DOKUZ EYLÜL UNIVERSITY
GRADUATE SCHOOL OF NATURAL AND APPLIED SCIENCES

FINITE ELEMENT SIMULATION OF BALLISTIC IMPACT ON COMPOSITE PLATES

by
Bulut BERK

July, 2014
İZMİR

FINITE ELEMENT SIMULATION OF BALLISTIC IMPACT ON COMPOSITE PLATES

A Thesis Submitted to the
Graduate School of Natural and Applied Sciences of Dokuz Eylül University
In Partial Fulfillment of the Requirements for the Degree of Master of Science
in Mechanical Engineering, Mechanics Program

by
Bulut BERK

July, 2014
İZMİR

M.Sc THESIS EXAMINATION RESULT FORM

We have read the thesis entitled **"FINITE ELEMENT SIMULATION OF BALLISTIC IMPACT ON COMPOSITE PLATES"** completed by **BULUT BERK** under supervision of **PROF.DR RAMAZAN KARAKUZU** and we certify that in our opinion it is fully adequate, in scope and in quality, as a thesis for the degree of Master of Science..

Prof.Dr. Ramazan KARAKUZU

Supervisor

Doç.Dr. Bülent Murat İGTEN

(Jury Member)

Doç.Dr. TUBA Alpyıldız

(Jury Member)

Prof.Dr. Ayşe OKUR
Director
Graduate School of Natural and Applied Sciences

ACKNOWLEDGEMENTS

First of all, I would like thank to my academic supervisor Prof. Dr. Ramazan Karakuzu because of his deep engineering knowledge and for advices in times of trouble. He showed really great patience to me and motivated me during this study.

I would like to express my gratitude to Dr. Ahmet Kaan Toksoy for performing my experimental tests and adding benefits to my thesis a lot.

Another thanks go to Research Assistant Volkan Arıkan for helping to find mechanical properties of specimens and for manufacturing processes.

This thesis was supported by Ministry of Science, Industry and Technology (01421.STZ-2012-1). I would also thank to Roketsan Missiles Inc. for financial support during this study.

My parents Münire, Namık and my brothers Ufuk and Umut deserve big thanks for standing always beside me and providing motivation over my entire life.

Lastly, I would like to thank to my love Merve. I felt her endless support during this study and will never forget.

Bulut BERK

FINITE ELEMENT SIMULATION OF BALLISTIC IMPACT ON COMPOSITE PLATES

ABSTRACT

In this study, effect of reinforcement type and different numerical composite damage material models were investigated in high velocity impact applications. Aramid and carbon-aramid hybrid fibers were used as a reinforcement material and epoxy was used as matrix in the composite plate. Both experimental and numerical methods were performed for understanding energy absorption mechanisms.

7.62 M61 type AP (Armor Piercing) projectiles were used in experimental procedure as strikers. Residual velocities were measured by velocity measurement traps. Six different velocities were used for both composites which have different reinforcements.

For numerical study, ANSYS was used as pre-processor and LS-Dyna was used as solver. Two failure models were used for composite materials which are MAT 22 (Mat_Composite_Damage) and MAT 59 (Mat_Composite_Failure_Solid_Model). Three different numerical models were created; MAT 22 with layered composite which was modeled as solid plies, MAT 59 with a layered composite which was modeled as solid plies and MAT 59 with single layer. Layered modeling technique was preferred because of weave style of composites. For modeling delamination, contact with tie-break option was used between composite layers.

After performing experimental and numerical procedure, good agreement was obtained in terms of ballistic limit velocities and residual velocities of projectile between experimental and numerical methods.

Keywords: Ballistic impact, 7.62 AP, aramid/epoxy, carbon-aramid/epoxy, LS-Dyna, numerical simulation

KOMPOZİT PLAKLAR ÜZERİNE BALİSTİK DARBENİN SONLU ELEMAN SİMÜLASYONU

ÖZ

Bu çalışmada, yüksek hızda darbe uygulamalarında, takviye tipinin etkisi ve farklı nümerik kompozit hasar modelleri incelenmiştir. Kompozit plakalarda, aramid ve karbon-aramid hibrid kumaşlar takviye elemanı olarak, epoksi ise reçine olarak kullanılmıştır. Enerji sönümleme mekanizması hem deneysel hem de nümerik yöntemlerle oluşturulmaya çalışılmıştır.

Deneysel prosedürde, 7.62 M61 tip AP (Armor Piercing) mermi tipi kullanılmıştır. Hız ölçüm kapanı yardımıyla çıkış hızları tespit edilmiştir. Her iki kompozit için altı farklı mermi hızı kullanılmıştır.

Nümerik çalışmada, ANSYS yazılımı ön işlemci olarak, LS-Dyna ise çözücü olarak kullanılmıştır. Kompozit malzemeler için, MAT 22 (Mat_Composite_Damage) ve MAT 59 (Mat_Composite_Failure_Solid_Model) olmak üzere olmak üzere iki farklı malzeme modeli kullanılmıştır. Üç farklı nümerik model oluşturulmuş olup, bunlar tabakalı kompozit modeli ve MAT 22, tabakalı kompozit modeli ve MAT 59 ve tek tabakalı kompozit modeli ve MAT 59 kombinasyonlarıdır. Örgü yapısından dolayı tabakalı modelleme tercih edilmiştir. Delaminasyon modellenmesi için, kompozit tabakalar arasında ayrılma özelliğine sahip kontak mekanizması kullanılmıştır.

Nümerik ve deneysel yöntemler uygulandıktan sonra, balistik hız ve mermi çıkış hızları baz alındığında, nümerik ve deneysel yöntemler arasında iyi bir uyum yakalanmıştır.

Anahtar kelimeler: Balistik çarpışma, 7.62 AP, aramid/epoksi, karbon-aramid/epoksi, LS-Dyna, nümerik benzetim

CONTENTS

Page

THESIS EXAMINATION RESULT FORM ii
ACKNOWLEDGEMENTS iii
ABSTRACT iv
ÖZ v
LIST OF FIGURES x
LIST OF TABLES xiv

CHAPTER ONE-INTRODUCTION 1

CHAPTER TWO-COMPOSITE MATERIALS AND MANUFACTURING TECHNIQUES 5

2.1 Composite Materials and Applications 5
2.1.1 Classification Based on Matrix Materials 6
2.1.1.1 Polymer Matrix Composites (PMC) 7
2.1.1.2 Metal Matrix Composites (MMC) 7
2.1.1.3 Ceramic Matrix Composites (CMC) 7
2.1.2 Classification Based on Type of Reinforcements 7
2.1.2.1 Fiber-reinforced Composites 8
2.1.2.2 Particle-reinforced Composites 8
2.1.2.3 Structural Composites 9
2.2 Components of Composite Materials 10
2.2.1 Fibers 10
2.2.1.1 Glass Fibers 10
2.2.1.2 Carbon Fibers 11
2.2.1.3 Aramid Fibers 12
2.2.2 Matrix Materials 12
2.2.2.1 Polymer Matrix Materials 12
2.2.2.1.1 Thermosets 12
2.2.2.1.2 Thermoplastics. 13

2.2.2.2 Nonpolymer Matrix Materials 13
2.3 Manufacturing Techniques of Composite Materials 13
2.3.1 Hand Lay-up 14
2.3.2 Spray-up 14
2.3.3 Autoclave Curing 15
2.3.4 Filament Winding 16
2.3.5 Vacuum Bag Molding 17
2.3.6 Vacuum Assisted Resin Infusion Molding 18
2.3.7 Pultrusion 18
2.3.8 Compression Molding 19
2.3.9 Resin Transfer Molding 20
2.3.10 Structural Reaction Injection Molding 21

CHAPTER THREE-BALLISTIC IMPACT SIMULATION THEORY 22

3.1 Theory Overview 22
3.2 Formulations of Explicit Dynamics 23
3.2.1 Lagrangian Approach 23
3.2.2 Eulerian Approach 23
3.2.3 Arbitrary Lagrangian-Eulerian (ALE) Approach 23
3.2.4 Smoothed Particle Hydrodynamics (SPH) Approach 24
3.3 Time Integration of Explicit Dynamics 25
3.4 Mass, Momentum and Energy Conversation 26
3.5 Penetration Mechanisms on Composite Plates 28
3.6 Material Models for Composite Materials in Numerical Simulations 29
3.7 Delamination Modeling 32

CHAPTER FOUR-MANUFACTURING PROCESS, MECHANICAL PROPERTIES OF COMPOSITE MATERIALS AND EXPERIMENTAL PROCEDURE 33

4.1 Manufacturing Steps 33
4.2 Mechanical Properties of Composite Materials 36
4.3 Experimental Procedure 39

4.3.1 Ballistic Setup 39
4.3.2 Properties of Projectile 40

CHAPTER FIVE-BALLISTIC IMPACT SIMULATION PROCEDURE 42

5.1 Modeling Details 42
5.2 Material Models 44
5.2.1 Material Model of Projectile 44
5.2.2 Material Models of Composite Materials 44
5.3 Geometries 45
5.3.1 Projectile Geometry 45
5.3.2 Geometries of Composite Materials 46
5.4 Finite Element Models 48
5.4.1 Finite Element Model of Projectile 48
5.4.2 Finite Element Model of Composite Materials 49
5.5 Contact Mechanisms 51
5.6 Boundary Conditions and Initial Velocity 52

CHAPTER SIX-EXPERIMENTAL AND NUMERICAL RESULTS 54

6.1 Experimental Results 54
6.1.1 Experimental Results of Aramid/Epoxy Composites 54
6.1.2 Experimental Results of Carbon-Aramid/Epoxy Composites 56
6.1.3 Ballistic Limit Velocity 57
6.2 Numerical Results 60
6.2.1 Numerical Results of Layered Composites with MAT 22 61
6.2.1.1 Aramid/Epoxy Composite 61
6.2.1.2 Carbon-Aramid/Epoxy Composite 64
6.2.2 Numerical Results of Layered Composites with MAT 59 66
6.2.2.1 Aramid/Epoxy Composite 66
6.2.2.2 Carbon-Aramid/Epoxy Composite 68
6.2.3 Numerical Results of Single Layer Composite with MAT 59 70
6.2.3.1 Aramid/Epoxy Composite 70
6.2.3.2 Carbon-Aramid/Epoxy Composite 72

6.3 Comparison Between Numerical and Experimental Results 73
6.3.1 Aramid/Epoxy Composite 73
6.3.2 Carbon-Aramid/Epoxy Composite 76

CHAPTER SEVEN-CONCLUSION AND DISCUSSION 79

REFERENCES 81

APPENDICES 85

LIST OF FIGURES

Page

Figure 2.1 Use of fiber-reinforced composites in Boeing 777 5
Figure 2.2 Schematic of integral armor design 6
Figure 2.3 Classification of composite materials 7
Figure 2.4 Tensile properties of a fibrous composite 8
Figure 2.5 Schematic of continuous fibrous and particulate composite 9
Figure 2.6 Laminated composite structure 9
Figure 2.7 Glass fiber 11
Figure 2.8 PAN based carbon fiber 11
Figure 2.9 Kevlar 12
Figure 2.10 Hand lay-up 14
Figure 2.11 Spray-up 15
Figure 2.12 Autoclave curing 16
Figure 2.13 Schematic illustration of filament winding 17
Figure 2.14 Schematic illustration of vacuum bag molding 18
Figure 2.15 Schematic illustration of vacuum infusion process 18
Figure 2.16 Schematic illustration of pultrusion 19
Figure 2.17 Schematic illustration of compression molding 20
Figure 2.18 Schematic illustration of resin transfer molding 21
Figure 2.19 Schematic illustration of SRIM 21
Figure 3.1 Implicit and explicit code applications 22
Figure 3.2 Lagrangian, Eulerian and ALE mesh 24
Figure 3.3 Pure SPH modeling of bird strike impact problem 25
Figure 3.4 Schematic illustration of Lagrangian computation cycle 28
Figure 3.5 Penetration damage mechanism during impact 28
Figure 3.6 Principal damage modes 29
Figure 4.1 Weave styles of fabrics, (a) carbon-aramid (b) aramid 33
Figure 4.2 Lamination process 34
Figure 4.3 Before resin infusion process 34
Figure 4.4 Resin progression 35

Figure 4.5 Composite material with material directions 36
Figure 4.6 Shimadzu AG-X tensile testing machine 37
Figure 4.7 Schematic illustration of V-notched shear test specimen 38
Figure 4.8 Schematic illustration of experimental setup 40
Figure 4.9 7.62 mm AP projectile (a) cartridge (b) cross-sectional view of projectile 41
Figure 5.1 Boundary conditions of composite materials 43
Figure 5.2 Simulation start-up 43
Figure 5.3 Projectile geometry 46
Figure 5.4 Geometry of composite materials 46
Figure 5.5 Through-thickness view of layered composite materials (a) aramid (b) carbon-aramid 47
Figure 5.6 Through-thickness view of single layer composite 47
Figure 5.7 Eight node hexahedron solid element 48
Figure 5.8 Front view of finite element model of projectile 48
Figure 5.9 Top view of finite element model of projectile 49
Figure 5.10 Top view of finite element model of composite materials 49
Figure 5.11 Detailed view of fine mesh region 50
Figure 5.12 Through-thickness view of layered composite materials (a) aramid (b) carbon-aramid 50
Figure 5.13 Through-thickness view of single layer composite material 51
Figure 5.14 Nodes in symmetry boundary conditions 52
Figure 5.15 Fixing condition 52
Figure 5.16 Nodes of core subjected to initial velocity 53
Figure 6.1 First specimen of aramid/epoxy composite material after ballistic tests a)front side b) back side 54
Figure 6.2 Second specimen of aramid/epoxy composite material after ballistic tests a) front side b) back side 55
Figure 6.3 Third specimen of aramid/epoxy composite material after ballistic tests a) front side b) back side 55
Figure 6.4 First specimen of carbon-aramid/epoxy composite material after ballistic tests a) front side b) back side 56

Figure 6.5 Second specimen of carbon-aramid/epoxy composite material after ballistic tests a) front side b) back side 56
Figure 6.6 Experimental initial vs. residual velocities of projectile for composite materials 57
Figure 6.7 Experimental initial vs. residual velocities of projectile including ballistic limit velocity 60
Figure 6.8 A sample of numerical simulation (Single layer aramid/epoxy composite with Mat 59, V_i: 852 m/s) 60
Figure 6.9 Perforation view of layered aramid/epoxy composites with MAT 22 after simulations for initial velocities (a) V_i: 852 m/s (b) V_i: 790 m/s 61
Figure 6.10 Velocity (mm/s) vs. time (s) curve of layered aramid/epoxy composite with MAT 22 for initial velocity V_i: 852 m/s 61
Figure 6.11 Velocity (mm/s) vs. time (s) curve of layered aramid/epoxy composite with MAT 22 for initial velocity V_i: 790 m/s 62
Figure 6.12 Initial vs. residual velocities of layered aramid/epoxy composite with MAT 22 after simulations 62
Figure 6.13 Initial velocity vs. residual velocity of layered aramid/epoxy composite with MAT 22 including ballistic limit velocity after simulations 63
Figure 6.14 Initial velocity vs. residual velocity of layered carbon-aramid/epoxy composite with MAT 22 after simulations 64
Figure 6.15 Initial velocity vs. residual velocity of layered carbon-aramid/epoxy composite with MAT 22 including ballistic limit velocity after simulations 65
Figure 6.16 Initial velocity vs. residual velocity of layered aramid/epoxy composite with MAT 59 after simulations 66
Figure 6.17 Initial velocity vs. residual velocity of layered aramid/epoxy composite with MAT 59 including ballistic limit velocity after simulations 67
Figure 6.18 Initial velocity vs. residual velocity of layered carbon-aramid/epoxy composite with MAT 59 after simulations 68
Figure 6.19 Initial velocity vs. residual velocity of layered carbon-aramid/epoxy composite with MAT 59 including ballistic limit velocity after simulations 69

Figure 6.20 Initial velocity vs. residual velocity of single layer aramid/epoxy composite with MAT 59 after simulations 70
Figure 6.21 Initial velocity vs. residual velocity of single layer aramid/epoxy composite with MAT 59 including ballistic limit velocity after simulations 71
Figure 6.22 Initial velocity vs. residual velocity of single layer carbon-aramid/epoxy composite with MAT 59 after simulations 72
Figure 6.23 Initial velocity vs. residual velocity of single layer carbon-aramid/epoxy composite with MAT 59 including ballistic limit velocity after simulations 73
Figure 6.24 Comparison of experimental and numerical results of aramid/epoxy composite 74
Figure 6.25 Comparison of experimental and numerical results of aramid/epoxy composite including ballistic limit velocity 75
Figure 6.26 Comparison of experimental and numerical results of carbon-aramid/epoxy composite 76
Figure 6.27 Comparison of experimental and numerical results of carbon-aramid/epoxy composite including ballistic limit velocity 78

LIST OF TABLES

Page

Table 4.1 Properties of reinforcements 35
Table 4.2 Properties of composite materials 35
Table 4.3 Mechanical properties of composite materials 39
Table 4.4 Initial velocities of projectiles for ballistic tests 40
Table 4.5 Some properties of 7.62 mm AP projectile 41
Table 5.1 Mechanical properties of core material 44
Table 5.2 Used values in simulations for composite materials 45
Table 6.1 Experimental initial and residual velocities of projectile for aramid composites 55
Table 6.2 Experimental initial and residual velocities of projectile for carbon-aramid composites 57
Table 6.3 Experimental initial, residual and ballistic limit velocities for aramid/epoxy composites 59
Table 6.4 Experimental initial, residual and ballistic limit velocities for carbon-aramid/epoxy composites 59
Table 6.5 Initial, residual and ballistic limit velocities of layered aramid/epoxy composite with MAT 22 after simulations 63
Table 6.6 Initial, residual and ballistic limit velocities of layered carbon-aramid/epoxy composite with MAT 22 after simulations 65
Table 6.7 Initial, residual and ballistic limit velocities of layered aramid/epoxy composite with MAT 59 after simulations 67
Table 6.8 Initial, residual and ballistic limit velocities of layered carbon-aramid/epoxy composite with MAT 59 after simulations 69
Table 6.9 Initial, residual and ballistic limit velocities of single layer aramid/epoxy composite with MAT 59 after simulations 71
Table 6.10 Initial, residual and ballistic limit velocities of single layer carbon-aramid/epoxy composite with MAT 59 after simulations 73
Table 6.11 Error percentages of numerical methods for aramid/epoxy composite considering ballistic limit velocities 73

Table 6.12 Error percentages of numerical methods for carbon-aramid/epoxy composite considering ballistic limit velocities 73

CHAPTER ONE

INTRODUCTION

Composite materials have become important recently in defense, aerospace and naval industry. The importance of composite materials appeared because of high strength, lightness, thermal insulation and corrosion resistance. It is not always possible to combine all advantages in a product so working conditions of the product should be considered well.

Ballistic impact of the materials is one of the most popular topics over last years. Penetration mechanisms continue to be developed by the experts. Besides the analytical approaches, numerical codes are widely used, finite element and finite difference methods are used popularly. Meshing methods may vary, over last years Lagrange, Euler, ALE and SPH formulations are used.

Hoof (1999) modeled a projectile and composite system where reinforcement of the composite material was woven Kevlar 29. In the thesis, the author considered and investigated many parameters and related sensitivities to models. Importance of mesh was also discussed with increasing number of elements in plane and through the thickness of the models. Two models, which were called as post failure and instantaneous, were discussed and instantaneous model which consists of load carrying capacity after failure showed more realistic results and post failure model was found more mesh sensitive.

Fawaz, Zheng, & Behdinan (2003) have simulated normal and oblique ballistic impact on ceramic-composite structure. Numerical model was simulated in LS-Dyna 3D with modeling composite by using type 59 orthotropic composite model (MAT_COMPOSITE_FAILURE_SOLID) and steel projectile with type 03 material model (MAT_PLASTIC_KINEMATIC). By using this material model for steel projectile, it could be seen deformation for the geometry. At the end of the work, it was observed that interlaminar stresses at the interface of ceramic-composite structure for oblique impact were found to be smaller than normal impact. Also the

erosion of the projectile for the oblique impact was found to be greater than normal impact. Energy distribution for both simulations was found similar.

Heimbs, Heller, & Middenford (2008) modeled low velocity impact procedure by LS-Dyna 3D and investigated the effect of compressive preloading. The composite was carbon fiber-reinforced epoxy and 24 plies were used. MAT 54 (MAT_ENHANCED_COMPOSITE_DAMAGE) shell theory was used for modeling composites. Striker was modeled with MAT 20 (MAT_RIGID). Also influence of number of shell layers, influence of element size, influence of contact penalty stiffness were investigated. Results between numerical and experimental methods were in good agreement.

Azevado, & Alves (2009) investigated a S2-glass/epoxy and bird system. As we know, bird strike is a major problem for aircraft industry. The system was simulated with LS-Dyna 3D which is a numerical code for explicit solutions. The bird was simulated by SPH elements as water because of behaving like water when impact occurs. Different simulation was adopted for the composite with pure FE and SPH algorithms. It was found that simulation results were similar to each other for this application despite different algorithms were applied.

Sevkat, Liaw, Delale, & Raju (2009) studied on S2-glass fiber/toughened composite beams. Both experimental and numerical methods were used. LS-Dyna 3D numerical code was used and user defined nonlinear orthotropic model, Chang-Chang linear orthotropic model and experimental results were compared. Good agreement was found between numerical and experimental methods. After verification of models, further FE simulations were performed for obtaining the ballistic limit velocity.

Guild, El-Habti, & Hogg (2010) modeled a FE model, which consisted of a projectile and composite structure in MSC Patran. The model was solved with a numerical code MSC Dytran. Delamination was modeled by using spring elements which were constraining two laminates and these constraints were related with some failure criteria. At the end of the work, it was found absorbed energy distribution by

fiber, matrix and delamination. It was proved that most of energy was absorbed by fibers.

Ahn, Nguyen, Park, Kweon, & Choi (2010) modeled a projectile and composite plate system by LS-Dyna 3D. Composite material was Kevlar 29/phenolic and impactor was modeled as elastic-plastic material. Contacts between laminates had tie-break options, so delamination occurred when specified criteria were met. Simulation results and test results in an earlier study (Hoof, 1999) were in good agreement.

Yang, & Dai (2010) modeled helmet, head and brain system by LS-Dyna 3D. Different projectile angles and different positions were modeled. The helmet's material was Kevlar and modeled with Chang-Chang failure criteria. The stress distribution for helmet and head were published after the simulation.

Deniz (2010) considered the effect of plate hardness on ballistic impact problems. 7.62 mm AP projectiles were used and for AISI 4340 steels, dynamic material models including Johnson-Cook strength models were preferred. After 2D and 3D numerical simulations by AUTODYN, good agreement was obtained between numerical and test results and it was proven that ballistic protection efficiency increased with increasing plate hardness values.

Ramadhan, Talib, Rafie, & Zahari (2013) investigated high ballistic impact and used a hybrid model. In this model, Aluminum 6061 T6 plate and Kevlar/epoxy was used. Aluminum was used as a variable in the model and placed in top, center and bottom. For solving this numerical model, Autodyn 3D was used and projectile, which has 7.62 mm diameter, was modeled by Johnson-Cook plasticity model and the softening was observed in the projectile. Experimental procedure was done by gas gun test setup and between numerical and experimental model, compatible results were found.

Yaghoubi, & Liaw (2013) investigated effect of fiber orientations to ballistic impact issue. The model consisted of combination of Aluminum 2024 T3 plate and S2-glass/epoxy. Experimental procedures were done by gas gun test setup and high

speed camera was also used. LS-Dyna 3D numerical code was used for solving this numerical model. For modeling delamination, stress based function was used. Besides comparison between V_{impact}-$V_{residual}$, $V_{ballistic}$ was written as a function of fiber orientation. The model which has $[0/90]_s$ fiber orientation was found most energy absorbing mechanism.

Mohan, & Velu (2014) worked analytically where the reinforcement material was glass fiber in the model. Delamination, friction between projectile and composite, tension failure, matrix failure were considered in the model. In this analytical model, some approximations like fully rigid behavior of the projectile and no strain energy, projectile impact on composite plate fully perpendicular, equal wave velocities for fiber and perpendicular fiber direction, considering the constant projectile deceleration were accepted.

Wielewski, Birkbeck, & Thomson (2013) has worked on an analytical approach. Most analytical approaches were interested in ballistic on single plate and was investigated multi-layer plates in this study. Hand lay-up Kevlar composites, which have 3, 6, 9, 12 layers, were used as combination of two of them. After experimental procedure, in the light of results best couple consisted of two 6 layered composites. Lambert-Jonas semi analytical equation, which is used for relation of impact and residual velocity, has been made available for multi-layer composite ballistic impact.

Manes, Lumassi, Giudici, & Giglio (2013) has worked on impact on helicopter tail rotor drive shaft numerically and experimentally. Drive shaft was produced by Aluminum 6061 T6 material and Johnson-Cook plasticity and Bao-Wierzbicki ductile fracture model were considered for this material. While modeling the projectile, core and shell were considered separately. Abaqus Explicit were used for solving numerical simulation. Numerical and experimental results were in good agreement**.**

In this study, high velocity impact behaviors of aramid/epoxy and carbon-aramid/epoxy composites were examined experimentally. After performing these tests, three numerical procedures with two different material models were performed by an explicit solver.

CHAPTER TWO

COMPOSITE MATERIALS AND MANUFACTURING TECHNIQUES

2.1 Composite Materials and Applications

Composite materials are combination of two or more materials which have basically different chemical composition and shape with a microscopic or macroscopic way. The new combined material may show different individual properties from these components. Composite materials are used in many industries as aerospace, defense, naval, marine, space, sports and civil engineering applications.

Aerospace industry has increased the usage of composite materials for providing benefits. As it is known, the composite materials have bigger strength to weight ratios than metals. This advantage simply reduces fuel consumption, moreover provides better resistance for some applications. Corrosion resistance also plays an important role for the fatigue behavior. Usage of composite materials has begun in military, in recent years civil aircraft have increased composite usage fast. From the beginning, many components like radome, engine cowls, tail planes, elevators, floor panels have been produced as composite materials (Figure 2.1). In the industry, mostly fiber reinforced composites are chosen. This type includes mostly glass and carbon fibers.

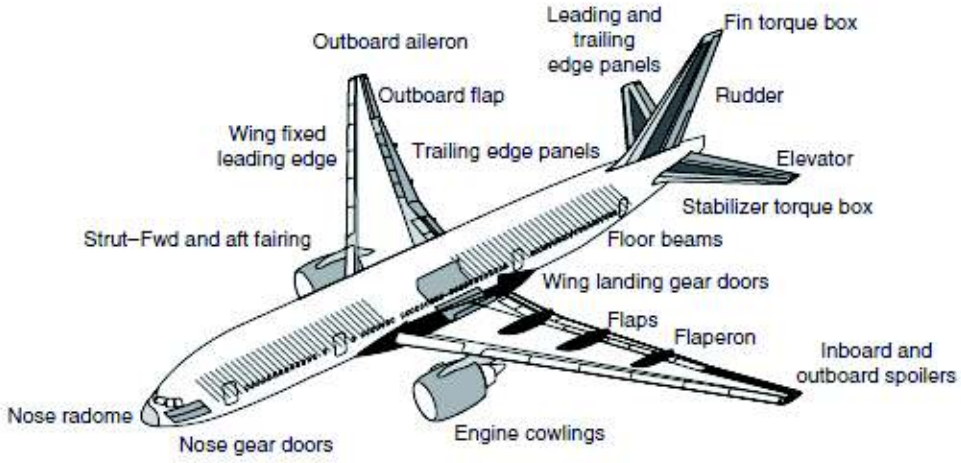


Figure 2.1 Use of fiber-reinforced composites in Boeing 777 (Mallick, 2007)

Composite materials are also used for numerous applications in defense industry (Figure 2.2). Low weight is also major component for body armor systems in defense industry because of carrying limitation of people. Despite its static behavior, composites are mostly designed for energy absorbing mechanisms in defense industry. Body armor systems (helmets, vests etc.), spall effects in armored vehicles are most popular topics in theoretical and numerical approaches.

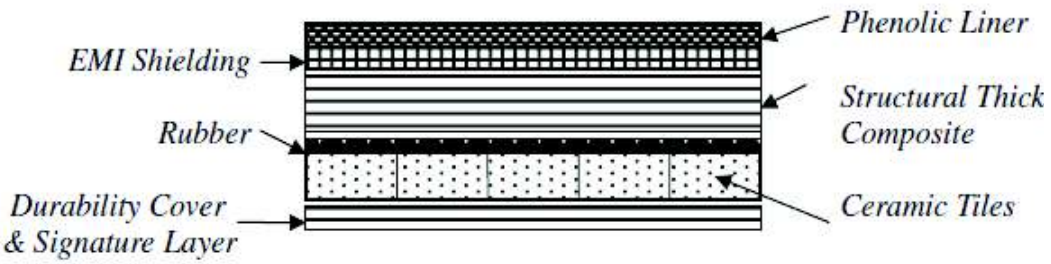


Figure 2.2 Schematic of integral armor design (Vaidya, Abraham, & Bhide, 2001)

Naval and marine industries have been also effected by composite materials benefits. Thermal conductivity, acoustic performance, corrosion resistance, fatigue and impact behavior are considerable factors in naval industry. Most of early applications have begun to overcome the corrosion problem of steel and aluminum and environmental weakness problems of wood**.** Early time and recently glass fiber reinforced polymers are mostly chosen because of low cost of the material. For the advanced applications, carbon fibers and aramids may be added next to glass fiber. Also sandwich composites usage can't be ignored.

Composite materials can be divided into two categories based on matrix materials and type of reinforcements.

2.1.1 Classification Based on Matrix Materials

Composite materials can be divided into three categories based on matrix materials.

2.1.1.1 Polymer Matrix Composites (PMC)

Polymer matrix composites are mostly used type of composites. Glass, carbon and aramids are used mostly. These composites are used in various applications including defense and aerospace industry. This type of composite is also called as Fiber Reinforced Polymers. They are relatively cheap and easy to produce.

2.1.1.2 Metal Matrix Composites (MMC)

This type of composites can be processed by several techniques and mostly used in automotive industry. The main purpose of creating this type is reducing density. It is usually used aluminum as matrix material but also magnesium and titanium are popular.

2.1.1.3 Ceramic Matrix Composites (CMC)

Ceramic matrix composites are usually preferred for high temperature applications. These materials are reinforced with short fibers or whiskers for improving the ductility of material.

2.1.2 Classification Based on Type of Reinforcements

Composite materials can be divided into three categories based on reinforcing material structure (Figure 2.3).

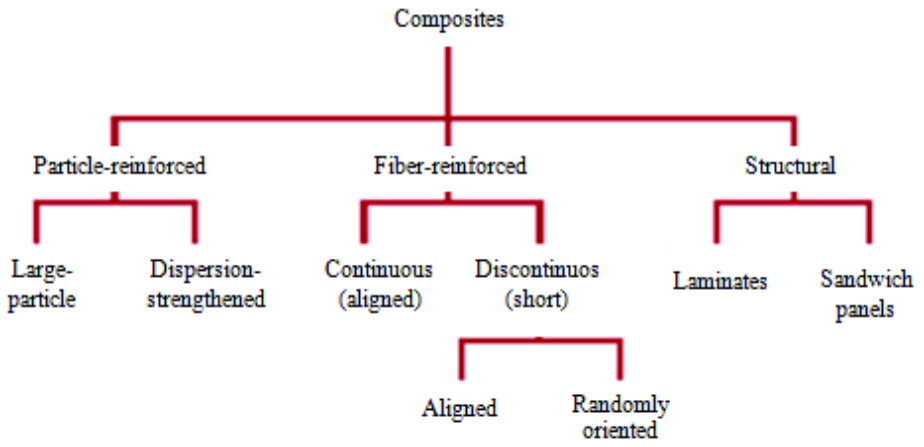


Figure 2.3 Classification of composite materials (Mansur, 2011)

2.1.2.1 Fiber-reinforced Composites

Fibrous composites contain a material which is dominant volumetrically and provide reinforcement at any direction. Moreover for bonding fibers and matrix, a fine interphase region is necessary. The advantage of this type is that strength of the material, which forms the matrix, can be upgraded to higher or desirable values. It can be reached to desirable values by changing material type and orientation of fibers. Mechanical properties of fibrous composites are usually between mechanical properties of fiber and mechanical properties of matrix (Figure 2.4).

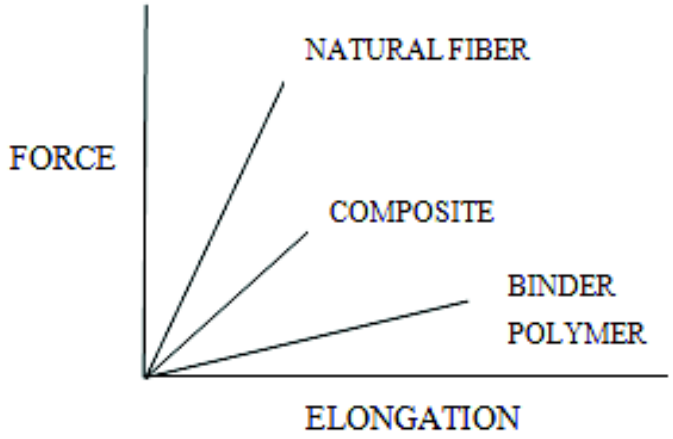


Figure 2.4 Tensile properties of a fibrous composite (Kamath, 2004)

Reinforced fibrous composites can be used as aligned to matrix in continuous or discontinuous phase. These fibers can have critical lengths for transferring loads to matrix or shorter lengths than critical length. Reinforced fibers can also be distributed randomly.

2.1.2.2 Particle-reinforced Composites

This type of composite includes one or more material that one dispersed in another one (Figure 2.5). Particles may have any shape like spherical, ellipsoidal or irregular. Particulate composites can be produced by simpler manufacturing techniques. This type of composite mostly has low strength and can be brittle based on distribution of particles.

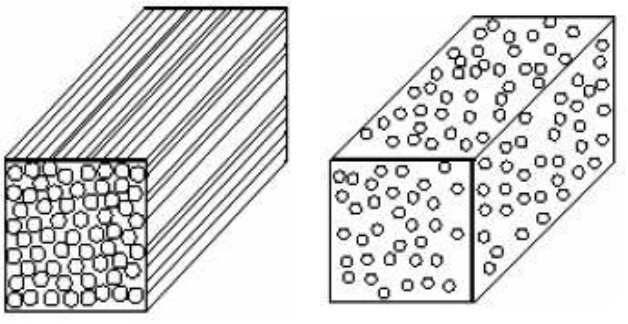


Figure 2.5 Schematic of continuous fibrous and particulate composite (Deo, 2010)

2.1.2.3 Structural Composites

Structural composites are type of composites that consist of at least two different layers that are used and bonded together (Figure 2.6). Laminated composites description is mostly used for plastic based composites and can also be called as laminated fibrous composites which can consist of glass, carbon and aramid and various type of resins but metals and sandwich panels can be included in this type of composites.

Sandwich panels consist of layers which have mostly good strength and a core based on application situation from low strength to high strength. The usage of sandwich panel varies and can be used from thermal isolation to improving strength applications.

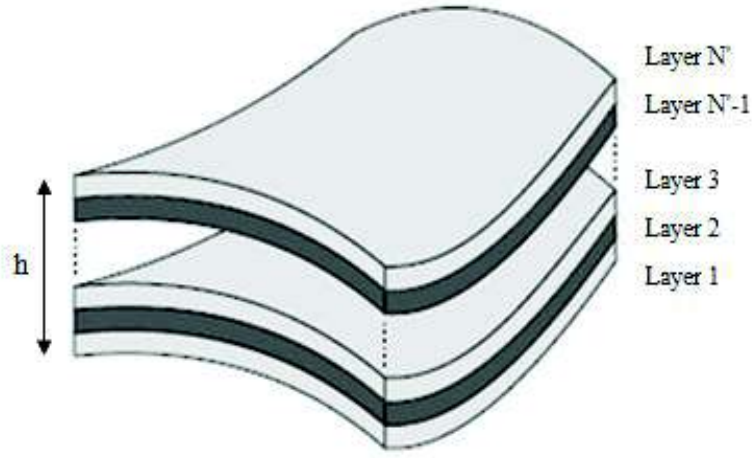


Figure 2.6 Laminated composite structure (Stegmann, 2005)

2.2 Components of Composite Materials

Composite material has two or more distinct materials which are generally called as fiber and matrix. Matrix material holds fibers with a fine interface and has to transfer loads to fibers. For sandwich panels, core materials are also important.

2.2.1 Fibers

Fibers usually have very big length to diameter ratio. They have high strength and are used to strengthen matrix materials. Fibers can be short and long based on manufacturing processes. Also fibers can be continuous, discontinuous and randomly oriented. Boron, aluminum oxide and other materials can be used as reinforcement for special applications but will not be introduced. Glass, carbon and aramid fibers are described as follows.

2.2.1.1 Glass Fibers

Glass fibers are general purpose fibers which have various types (Figure 2.7). Strength properties are lower than other fibers but they are much cheaper. Glass fibers can be categorized in many categories based on some required properties.

- A Glass : High alkali glass
- C Glass : Chemical stability for corrosion
- D Glass : Low dielectric constant
- E Glass : Good electrical resistance
- R Glass : Strength and corrosion
- S Glass : Providing high strength



Figure 2.7 Glass fiber (Ipek, 2005)

2.2.1.2 Carbon Fibers

Carbon fiber is the fiber type which has high strength and used in mostly aerospace, nuclear, automotive and marine industries. Most used carbon fibers are PAN (polyacrylnitrile) fiber which has low stiffness and high tensile and compressive strength and Pitch fiber which has high strength and high tensile and low compressive strength. Despite the strength properties, carbon fibers are expensive. For this issue, investigations on low cost carbon fibers are still continuing.

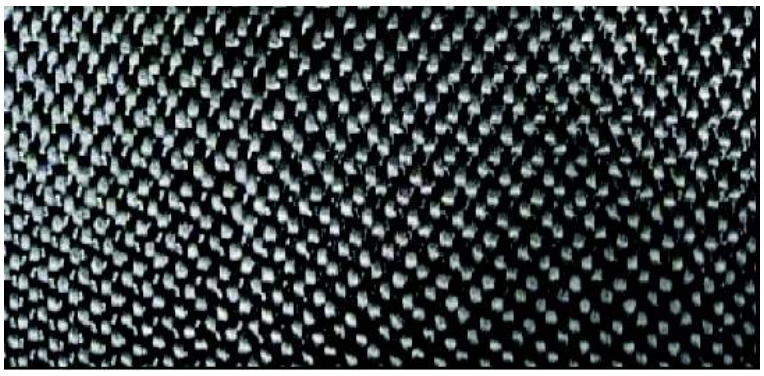


Figure 2.8 PAN based carbon fiber (Liu, 2010)

2.2.1.3 Aramid Fibers

Aramid fibers are mostly used in military industry for ballistic applications (Figure 2.9). These fibers have some advantages over glass and carbon fibers. High stiffness, low density, high tensile and low compressive strength, ductility are most stunning properties of this kind of fibers.

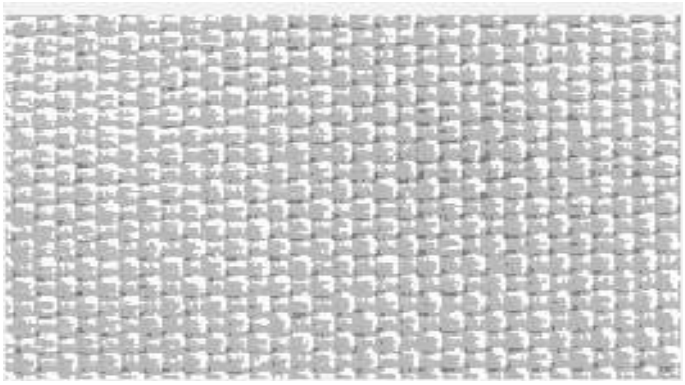


Figure 2.9 Kevlar (Ipek, 2005)

2.2.2 Matrix Materials

Composites can be classified based on matrix materials and divided into three major categories. So matrix materials can be polymeric and nonpolymeric including metal and ceramics materials and polymeric matrix materials are mostly used in these days based on working conditions. Matrix materials are main parts of composites and hold fibers within them and transfer loads to fibers. After fiber failure, composite show basically characteristic of matrix.

2.2.2.1 Polymer Matrix Materials

This type of matrix divided into two main categories including thermosets and thermoplastics. Today thermosets play a major role in the industry over thermoplastics.

2.2.2.1.1 Thermosets. Thermosetting resins include dominantly polyester, vinyl ester and epoxy. Polyester resin is one of the most common unsaturated resin particularly used in marine industry. Polyester resin has good chemical resistance but

flammable. Due to being inexpensive, polyester resins are preferable. Vinyl ester shows strength properties between polyester and epoxy. It has very good chemical resistance. Because of molecular chain, this type is tougher than polyester. Vinyl ester has moderate price. Epoxy is used for high quality composites. This type of resin has good strength properties and is also preferred in aerospace and defense applications.

2.2.2.1.2 Thermoplastics. Thermoplastic resins include PP (polypropylene), PE (polyethylene), PEEK (polyether ether ketone), PTFE (teflon). This type of resin needs to be formed with different manufacturing process. Resin is heated and becomes a liquid than with cooling it solidifies. Thermoplastics have larger ductility than thermosets. Also these resins have good impact resistance. Thermoplastics are more temperature resistant but more expensive. Recycling issue is more possible and can be heated and remolded again.

2.2.2.2 Nonpolymer Matrix Materials

This group can be divided into two categories which are metal matrix and ceramic matrix materials. For metal matrix materials aluminum, copper, titanium can be said. For ceramics matrix materials aluminum oxide, zirconia and silicium carbide can be said.

2.3 Manufacturing Techniques of Composite Materials

Composite materials can be produced by different manufacturing techniques and manufacturing depends on geometry, desired quality, cost and experience. These techniques may roughly divide into two categories as open and closed molding. In open molding, the process is done under the effect of atmosphere. In closed molding, the process is done with the aid of molds or vacuum bags that block the effect of atmosphere. These types have their own advantages and so concepts which are described above are important before production.

2.3.1 Hand Lay-up

Hand lay-up is the oldest technique for producing a composite material (Figure 2.10). Desired thickness can be reached and this process has low tooling costs. Complex geometries can be produced with experienced operators. Slow process, unwanted gaps and lack of adaptation to mass production can be said as disadvantages. Turbine blades and marine applications like boat hulls and kite boards can be produced with this technique.



Figure 2.10 Hand lay-up (Keulen, 2006)

Steps of the procedure can be listed as follows.

- Mold is coated by gel.
- Fibers and resins are placed on the mold and this process keeps on until desired thickness is reached.
- Part is cured and it can be removed from mold with a single piece.

2.3.2 Spray-up

Spray-up is also open molding production technique usually used for small boats and sandwich panels. Gel coat is optional and depends on manufacturer for a surface finish quality. With this technique, continuous fibers are chopped with a chopping mechanism and discontinuous short fibers are provided and liquid resins are sprayed

onto mold together with the aid of a nozzle or a gun (Figure 2.11). This process is simple, low cost and has easy setup. Because of chopped fibers, desired strength may not be available and this can be said as a disadvantage.



Figure 2.11 Spray-up (Keulen, 2006)

2.3.3 Autoclave Curing

Autoclave curing which is usually performed for aerospace and ballistic applications is a vessel that controls temperature and pressure for polymeric composite materials to remove unwanted air (Figure 2.12). The machine applies pressure with temperature. After curing operation composite material has better resin-fabric ratio so strength properties are improved to better levels. Cost can be said as a disadvantage and the process is not suitable for small parts.



Figure 2.12 Autoclave curing (Wang, & Shie, 2009)

2.3.4 Filament Winding

Filament winding is a continuous process that controls oriented fibers which are wound around a rotating mandrel (Figure 2.13). The process continues until desired thickness is reached. Fibers can be pre-impregnated. Another technique except pre-impregnation, fibers go through resin bath before wound operation. Curing operation is necessary for removing mandrel and part shapes are limited to cylindrical or spherical shapes because of structure of the process. Process is adaptable to mass production. High strength can be achieved. Process is suitable for pressure vessels, water, gas and storage tanks.

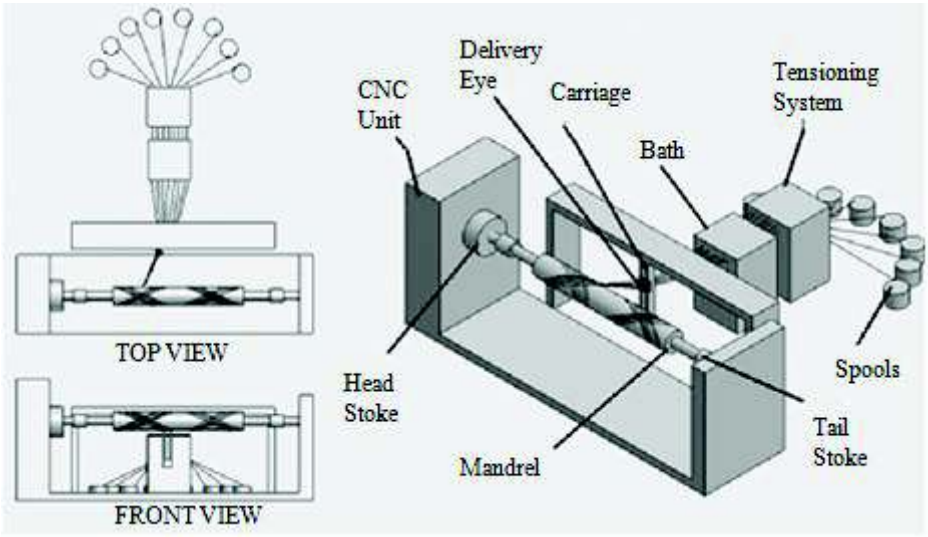


Figure 2.13 Schematic illustration of filament winding (Balya, 2004)

2.3.5 Vacuum Bag Molding

Vacuum bag molding has appeared in order to eliminate the shortcomings of open molding processes. This technique has steps as follows (Figure 2.14).

- Fibers and resins are placed on mold as wet lay-up.
- A flexible film (nylon, PVA etc) is placed over wet lay-up.
- A vacuum is started and atmospheric pressure compresses laminates.

Vacuum bagging has important advantages over hand lay-up. First of all efficient laminating can be done. Improved strength can be achieved because of removing trapped air and emptying excessive resin from laminates, with this feature this technique decreases resin cost.

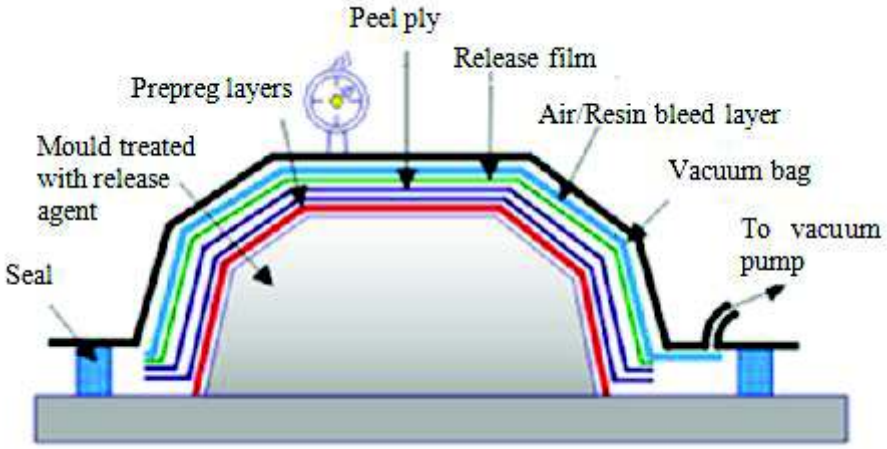


Figure 2.14 Schematic illustration of vacuum bag molding (Shukla, 2011)

2.3.6 Vacuum Assisted Resin Infusion Molding

Vacuum assisted resin infusion molding is a various application of vacuum bag molding. The difference between bag and infusion is that resin is entered to mold after vacuum is started and air is almost evacuated (Figure 2.15). So reinforcements are already ready and resin comes after vacuum operation. Also position of reinforcements may be well defined and excessive resin problem is resolvable. Desired mechanical properties of composite materials which are produced with vacuum infusion technique can be achieved.

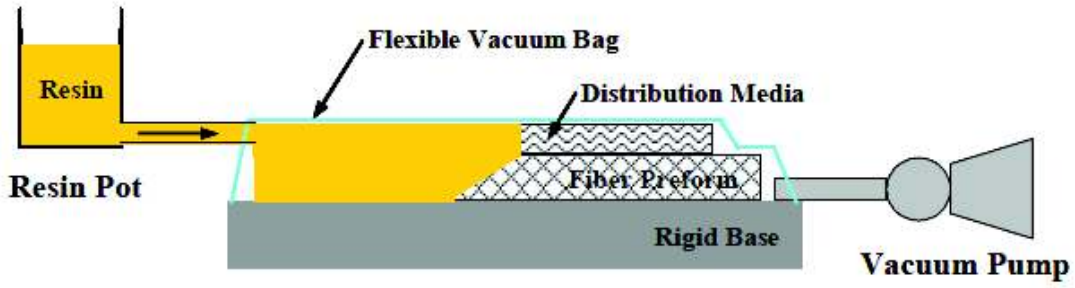


Figure 2.15 Schematic illustration of vacuum infusion process (Grimsley, 2005)

2.3.7 Pultrusion

Pultrusion is a continuous process for manufacturing products that have constant profiles such as pipe, beams and structural shapes. Roving fibers go through resin

bath with a guide puller and then formed (Figure 2.16). Multiple rows can be used with an automated process. After forming, curing process takes place. Lastly cutting is done after forming and curing operation. These products which are manufactured with this technique have high strength properties with providing enough fiber contents. This technique has a disadvantage because of limited to uniform cross sections.

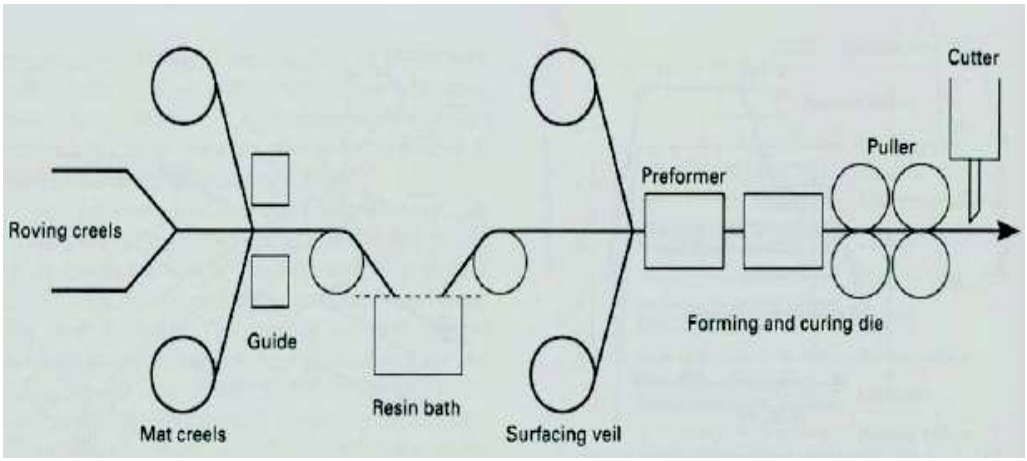


Figure 2.16 Schematic illustration of pultrusion (Bundy, 2005)

2.3.8 Compression Molding

Compression molding is a closed molding process that has couple molds which are called male and female molds and these molds are controlled by mechanical or hydraulic presses (Figure 2.17). Mostly heated molds form composites. This technique has several kinds as follows.

- Bulk molding compound
- Sheet molding compound
- Thick molding compound
- Liquid composite molding

Complex geometries like holes can be produced by this technique with aid of single or multiple cavities. Fast molding and automated process can be said as an advantage. Chopped fibers may decrease desired strength values.

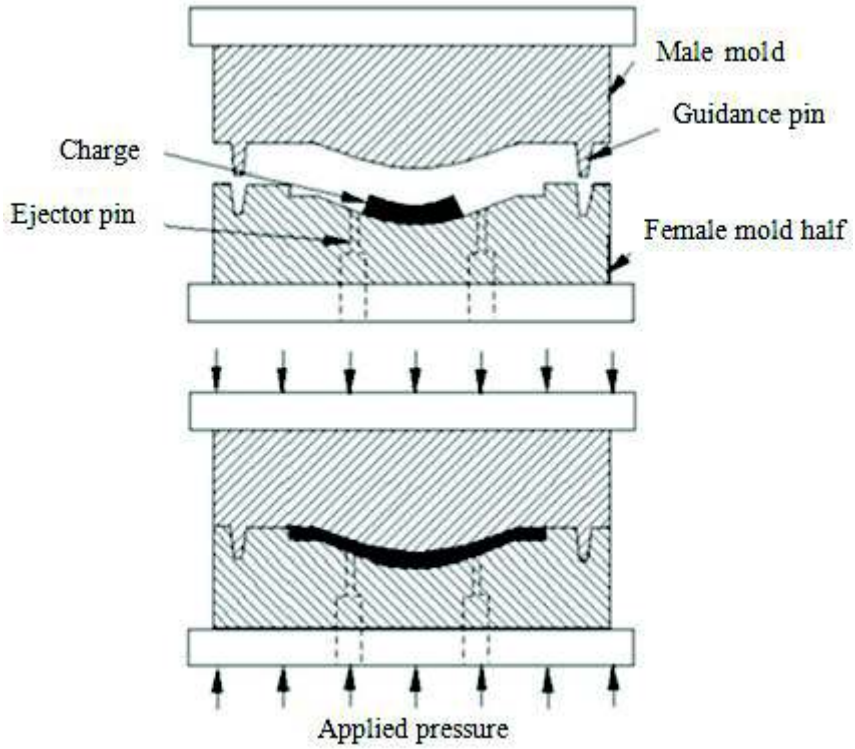


Figure 2.17 Schematic illustration of compression molding (Dhananjayan, 2013)

2.3.9 Resin Transfer Molding

Resin transfer molding is a closed molding process which has two molds, reinforcements are placed in these molds and resin is injected into these molds for producing advanced continuous fiber reinforcements (Figure 2.18). All fibers can be used with forms such as mat and woven. After resin transfers, molds are heated and curing cycle starts and resin solidifies. Gel coat may be used for better surface finish quality. One of advantage is fast production and this process is adaptable to mass production. Higher fiber-resin ratio can be provided so after manufacturing, finalized product is lighter and has more strength. Complex shapes can be manufactured by cavities. Tooling costs are high and also molds are controlled by hydraulic presses. Some automotive products such as auto body panels, wind turbine blades can be manufactured.

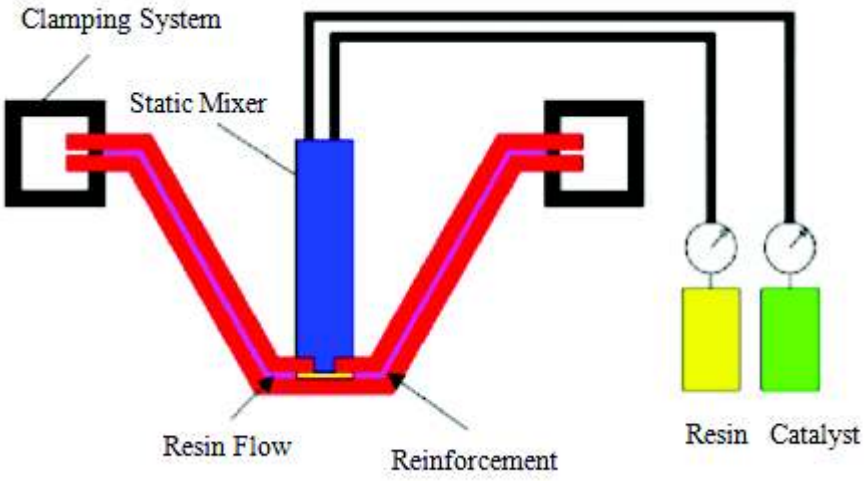


Figure 2.18 Schematic illustration of resin transfer molding (Ipek, 2005)

2.3.10 Structural Reaction Injection Molding

Structural reaction injection molding (SRIM) is a process which molds already contain short fibers as reinforcements and two resins are forced to combine at high velocities and injected into mold (Figure 2.19). After injection process, curing operation starts. This technique can be automated and fast production can be achieved. Isotropic material behavior is also possible. High fiber content is not available so mostly desired strength can't be reached.

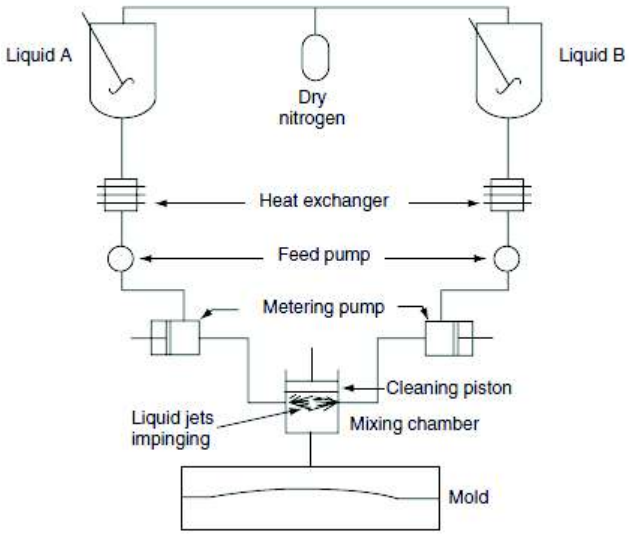


Figure 2.19 Schematic illustration of SRIM (Mallick, 2007)

CHAPTER THREE

BALLISTIC IMPACT SIMULATION THEORY

3.1 Theory Overview

Materials show different behaviors depending on strain rate and temperature. Two different approaches are mostly used for solving dynamic applications which are known as implicit and explicit solvers. There are three different phases which are known as static, quasi-static and dynamic (Figure 3.1). General engineering materials are used for low strain applications and subjected to static equilibrium. These materials show static responses and strain rate effects are mostly excluded. Quasi-static phase is between static and dynamic phases and internal and external forces difference is nearly zero. Dynamic phase includes impact, metal forming and explosion events. For providing true behavior of materials, strain rate effects should be included.

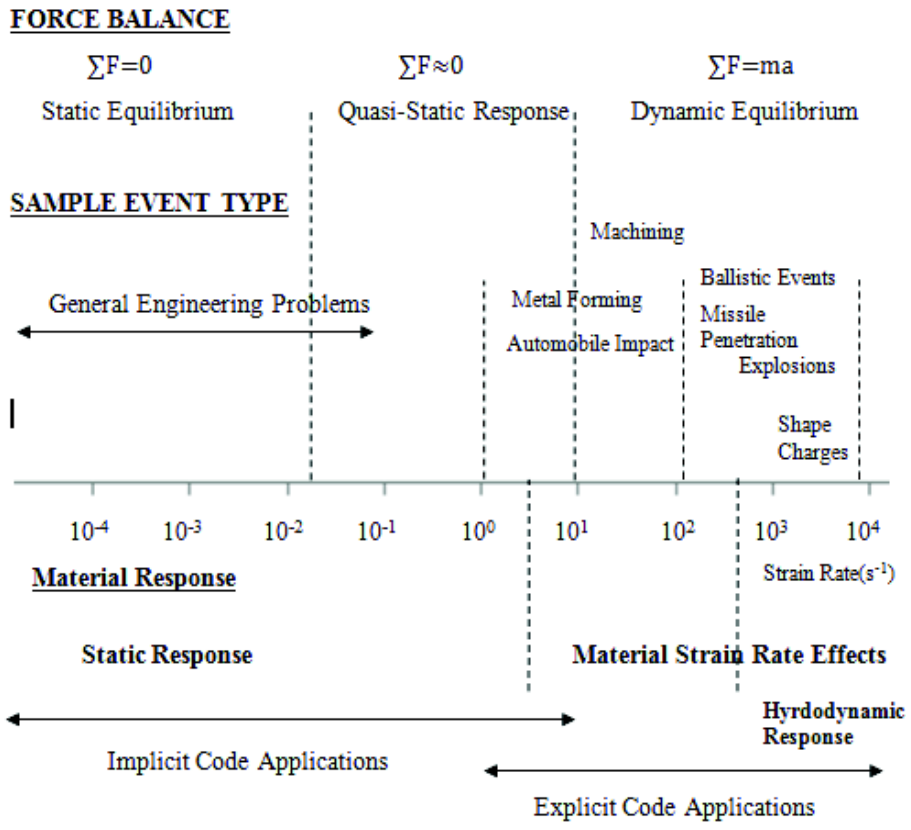


Figure 3.1 Implicit and explicit code applications (Deniz, 2010)

3.2 Formulations of Explicit Dynamics

Explicit dynamics theory has some advantages which are non-convergence issues and time over implicit dynamics theory. It is known that different approaches are used in explicit finite elements method. Four formulations are popularly used which are known as Lagrangian, Eulerian, ALE (Arbitrary Lagrangian-Eulerian) and a mesh free method called as SPH (Smoothed Particle Hydrodynamics).

3.2.1 Lagrangian Approach

This approach is the most popular technique in ballistic impact penetration models. The method uses material coordinates which is also known as Lagrangian coordinates. Nodes of mesh move and distort with material and no material transfer between elements (Figure 3.2). With this method, less computational time may be provided than other approaches. Conversation of mass is provided automatically. This approach may lead inaccurate results and time steps may decrease depending on element characteristic dimension for large deformation problems. For better results while running large deformation problems, remeshing may be required and this can lead extra computational time.

3.2.2 Eulerian Approach

This approach is ideal for modeling fluid, gas flow and large deformations of solids. The method includes a fixed mesh in space and material moves in this region, so material transfer between elements is possible (Figure 3.2). Conversation of mass, momentum and energy is satisfied. More computational time is needed than Lagrangian approach and for some setups, free space must be meshed.

3.2.3 Arbitrary Lagrangian-Eulerian (ALE) Approach

Arbitrary Lagrangian Eularian approach is combination of Lagrangian and Eularian methods. It can be said that this approach has two meshes, one is placed to background and can move in space and the other one is attached to background mesh and can move through the background mesh (Figure 3.2). Eulerian mesh is fixed and ALE mesh can move in space and this can be said as a difference. Conversation of

mass, momentum and energy is satisfied. This method is generally slower than other methods which are mentioned above and still under development.

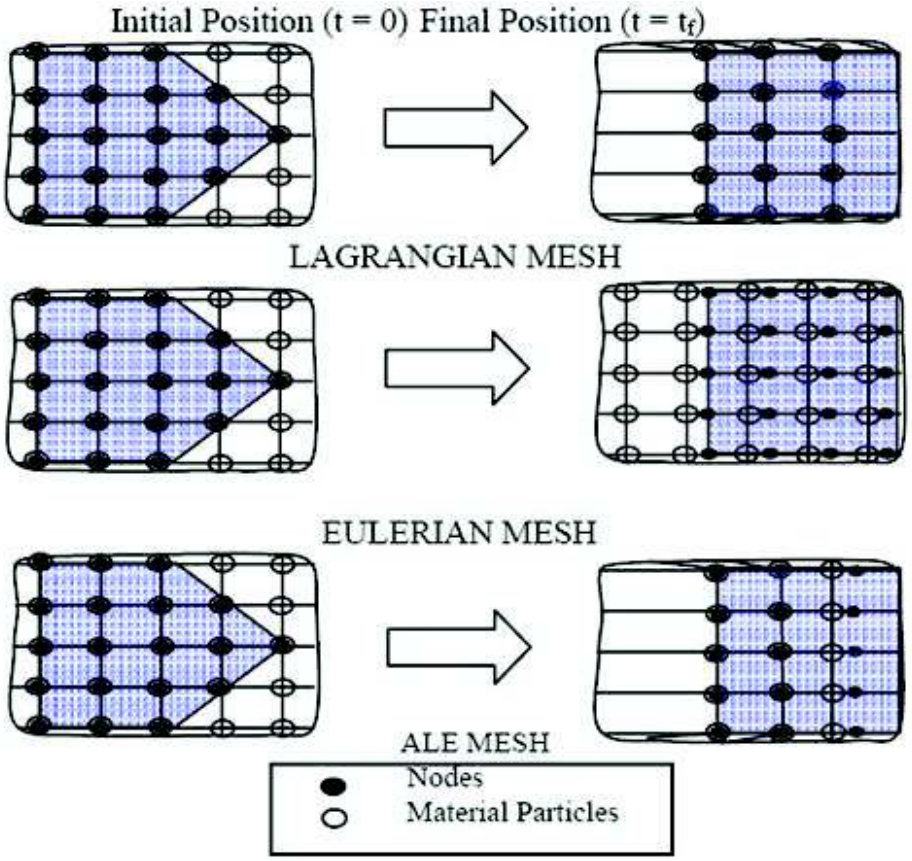


Figure 3.2 Lagrangian, Eulerian and ALE mesh (Goyal, Huertas, & Vasko, 2013)

3.2.4 Smoothed Particle Hydrodynamics (SPH) Approach

Smoothed Particle Hydrodynamics (SPH) is a mesh-free method which is still under development. In ballistic impact topic, hyper-velocity and spall effect issue may be investigated. With this technique, complex material models may be simulated (Figure 3.3). Modeling excessive local material distortion is possible. Instability in tension, zero energy modes and high computational time may be said as disadvantages of this method.

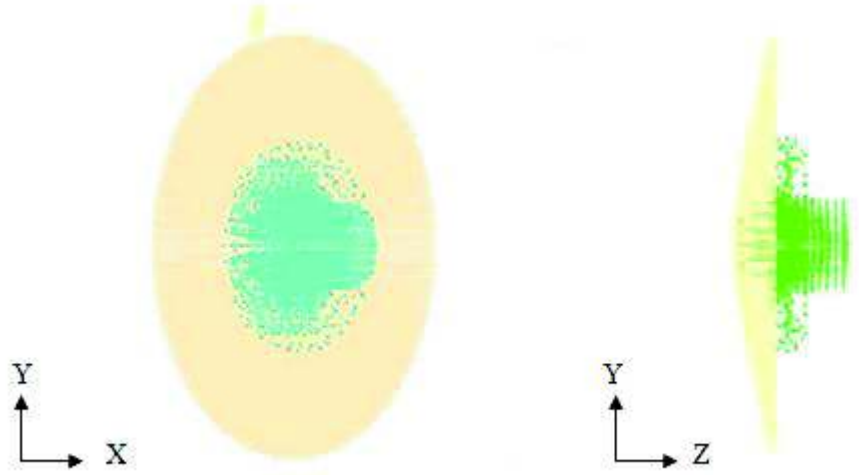


Figure 3.3 Pure SPH modeling of bird strike impact problem (Azevado et al, 2009)

After evaluation of advantages and disadvantages of element formulations which are mentioned above, Lagrangian approach is chosen for corresponding numerical simulations.

3.3 Time Integration of Explicit Dynamics

Explicit Dynamics solvers usually use central difference integration theme. This integration has advantages such as not having convergence checks, not requiring any iteration and no inversion of global stiffness matrix. For dynamic events such as high velocity impacts, damping effects are usually ignored and the equation may be written as shown below.

$$[M]\{\ddot{x}\} + [K]\{x\} = \{F(t,x)\} \tag{3.1}$$

where, $[M]$ is mass matrix, $[K]$ is stiffness matrix and $\{F(t,x)\}$ is load vector. $\{\ddot{x}\}$ and $\{x\}$ represents system acceleration and system displacement vectors.

Acceleration and velocity are expressed via formulas which are mentioned as follows. These equations solutions allow us to find positions of nodes for the next time step and generate a cycle from beginning to end time.

$$\{\dot{x}_{j+1}\} = \frac{1}{\Delta t}\left[\{x_{j+1}\} - \{x_j\}\right] \tag{3.2}$$

$$\{\ddot{x}_j\} = \frac{1}{2\Delta t}\left[\{\dot{x}_{j+1}\} - \{\dot{x}_{j-1}\}\right] \tag{3.3}$$

where, $\{\dot{x}_{j+1}\}$ is velocity vector of next time step, $\{x_{j+1}\}$ is displacement vector of next time step, $\{x_j\}$ is displacement vector of current time step and Δt is time step increment. Also $\{\ddot{x}_j\}$ is acceleration vector of current time step, $\{\dot{x}_{j+1}\}$ is velocity vector of next time step, $\{\dot{x}_{j-1}\}$ is velocity vector of previous time step.

Time increment is mostly calculated by solvers depending on element characteristic dimensions and sound wave speed which are associated with element types and sizes. Mostly solvers provide a stability time step factor to allow users to decrease this time step. For example this factor in LS-Dyna is already set 0.9 by default.

3.4 Mass, Momentum and Energy Conversation

Three basic equations including conversation of mass, momentum and energy are solved in Lagrange coordinates.

Conversation of mass is automatically satisfied. The mesh moves and distorts depending on material model, initial boundary conditions and forces, so density can be always calculated by initial mass and current volume.

$$\rho = \frac{\rho_0 V_0}{V} = \frac{m}{V} \tag{3.4}$$

where ρ is density at any time, ρ_0 is initial density, $V_0$is initial volume, V is volume at any time and m is mass.

Conversation of momentum is satisfied by the equation as shown below. These partial differential equations of stress tensor σ_{ij}, can be expressed by acceleration.

$$\rho\ddot{x} = \frac{\partial \sigma_{xx}}{\partial x} + \frac{\partial \sigma_{xy}}{\partial y} + \frac{\partial \sigma_{xz}}{\partial z} \tag{3.5}$$

$$\rho\ddot{y} = \frac{\partial \sigma_{yx}}{\partial x} + \frac{\partial \sigma_{yy}}{\partial y} + \frac{\partial \sigma_{yz}}{\partial z} \tag{3.6}$$

$$\rho\ddot{z} = \frac{\partial \sigma_{zx}}{\partial x} + \frac{\partial \sigma_{zy}}{\partial y} + \frac{\partial \sigma_{zz}}{\partial z} \tag{3.7}$$

Energy conversation equation is shown below. The pressure p has two variables as density ρ and specific internal energy e and these variables form an equation of state.

$$p = f(\rho, e) \tag{3.8}$$

This equation must be solved with conversation of energy.

$$\rho\dot{e} = \sigma_{xx}\,\dot{\varepsilon}_{xx} + \sigma_{yy}\,\dot{\varepsilon}_{yy} + \sigma_{zz}\,\dot{\varepsilon}_{zz} + 2\sigma_{xy}\,\dot{\varepsilon}_{xy} + 2\sigma_{yz}\,\dot{\varepsilon}_{yz} + 2\sigma_{zx}\,\dot{\varepsilon}_{zx} \tag{3.9}$$

where $\dot{\varepsilon}_{xx}, \dot{\varepsilon}_{yy}, \dot{\varepsilon}_{zz}, \dot{\varepsilon}_{xy}, \dot{\varepsilon}_{yz}, \dot{\varepsilon}_{zx}$ are strain rates. Strain rates can be expressed by velocities.

$$\dot{\varepsilon}_{xx} = \frac{\partial \dot{x}}{\partial x} \qquad \dot{\varepsilon}_{yy} = \frac{\partial \dot{y}}{\partial y} \qquad \dot{\varepsilon}_{zz} = \frac{\partial \dot{z}}{\partial z} \tag{3.10}$$

$$2\dot{\varepsilon}_{xy} = \frac{\partial \dot{x}}{\partial y} + \frac{\partial \dot{y}}{\partial x} \qquad 2\dot{\varepsilon}_{yz} = \frac{\partial \dot{y}}{\partial z} + \frac{\partial \dot{z}}{\partial y} \qquad 2\dot{\varepsilon}_{zx} = \frac{\partial \dot{z}}{\partial x} + \frac{\partial \dot{x}}{\partial z} \tag{3.11}$$

Steps of Lagrangian computation cycle can be discretized which are shown in Figure 3.4.

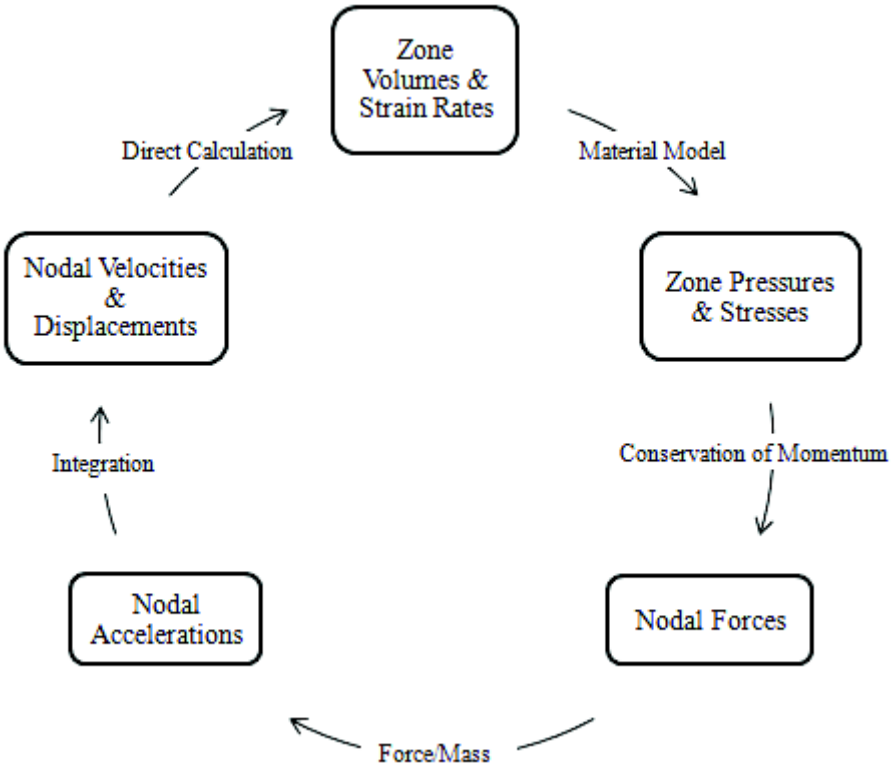


Figure 3.4 Schematic illustration of Lagrangian computation cycle (Deniz, 2010)

3.5 Penetration Mechanisms on Composite Plates

During high velocity impact on composites, penetration mechanism can be divided into three major categories (Figure 3.5).

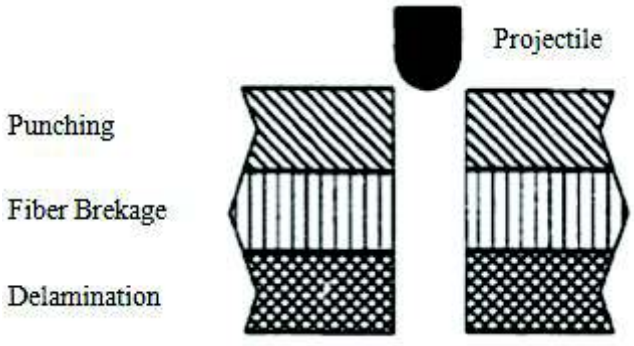


Figure 3.5 Penetration damage mechanism during impact (Hoof, 1999)

- **Punching:** This phase includes projectile' s first touch to composite. While projectile hits, compression occurs and through thickness shear stresses damage composite and punching occurs (Figure 3.6).

- **Fiber breakage:** In this phase, progress of projectile continues, tension on fibers occurs and tensile stress failure may be seen if stresses exceed limits of composite tensile strength (Figure 3.6).

- **Delamination:** This phase is one of the most important composite engineering mechanism and investigated by engineers over last years. This mechanism may be modeled by stress based or fracture mechanics theories (Hoof, 1999). In this phase, after tensile failure of fibers, interlaminar shear and interlaminar normal stresses cause delamination growth (Figure 3.6).



Figure 3.6 Principal damage modes (Hoof, 1999)

3.6 Material Models for Composite Materials in Numerical Simulations

MAT 22 (Mat_Composite_Damage) which is also known as Chang-Chang failure model and MAT 59 material model (Mat_Composite_Failure_Solid_Model) were preferred for modeling composite failure in numerical simulations.

Corresponding relationships for Chang-Chang composite failure model are as follows (Hallquist, 2006). When any corresponding failure criteria exceed 1, it is considered that this element is failed for this mode.

- Longitudinal tension :

$$\left(\frac{\sigma_1}{X_t}\right)^2 + \bar{\tau} > 1, \quad \sigma_1 > 0 \tag{3.12}$$

- Transverse tension :

$$\left(\frac{\sigma_2}{Y_t}\right)^2 + \bar{\tau} > 1, \quad \sigma_1 > 0 \tag{3.13}$$

- Transverse compression :

$$\left(\frac{\sigma_2}{2S_{12}}\right)^2 + \left[\left(\frac{Y_c}{2S_{12}}\right)^2 - 1\right]\frac{\sigma_2}{Y_c} + \bar{\tau} > 1 \tag{3.14}$$

where, σ_1 is stress in fiber direction, X_t is longitudinal tensile strength, $\bar{\tau}$ is fiber matrix shearing term, σ_2 is stress in matrix direction, Y_t is transverse tensile strength, S_{12} is in-plane shear strength and Y_c is transverse compressive strength.

$$\bar{\tau} = \frac{\frac{{\tau_{12}}^2}{2G_{12}} + \frac{3}{4}\,\alpha{\tau_{12}}^4}{\frac{{S_{12}}^2}{2G_{12}} + \frac{3}{4}\,\alpha{\tau_{12}}^4} \tag{3.15}$$

where, τ_{12} is in-plane shear stress, G_{12} is in-plane shear modulus and α is nonlinear shear stress parameter. In plane stress-strain relationships are as follows.

$$\varepsilon_1 = \frac{1}{E_1}\,(\sigma_1 - \nu_{12}\,\sigma_2) \tag{3.16}$$

$$\varepsilon_2 = \frac{1}{E_2}\,(\sigma_2 - \nu_{12}\,\sigma_1) \tag{3.17}$$

$$\varepsilon_{12} = \frac{\tau_{12}}{2G_{12}} + \frac{\alpha{\tau_{12}}^3}{2} \tag{3.18}$$

where, ε_1 is strain in fiber direction, ν_{12} is Poisson's ratio, ε_2 is strain in matrix direction and ε_{12} is shear strain. If index 2 is replaced by 3 in any above criteria, failure theories are applied for the plane 1-3 (Sevkat et al, 2009).

Corresponding relationships for MAT 59 are as follows. When any corresponding failure criteria exceed 1, it is considered that this element is failed for this mode (Davis, 2012).

- Longitudinal tension :

$$\frac{{\sigma_1}^2}{{X_t}^2} + \frac{{\tau_{12}}^2}{{S_{12}}^2} + \frac{{\tau_{31}}^2}{{S_{31}}^2} > 1, \quad \sigma_1 > 0 \tag{3.19}$$

- Transverse tension (with longitudinal tension) :

$$\frac{{\sigma_2}^2}{{Y_t}^2} + \frac{{\tau_{12}}^2}{{S_{12}}^2} + \frac{{\tau_{23}}^2}{{S_{23}}^2} > 1, \quad \sigma_2 > 0 \tag{3.20}$$

- Through-thickness shear :

$$\frac{{\sigma_1}^2}{{X_t}^2} + \frac{{\tau_{31}}^2}{{S_{31}}^2} > 1, \quad \sigma_1 > 0 \tag{3.21}$$

- Through-thickness tension (delamination) :

$$\frac{{\sigma_3}^2}{{Z_t}^2} + \frac{{\tau_{23}}^2}{{S_{23}}^2} + \frac{{\tau_{31}}^2}{{S_{31}}^2} > 1, \quad \sigma_3 > 0 \tag{3.22}$$

- Through-thickness shear (with transverse tension) :

$$\frac{{\sigma_2}^2}{{Y_t}^2} + \frac{{\tau_{23}}^2}{{S_{23}}^2} > 1, \quad \sigma_2 > 0 \tag{3.23}$$

- Longitudinal compression :

$$\frac{{\sigma_1}^2}{{X_c}^2} > 1, \quad \sigma_1 < 0 \tag{3.24}$$

- Transverse compression :

$$\frac{{\sigma_2}^2}{(S_{12}+S_{23})^2} + \frac{\sigma_2}{Y_c}\left[\left(\frac{{Y_c}^2}{(S_{12}+S_{23})^2}\right) - 1\right] + \frac{{\tau_{12}}^2}{{S_{12}}^2} + \frac{{\tau_{31}}^2}{{S_{31}}^2} > 1, \quad \sigma_2 < 0 \tag{3.25}$$

- Through-thickness compression :

$$\frac{{\sigma_3}^2}{(S_{31}+S_{23})^2}+\frac{\sigma_3}{Z_c}\left[\left(\frac{{Z_c}^2}{(S_{31}+S_{23})^2}\right)-1\right]+\frac{{\tau_{31}}^2}{{S_{31}}^2}+\frac{{\tau_{23}}^2}{{S_{23}}^2}>1,\ \ \sigma_3<0 \qquad (3.26)$$

where, X_t is longitudinal tensile strength, τ_{12} is in-plane shear stress, τ_{23} and τ_{31} are transverse shear stresses, S_{12} is in-plane shear strength, S_{31} and S_{23} are transverse shear strengths, Y_t is transverse tensile strength, Z_t is normal tensile strength, X_c is longitudinal compressive strength, Y_c is transverse compressive strength and Z_c is normal compressive strength.

3.7 Delamination Modeling

As we know, several approaches are used for delamination modeling in numerical and analytical techniques. Delamination modeling is one of the major topics in composites and has been studied for many years. In this study, stress-based failure model which predicts delamination initiation was used. This approach is based on strength of materials approach.

This model theory is expressed as follows. This criterion depends on normal and shear strength values on layer interfaces. In LS-Dyna, this approach is reflected by contact tie-break option.

$$\left(\frac{\sigma_n}{S_n}\right)^2+\left(\frac{\sigma_s}{S_s}\right)^2\geq 1 \qquad (3.27)$$

where S_n is inter-laminar tension strength, S_s is inter-laminar shear strength.

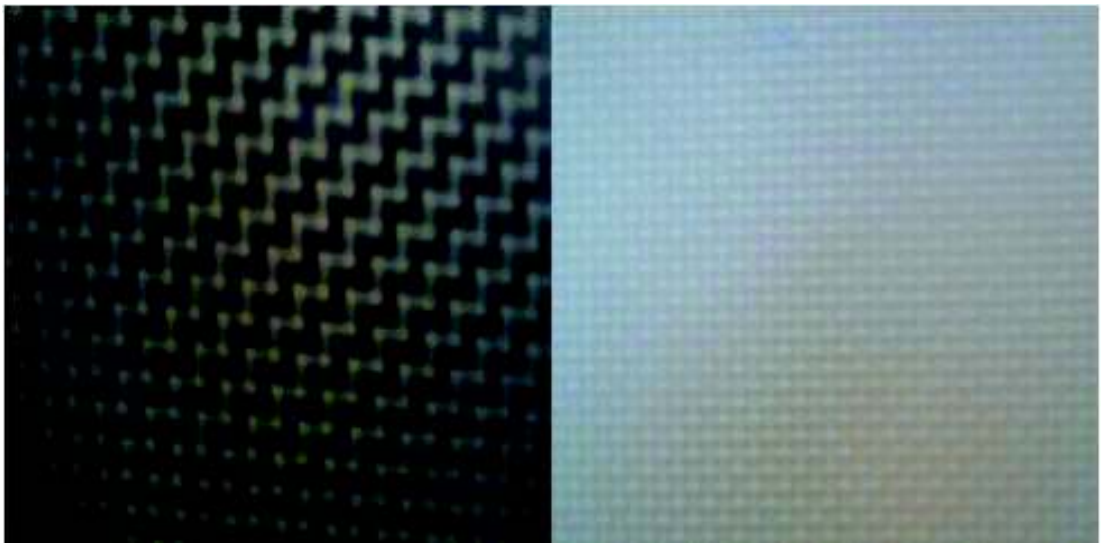
In this equation, when critical stress values are met, delamination occurs.

CHAPTER FOUR

MANUFACTURING PROCESS, MECHANICAL PROPERTIES OF COMPOSITE MATERIALS AND EXPERIMENTAL PROCEDURE

4.1 Manufacturing Steps

Vacuum assisted resin infusion molding technique was used for manufacturing specimens. Carbon-aramid fabrics have relatively thinner thickness so aramid fabrics were cut as 15 layers and carbon-aramid fabrics were cut as 38 layers to achieve desired thickness (Figure 4.1). These reinforcements have different properties, relatively (Table 4.1).



(a) (b)

Figure 4.1 Weave styles of fabrics, (a) carbon-aramid (b) aramid

Table 4.1 Properties of reinforcements

	Aramid	Carbon-aramid
Areal density (g/m^2)	410	210
Weave style	Plain	Twill

Second process is placement of fabrics on the tool geometry. Reinforcements were placed well and vacuum bag was prepared (Figure 4.2). Here one of the most

important things is disconnecting air relation with fabrics. So a good bonding was provided.

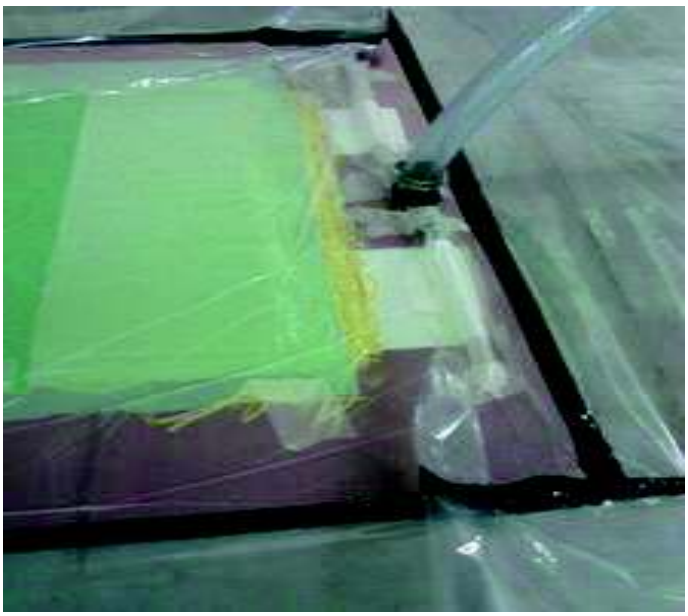


Figure 4.2 Lamination process

After placement of reinforcements, vacuum started and aim was to empty air from inside of bag to outside. Change of pressure was observed by pressure gage. After constant pressure was seen, setup was ready for injection of resin (Figure 4.3).



Figure 4.3 Before resin infusion process

After the vacuum pulled bag down, epoxy infusion was started. Epoxy was prepared with an appropriate hardener. Progression of resin can be seen in Figure 4.4.

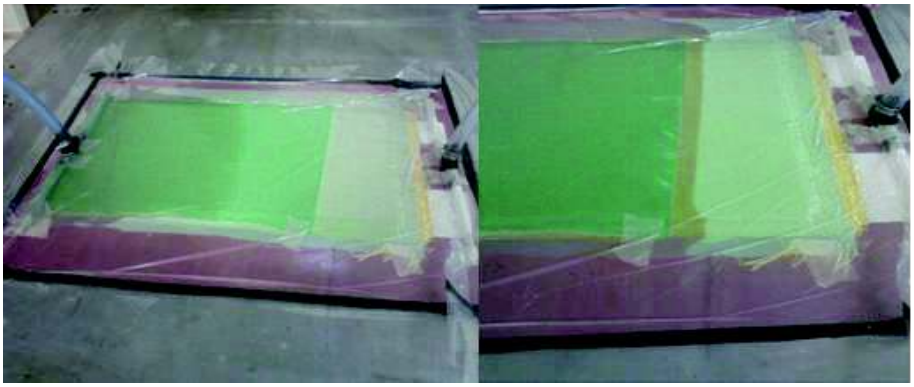


Figure 4.4 Resin progression

Curing process continued for 8 hours at 80 ^{0}C after resin infusion. Steps for composite manufacturing were finished once curing was performed.

Lastly, excessive region of specimens were cut by water jet. Water jet is a capable tool which is used for cutting variety of materials. While cutting is performed, tool uses high pressure water. The tool has advantage over conventional cutting processes which use heat, that there is no heat affected zone. This technique overcomes edge cracks, burrs and delamination, provides better finish quality also has high cutting velocity. After cutting process, desired specimens were obtained (Figure 4.5). Properties of composite materials can be seen in Table 4.2.

Table 4.2 Properties of composite materials

	Aramid composite	Carbon-aramid composite
Resin	Epoxy	Epoxy
Weight	905 g	930 g
In-plane dimensions (mm)	300*300 mm	300*300 mm
Thickness (mm)	9 mm	9 mm

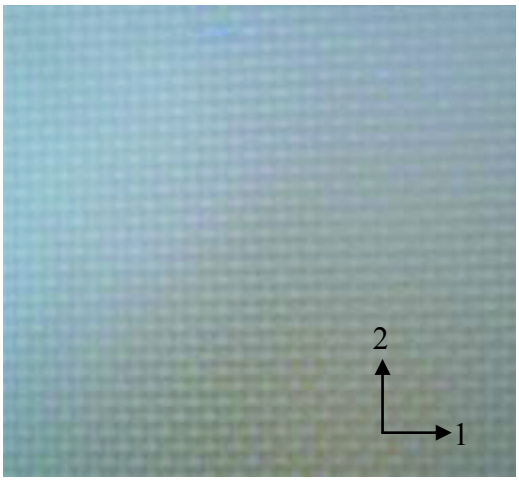


Figure 4.5 Composite material with material directions

4.2 Mechanical Properties of Composite Materials

Fiber reinforced composite materials are orthotropic materials which generally show different characteristics in fiber, matrix and through thickness direction. These characteristics may depend on fiber material, matrix material, fiber orientation etc.

For obtaining behaviors of composites, Shimadzu AG-X test machine was used (Figure 4.6). Strength values were obtained under static conditions. Different apparatus configurations were used for shear, tension and compression strength values.

These strength values are going to guide us before performing numerical simulation. So these values need to be accurately measured. For theoretical, despite linear brittle theory was used in numerical simulation, obtaining failure strains were also important for representing erosion cards in LS-Dyna. After tests, corresponding equations were used for measuring mechanical properties by ASTM standards.



Figure 4.6 Shimadzu AG-X tensile testing machine

$$\sigma_1 = \frac{P}{A} \qquad E_1 = \frac{\sigma_1}{\varepsilon_1} \qquad \nu_{12} = -\frac{\varepsilon_2}{\varepsilon_1} \tag{4.1}$$

where, σ_1 is stress in fiber direction, P is force and A is cross-sectional area perpendicular to fiber direction. E_1 is elasticity modulus in fiber direction, ε_1 is strain in fiber direction. ε_2 is strain perpendicular to fiber direction and ν_{12} is Poisson' s ratio.

$$X_t = \frac{P_{max}}{A} \qquad X_c = \frac{P_{max}}{A} \tag{4.2}$$

where, X_t is tensile strength in fiber direction, X_c is compression strength of composite material in transverse direction and P_{max} is load capacity of composite in fiber direction or transverse direction.

$$\tau_{12} = \frac{P}{A} \qquad G_{12} = \frac{\tau_{12}}{\gamma_{12}} \tag{4.3}$$

where, $\tau_{12}$is shear stress and G_{12} is shear modulus.

For finding shear strength S_{12}, V-notched shear tests were performed. For performing this test, corresponding specimens were prepared (Figure 4.7).

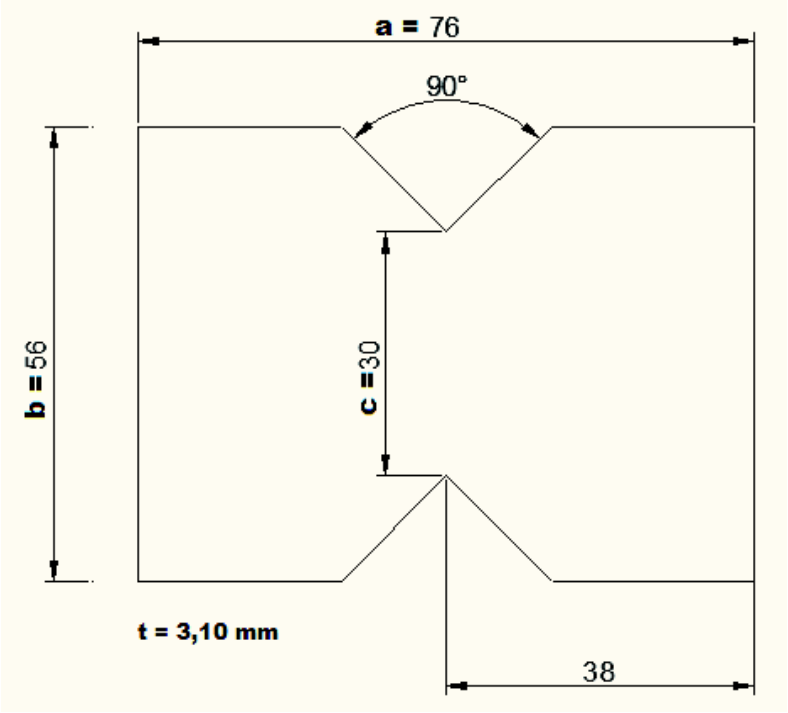


Figure 4.7 Schematic illustration of V-notched shear test specimen (Öğrenci, 2012)

$$S_{12} = \frac{P_{max}}{t.c} \tag{4.4}$$

where, S_{12} is shear strength, t is thickness and c distance between notches.

These tests were also performed in direction 2. Because of weave style of composite materials, close results were found in direction 1 and direction 2 and approaches were made as follows (Table 4.3).

$$E_1 = E_2 \qquad X_t = Y_t \qquad X_c = Y_c \tag{4.5}$$

Table 4.3 Mechanical properties of composite materials

	Aramid/epoxy	Carbon-aramid/epoxy
E_1 (MPa)	17230	47700
E_2 (MPa)	17230	47700
X_t (MPa)	425	552
X_c (MPa)	88	273
Y_t (MPa)	425	552
Y_c (MPa)	88	273
G_{12} (MPa)	5510	2345
S_{12} (MPa)	66	2345
ν_{12}	0.2	0.1

4.3 Experimental Procedure

4.3.1 Ballistic Setup

Test setup contains a gun barrel which is capable of 7.62 x 51 mm projectile shoot. This setup has also a laser system, so projectile velocities before impact were measured by this system.

Residual velocities were measured by velocity traps and oscilloscope. After the projectile hits the specimen and perforation occurs, time is calculated by oscilloscope between velocity traps and velocity of projectile can be calculated by distance and time (Figure 4.8).

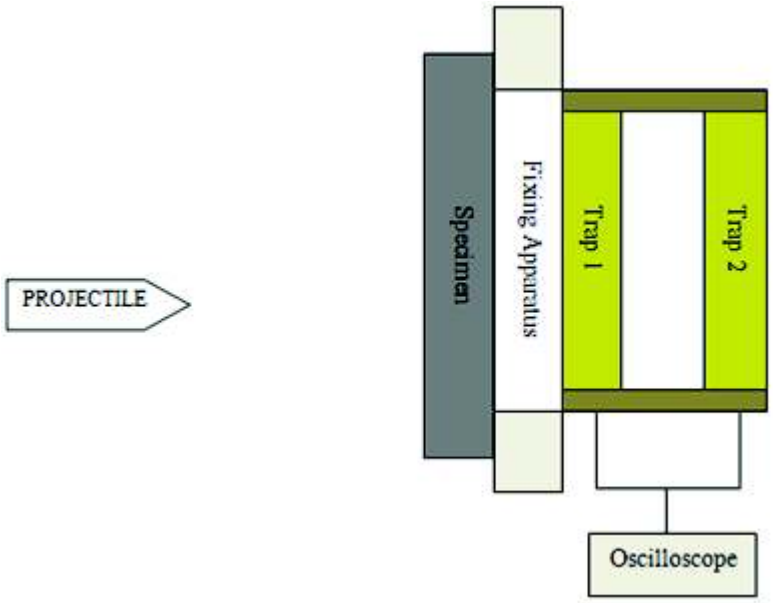


Figure 4.8 Schematic illustration of experimental setup

Ballistic tests were performed with six different velocities (Table 4.4).

Table 4.4 Initial velocities of projectiles for ballistic tests

	Aramid/epoxy	Carbon-aramid/epoxy
Projectile initial velocity 1 (m/s)	852	850
Projectile initial velocity 2 (m/s)	790	841
Projectile initial velocity 3 (m/s)	713	764
Projectile initial velocity 4 (m/s)	619	652
Projectile initial velocity 5 (m/s)	543	540
Projectile initial velocity 6 (m/s)	333	381

4.3.2 Properties of Projectile

7.62 x 51 mm M61 type AP projectiles were used for experimental tests. These projectiles consist of base filler, core and jacket. Penetrating mass is called as core and jacket protects core during firing of the barrel (Figure 4.9). Properties of this type o projectile can be seen in Table 4.5.

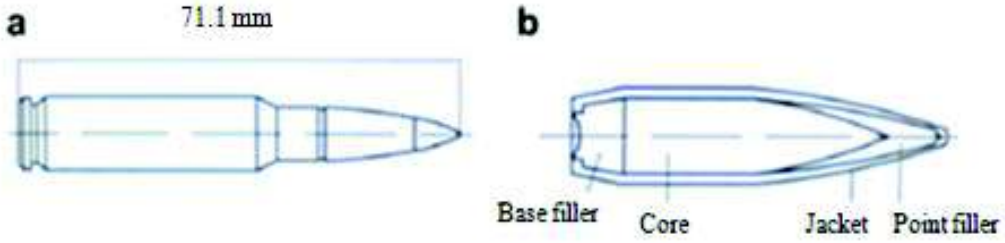


Figure 4.9 7.62 mm AP projectile (a) cartridge (b) cross-sectional view of projectile (Demir, Übeyli, & Yıldırım, 2008)

Table 4.5 Some properties of 7.62 mm AP projectile (Demir et al., 2008)

Type	Property
Cartridge length	71.12 ± 0.76 mm
Cartridge weight	25.47 ± 1.75 g
Case material	7.62 x 51 mm Brass (CuZn30)
Core material	DIN 100Cr6 (HRC 61-62)
Bullet weight	9.75 ± 0.1 g
Length of bullet	32.95 mm
Nose angle	Conical (cone half angle, $\alpha = 17^{o}$)

CHAPTER FIVE

BALLISTIC IMPACT SIMULATION PROCEDURE

5.1 Modeling Details

In this study, two type of composite materials and projectile system simulated by initial velocity conditions, residual velocities were observed and compared with experimental data.

LS-Dyna 3D was used for solving these simulations. Lagrangian approach was preferred because of the advantage of saving computational time. Solid modeling technique was preferred (Figure 5.2).

Three different numerical models were created which were combination of MAT 22 and layered composite which was modeled as solid plies, MAT 59 with a layered composite which was modeled as solid plies and MAT 59 with single layer. Layered modeling technique was preferred because of weave style of composites. MAT 59 with single layer modeling was also simulated because in-plane strengths are the same so only compression failure criteria are different from layered composite but with layer modeling and single layer modeling, differences may be observed on stiffness because of multiple layers. For modeling interaction of plies, contact with tie-break option was used between composite layers.

After considering boundary conditions, it is apparent that composite and projectile have two symmetry planes (Figure 5.1). Because of symmetry planes, 1/4 of model was used for corresponding simulations.

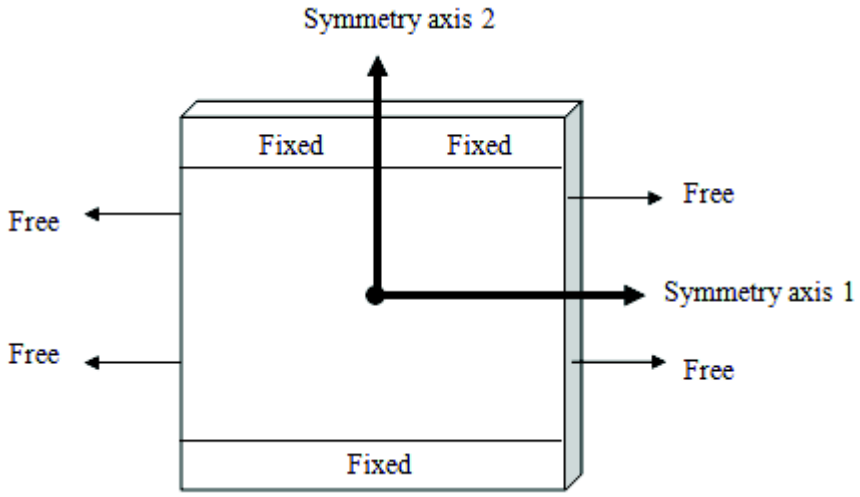


Figure 5.1 Boundary conditions of composite materials

Because of three simulation procedures, two different composite materials and six different velocities, thirty-six analyses were simulated totally.

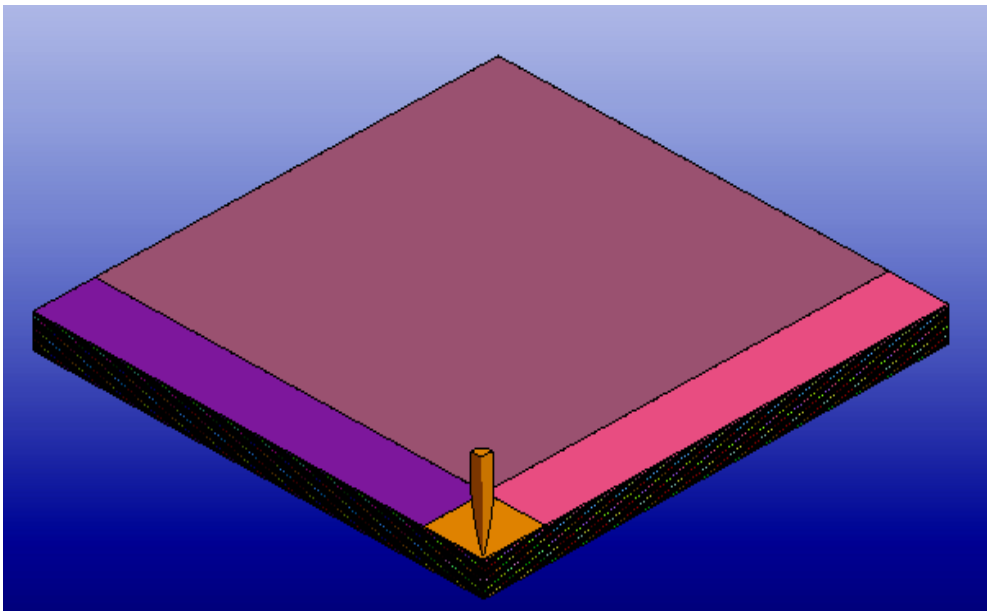


Figure 5.2 Simulation start-up

5.2 Material Models

5.2.1 Material Model of Projectile

Penetration mechanism is occurred by effects of hardened inner core so only core of the projectile was modeled. It was thought that brass and filler had negligible effects before simulation.

It is known that core has higher strength than composites, core was considered as rigid striker and it was thought no plastic deformation on core. For this reason, MAT 20 (Mat_Rigid) was used for modeling core material. Mechanical properties of core material are given in Table 5.1.

Table 5.1 Mechanical properties of core material (Fawaz et al, 2003)

	ρ (kg/m^3)	E (GPa)	ν
Steel core	7890	202	0.3

5.2.2 Material Models of Composite Materials

Corresponding material mechanical properties are shown as follows for MAT 59. In Mat 22 for both composites, nonlinear shear stress term α = 0 was used and it was considered linear brittle behavior.

For through-thickness mechanical properties of composite materials, it was assumed to be 0.6 times of in-plane mechanical properties (Table 5.2).

After failure occurs in elements for Lagrangian approach in LS-Dyna, erosion cards must be used for element erosion. MAT 00 (Mat_Add_Erosion) card was used for providing element erosion. These values were obtained from stress-strain curves, for aramid/epoxy composite, $\varepsilon_{mxp.}$= 0.048, $\varepsilon_{mnp.}$= -0.004 and $\varepsilon_{sh.}$ = 0.14 for carbon-aramid/epoxy composite $\varepsilon_{mxp.}$= 0.014, $\varepsilon_{mnp.}$= -0.005 and $\varepsilon_{sh.}$ = 0.095 were used.

Table 5.2 Used values in simulations for composite materials

	Aramid/epoxy	Carbon-aramid/epoxy
ρ (kg/m^3)	1117	1148
E_1 (MPa)	17230	47700
E_2 (MPa)	17230	47700
E_3 (MPa)	10338	28620
X_t (MPa)	425	552
X_c (MPa)	88	273
Y_t (MPa)	425	552
Y_c (MPa)	88	273
Z_t (MPa)	255	331
Z_c (MPa)	53	164
G_{12} (MPa)	5510	2345
G_{23} (MPa)	3300	1407
G_{32} (MPa)	3300	1407
S_{12} (MPa)	66	82
S_{23} (MPa)	40	49
S_{31} (MPa)	40	49
ν_{12}	0.2	0.1
ν_{23}	0.12	0.06
ν_{31}	0.12	0.06

5.3 Geometries

5.3.1 Projectile Geometry

Because of two symmetry boundary conditions of simulations, 1/4 of projectile was modeled (Figure 5.3).

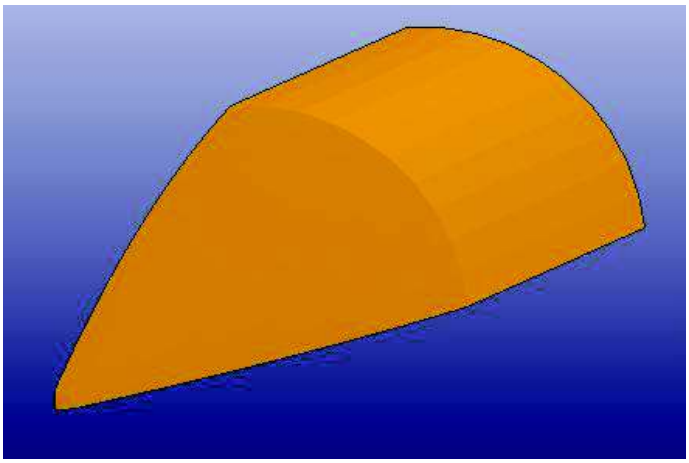


Figure 5.3 Projectile geometry

5.3.2 Geometries of Composite Materials

Because of two symmetry boundary conditions of simulations, 1/4 of composite materials were modeled (Figure 5.4).

For providing mesh density, local 20 x 20 mm cutting process was performed but mesh transition was provided between these parts (Figure 5.4).

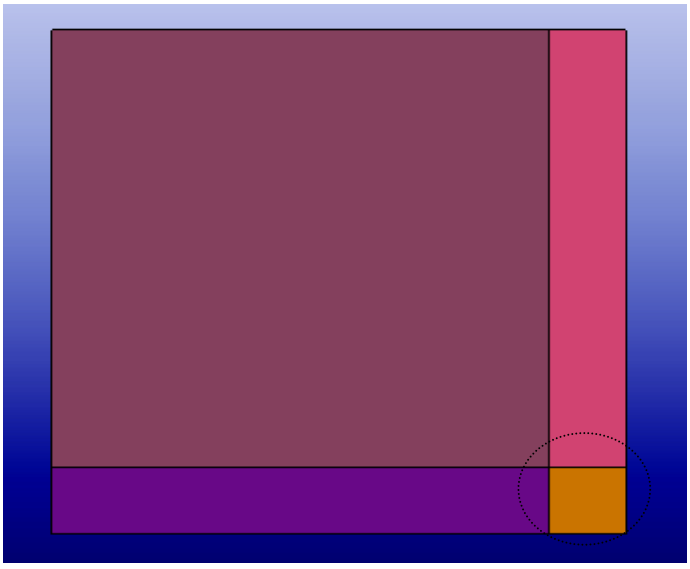
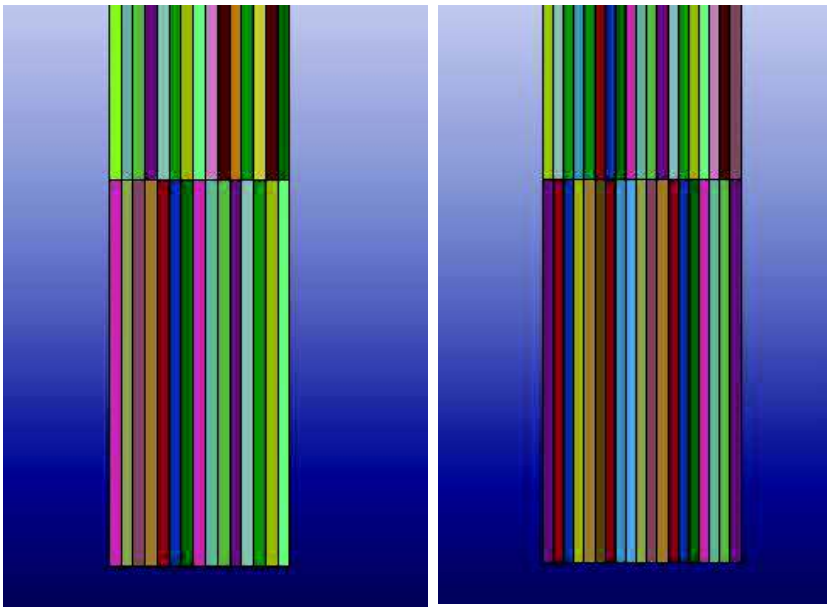


Figure 5.4 Geometry of composite materials

Through-thickness view of layered composite materials and single layer composite is shown in Figure 5.5 and 5.6.



(a) (b)

Figure 5.5 Through-thickness view of layered composite materials (a) aramid (b) carbon-aramid

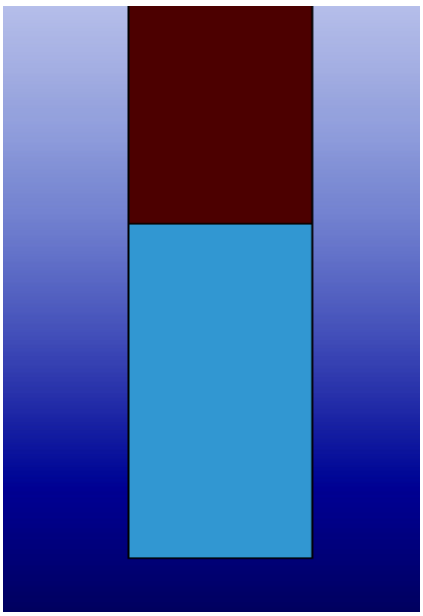


Figure 5.6 Through-thickness view of single layer composite

5.4 Finite Element Models

Eight node hexahedron constant stress solid elements were used for finite element model of projectile and composite materials (Figure 5.7). This element type has single Gaussian integration point and less computational time is an advantage.

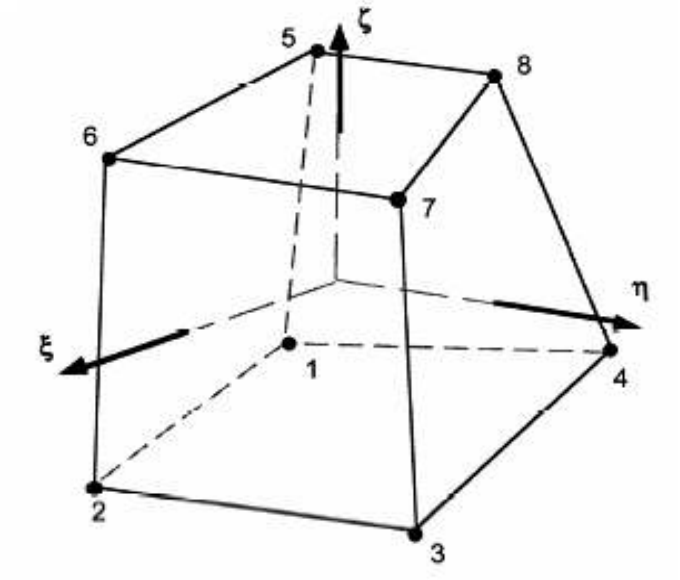


Figure 5.7 Eight node hexahedron solid element (Hallquist, 2006)

5.4.1 Finite Element Model of Projectile

Because of 1/4 model of projectile and rotational symmetry of geometry, fine model could be created for projectile. Front and top views of finite element model of projectile are shown in Figures 5.8-9.

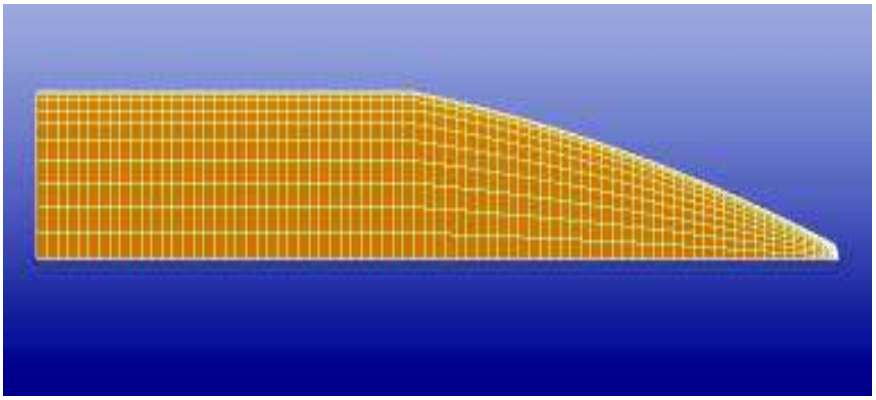


Figure 5.8 Front view of finite element model of projectile

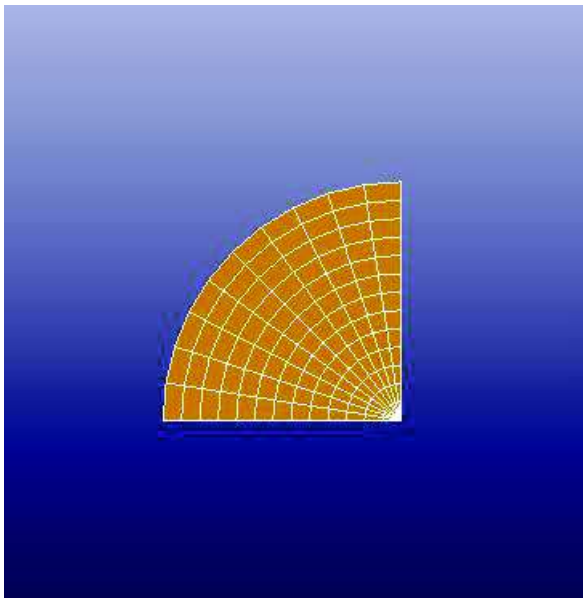


Figure 5.9 Top view of finite element model of projectile

5.4.2 Finite Element Model of Composite Materials

For providing mesh density for the regions which the projectile hits, cutting process was performed and four different parts were created in a single ply. Mesh transition were provided between these parts (Figure 5.10).

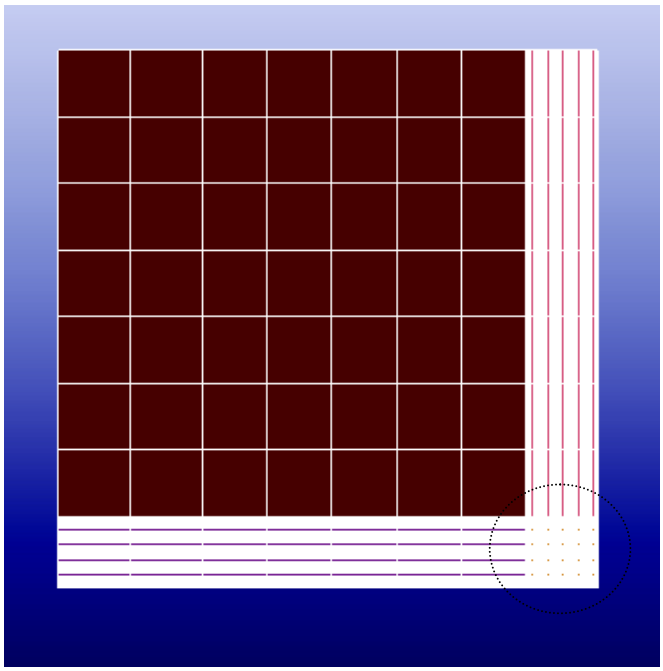


Figure 5.10 Top view of finite element model of composite materials

Because of multi-body part modeling, elements of two regions have poor aspect ratios because of using coarser mesh in order to reduce computational time. Despite regions which have poor aspect ratios, very fine mesh was provided at the desired locations (Figure 5.11).

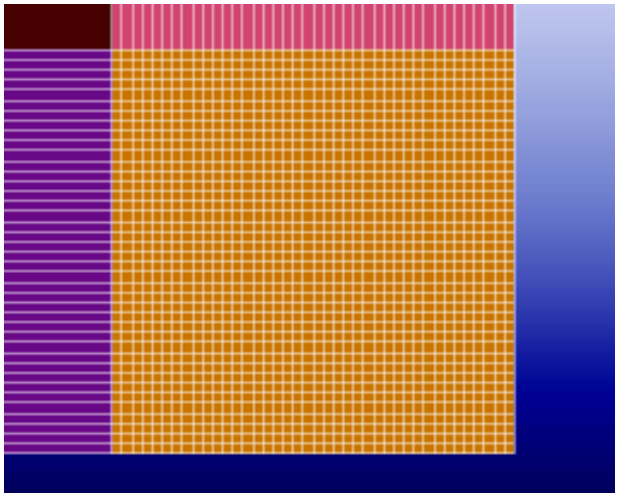
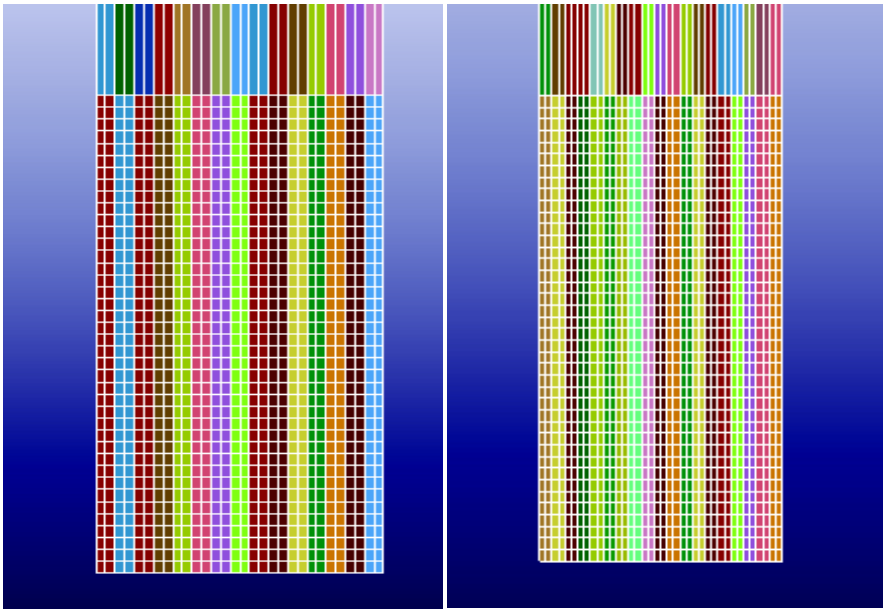


Figure 5.11 Detailed view of fine mesh region

Two elements were used in the thickness direction for a single ply for layered composites (Figure 5.12).



(a) (b)

Figure 5.12 Through-thickness view of layered composite materials (a) aramid (b) carbon-aramid

For single layer composite, same element sizes were preferred in order to reduce mesh dependence of simulations. As it is obvious that with same element sizes, finite element model with same in-plane and through thickness conditions was provided (Figure 5.13).

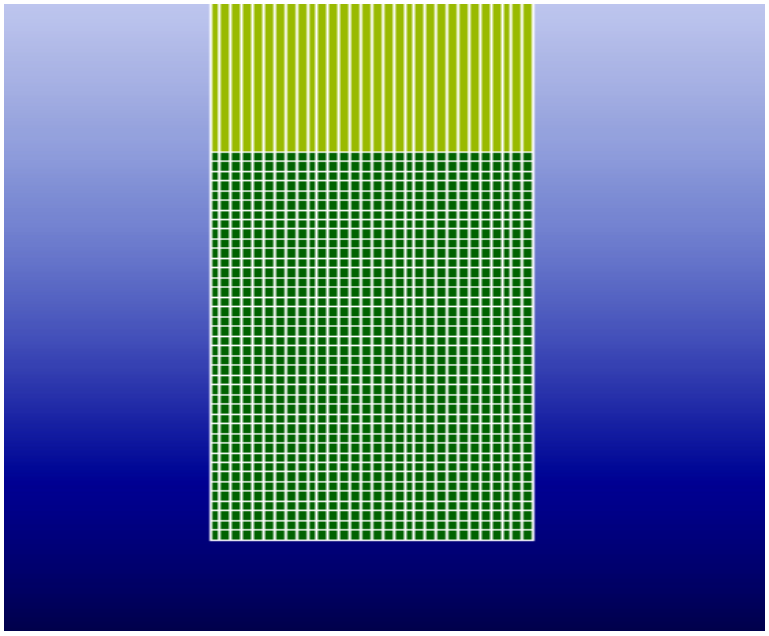


Figure 5.13 Through-thickness view of single layer composite material

5.5 Contact Mechanisms

Interaction of different bodies is reflected by contact cards and LS-Dyna offers many options for reflecting this behavior. Contact algorithms are divided roughly into three categories which are single surface contact, surface to surface contact and node to surface contact.

Contact_Eroding_Surface_To_Surface card was used between projectile and composite plies. This card provides additional advantage by deleting failed elements from the calculations.

Contact_Automatic_One_Way_Surface_To_Surface_Tiebreak card was used between composite plies. This card provides additional advantage by modeling delamination failure criteria between composite plies. When certain criteria are met

depending on stress based approach or fracture mechanics approach, delamination occurs.

5.6 Boundary Conditions and Initial Velocity

Due to long solving times, symmetry boundary conditions were generated in order to reduce computational time. The nodes inside of cut planes were constrained in direction depending on cut plane normal (Figure 5.14).

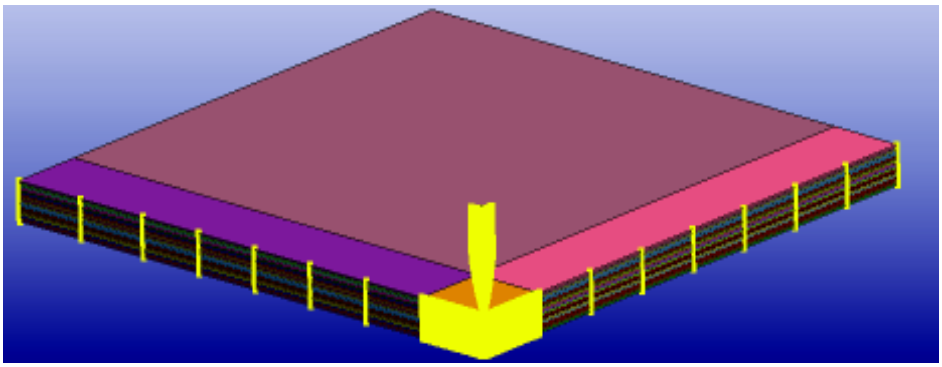


Figure 5.14 Nodes in symmetry boundary conditions

After consideration of test setup, rectangles were drawn with dimensions 150 mm x 40 mm to top and bottom faces of composite materials. All nodes inside of this rectangle were fixed in all directions (Figure 5.15).

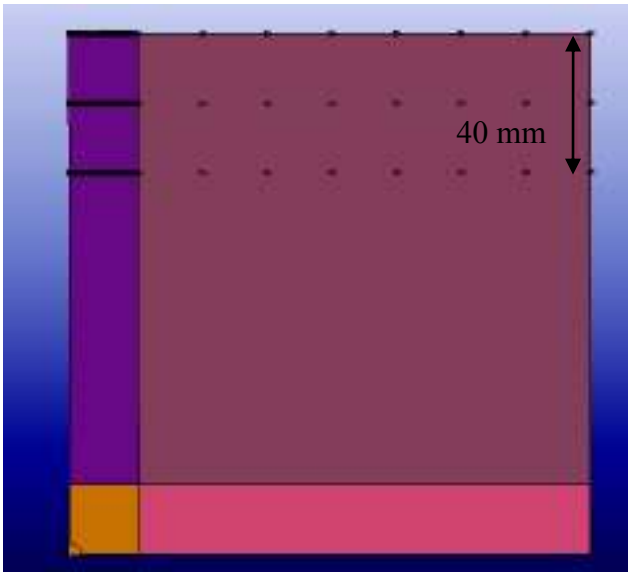


Figure 5.15 Fixing condition

Initial_Velocity_Rigid_Body card was used for providing initial velocity for steel core. After selecting rigid body with this card, it gives velocity to all nodes of body (Figure 5.16).

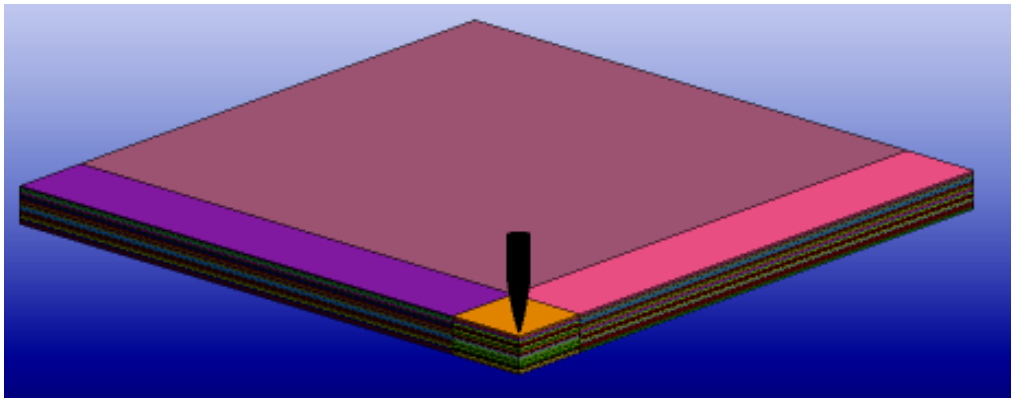


Figure 5.16 Nodes of core subjected to initial velocity

CHAPTER SIX

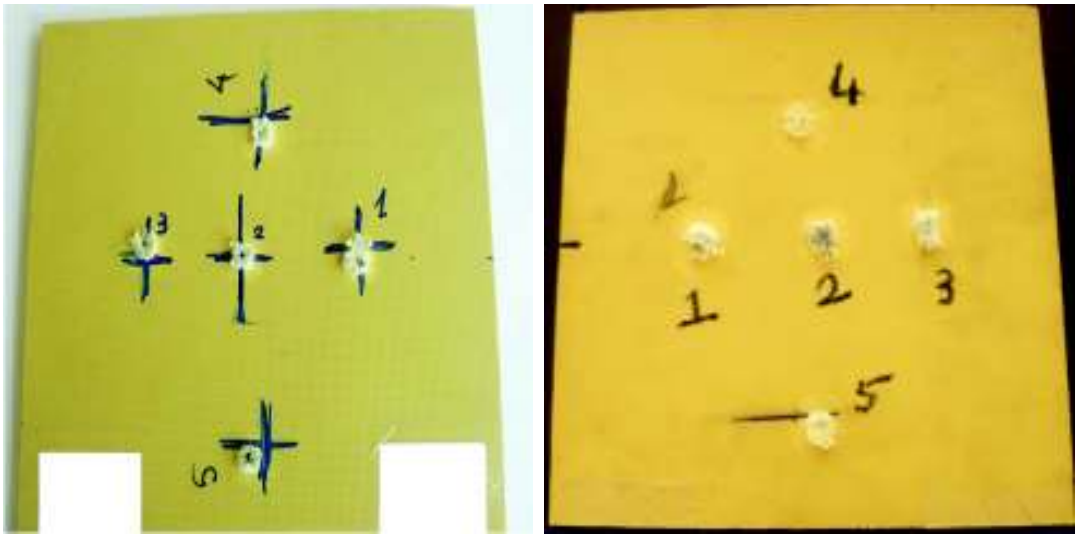
EXPERIMENTAL AND NUMERICAL RESULTS

6.1 Experimental Results

After performing ballistic tests, residual velocities of projectiles were obtained by velocity traps. It is obvious that deformation is very local on composite materials because of projectile impact, multiple shots were made on a layered composite.

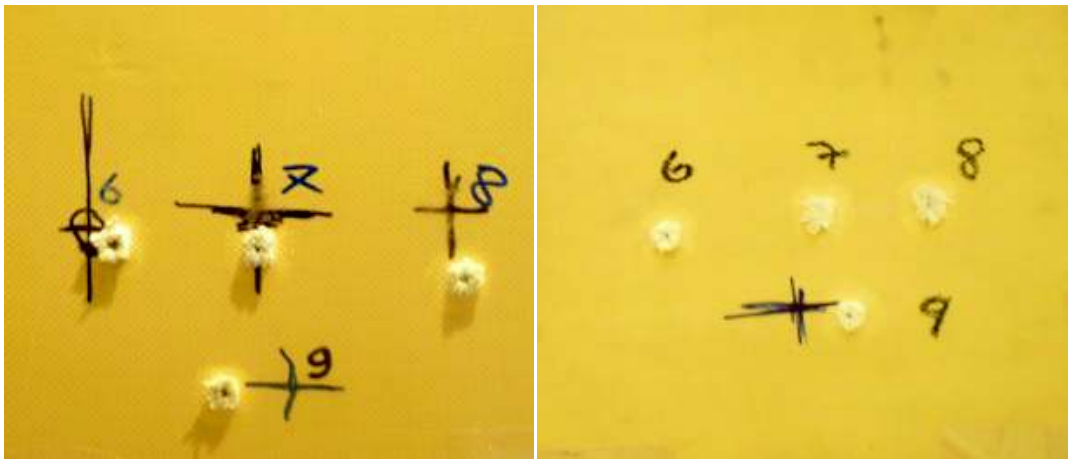
6.1.1 Experimental Results of Aramid/Epoxy Composites

Twelve shots were performed to aramid/epoxy composites (Figure 6.1-3). Some trials were made and time could not be calculated by oscilloscope for one shot. Six initial and residual velocities were obtained during ballistic tests (Table 6.1).



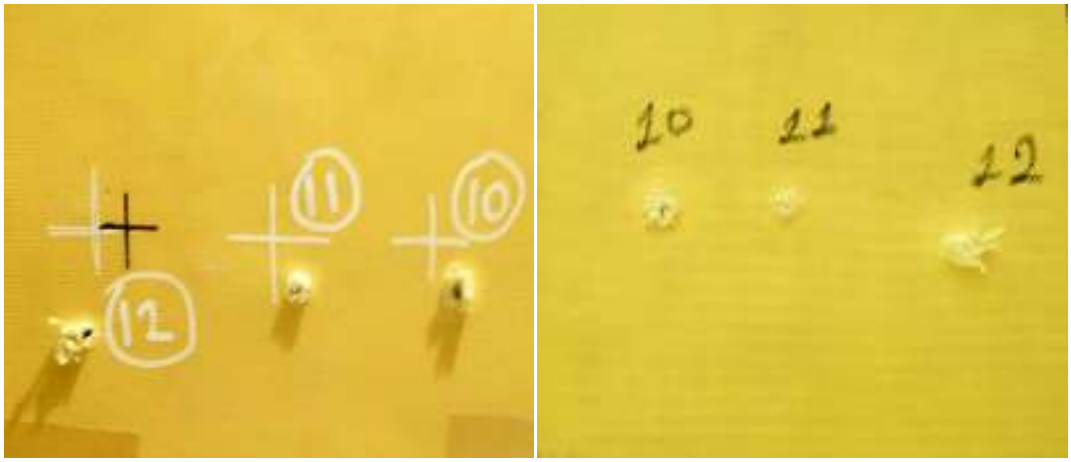
(a) (b)

Figure 6.1 First specimen of aramid/epoxy composite material after ballistic tests (a) front side (b) back side



(a) (b)

Figure 6.2 Second specimen of aramid/epoxy composite material after ballistic tests (a) front side (b) back side



(a) (b)

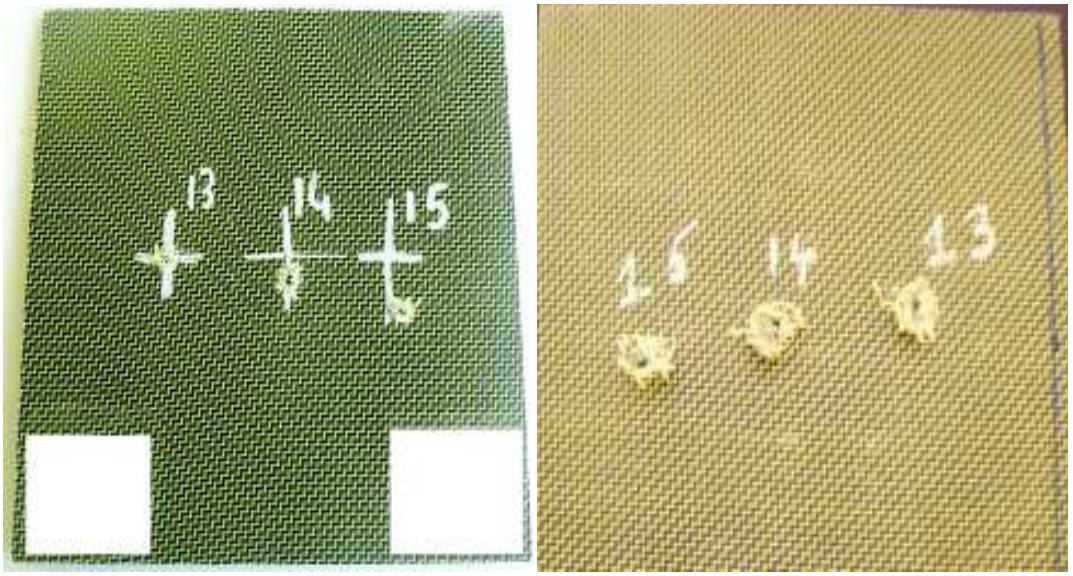
Figure 6.3 Third specimen of aramid/epoxy composite material after ballistic tests (a) front side (b) back side

Table 6.1 Experimental initial and residual velocities of projectile for aramid composites

Shot number	Initial velocity - V_i (m/s)	Residual velocity - V_r (m/s)
3	852	817
5	790	742
7	713	657
8	619	579
9	543	498
10	333	259

6.1.2 Experimental Results of Carbon-Aramid/Epoxy Composites

Six shots were performed to carbon-aramid/epoxy composites (Figure 6.4-5). Six initial and residual velocities were obtained during ballistic tests (Table 6-2).



(a) (b)

Figure 6.4 First specimen of carbon-aramid/epoxy composite material after ballistic tests (a) front side (b) back side



(a) (b)

Figure 6.5 Second specimen of carbon-aramid/epoxy composite material after ballistic tests (a) front side (b) back side

Table 6.2 Experimental initial and residual velocities of projectile for carbon-aramid composites

Shot number	Initial velocity - V_i (m/s)	Residual velocity - V_r (m/s)
17	850	820
13	841	805
14	764	724
15	652	626
16	540	489
18	381	352

Initial velocity versus residual velocity diagram is drawn by using obtained datas and given in Figure 6.6.

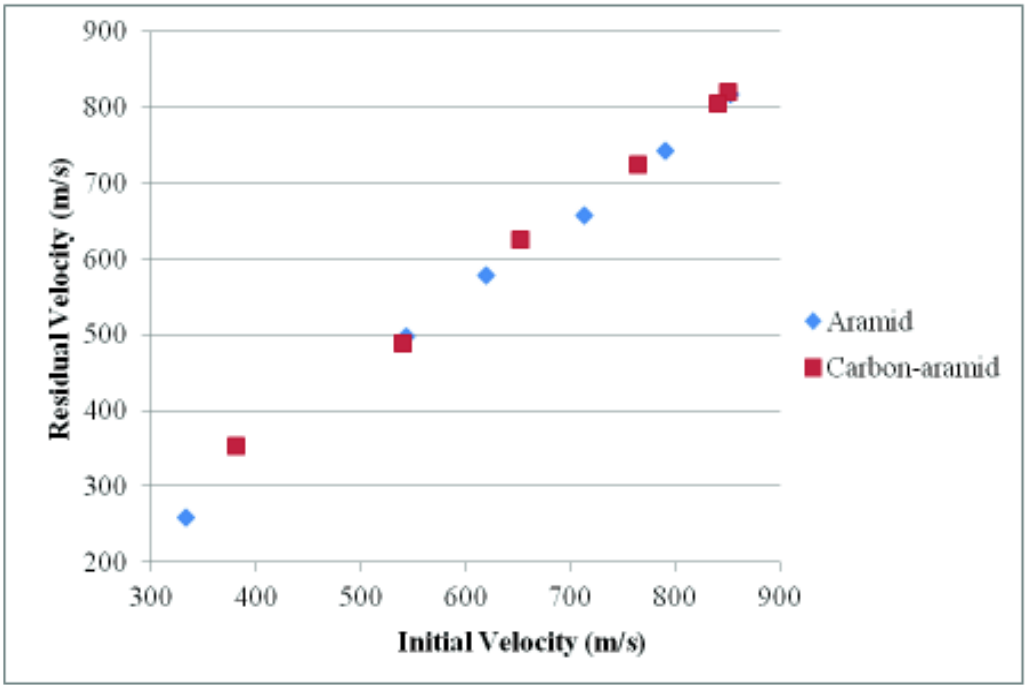


Figure 6.6 Experimental initial vs. residual velocities of projectile for composite materials

6.1.3 Ballistic Limit Velocity

Ballistic limit velocity is the lowest velocity in order to provide total penetration of laminate (Abrate, 2007).

Ballistic limit velocity (V_b) is also known as V_{50} and V_{50} means the velocity which is required to penetrate probability at least 50 % of all tests.

Many approaches were made for calculating ballistic limit velocity based on energies, forces etc.

$$U_i - U_r = U_p \text{ (Abrate, 2007)} \tag{6.1}$$

where, U_i is initial kinetic energy, U_r is residual kinetic energy and U_p is penetration energy.

$$U_i = \frac{1}{2} m_i V_i^2 \tag{6.2}$$

$$U_r = \frac{1}{2} m_r V_r^2 \tag{6.3}$$

where m_i is initial mass of projectile, m_r is residual mass of projectile, V_i is initial velocity of projectile and V_r is residual velocity of projectile.

After projectile is thought to be rigid and $m_i = m_r = m$, also no material loss because of erosion of composite, equations are as follows.

$$U_p = \frac{1}{2} m V_i^2 - \frac{1}{2} m V_r^2 \tag{6.4}$$

$$U_p = \frac{1}{2} m (V_i^2 - V_r^2) \tag{6.5}$$

$$\frac{1}{2} m V_b^2 = \frac{1}{2} m (V_i^2 - V_r^2) \tag{6.6}$$

$$V_b^2 = V_i^2 - V_r^2 \tag{6.7}$$

$$V_b = \sqrt{V_i^2 - V_r^2} \tag{6.8}$$

During finding average ballistic limits for experimental and numerical methods, maximum and minimum values were removed from data set in order to achieve a clearer range. Experimental initial, residual and ballistic limit velocities for aramid/epoxy and carbon-aramid/epoxy composites are given in Table 6.3-4, respectively.

Table 6.3 Experimental initial, residual and ballistic limit velocities for aramid/epoxy composites

Initial velocity V_i (m/s)	Residual velocity V_r (m/s)	Ballistic limit velocity V_b (m/s)
852	817	241.69
790	742	271.17
713	657	276.98
619	579	218.90
543	498	216.43
333	259	209.30
		Average ballistic limit velocity V_b = 237.05 m/s

Table 6.4 Experimental initial, residual and ballistic limit velocities for carbon-aramid/epoxy composites

Initial velocity V_i (m/s)	Residual velocity V_r (m/s)	Ballistic limit velocity V_b (m/s)
850	820	223.83
841	805	243.43
764	724	243.97
652	626	182.29
540	489	229.08
381	353	143.36
		Average ballistic limit velocity V_b = 219.79 m/s

After finding ballistic limit velocities of composite materials, actual function of initial velocity and residual velocity diagram is given in Figure 6.7.

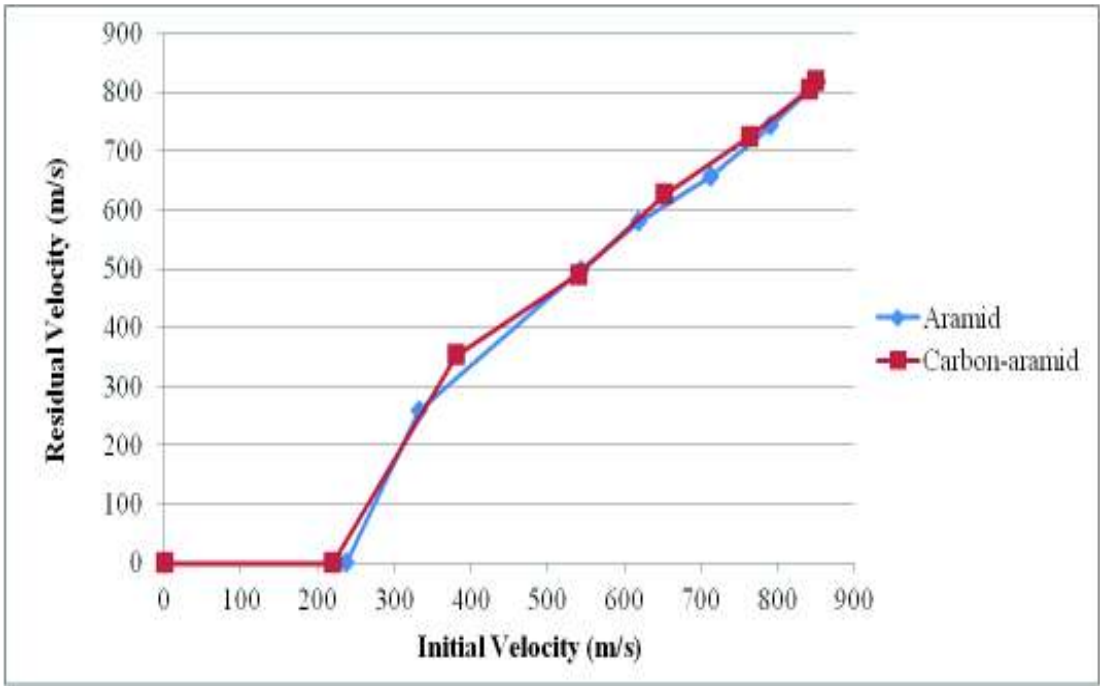


Figure 6.7 Experimental initial vs. residual velocities of projectile including ballistic limit velocity

6.2 Numerical Results

After numerical simulations, perforation was observed in the composites for all velocities.

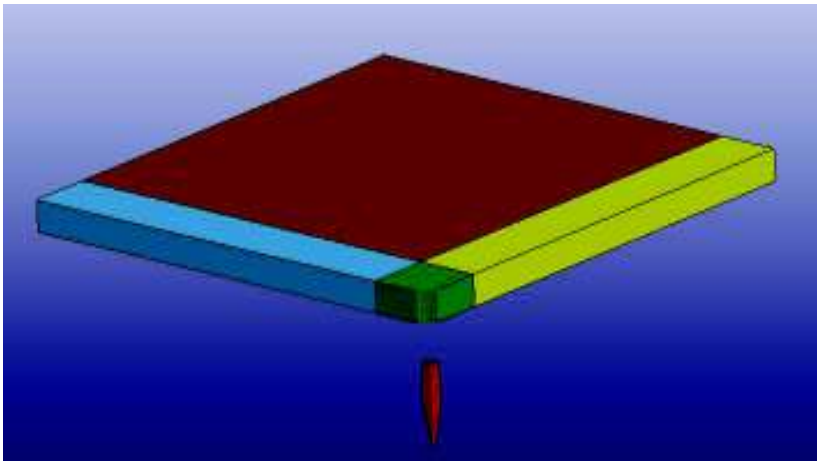
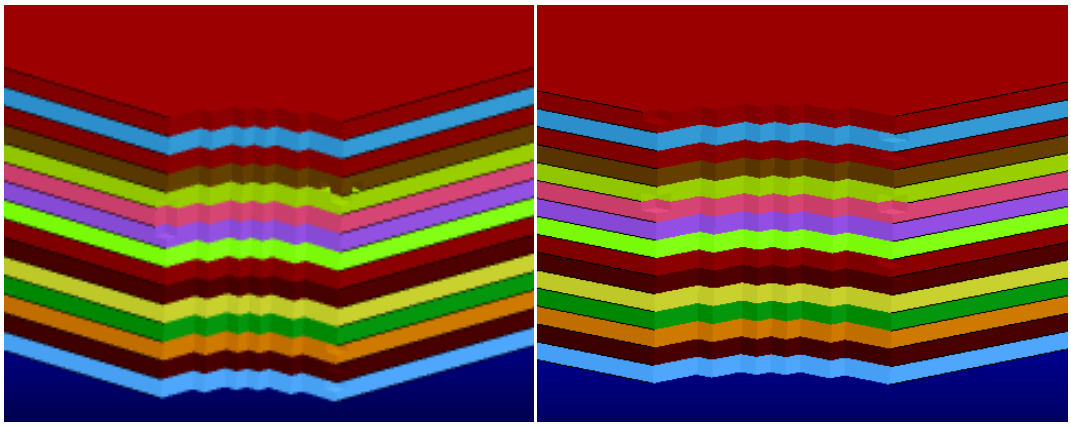


Figure 6.8 A sample of numerical simulation (Single layer aramid/epoxy composite with Mat 59, V_i: 852 m/s)

6.2.1 Numerical Results of Layered Composites with MAT 22

6.2.1.1 Aramid/Epoxy Composite

After performing simulations of layered aramid/epoxy composite with MAT 22, it was seen that diameters of projectile entrance and exit holes were close to each other (Figure 6.9).



(a) (b)

Figure 6.9 Perforation view of layered aramid/epoxy composites with MAT 22 after simulations for initial velocities (a) V_i: 852 m/s (b) V_i: 790 m/s

Velocity versus time curves for layered aramid/epoxy composites with MAT 22 for initial velocities V_i: 852 m/s and V_i: 790 m/s can be seen in Figure 6.10-11. Other detailed results are given in Appendix A.

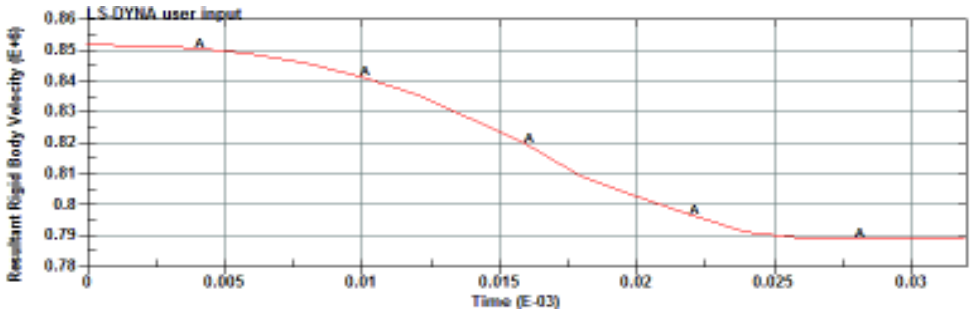


Figure 6.10 Velocity (mm/s) vs. time (s) curve of layered aramid/epoxy composite with MAT 22 for initial velocity V_i: 852 m/s

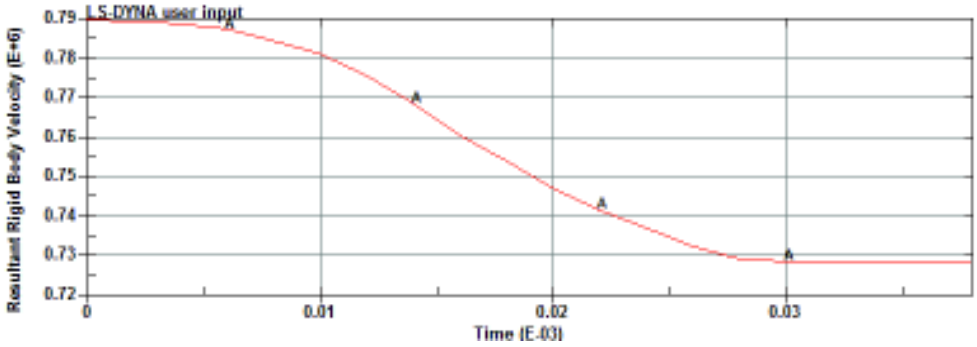


Figure 6.11 Velocity (mm/s) vs. time (s) curve of layered aramid/epoxy composite with MAT 22 for initial velocity V_i: 790 m/s

Initial velocity versus residual velocity diagram of layered aramid/epoxy composite with MAT 22 is drawn by using obtained data from simulations and shown in Figure 6.12.

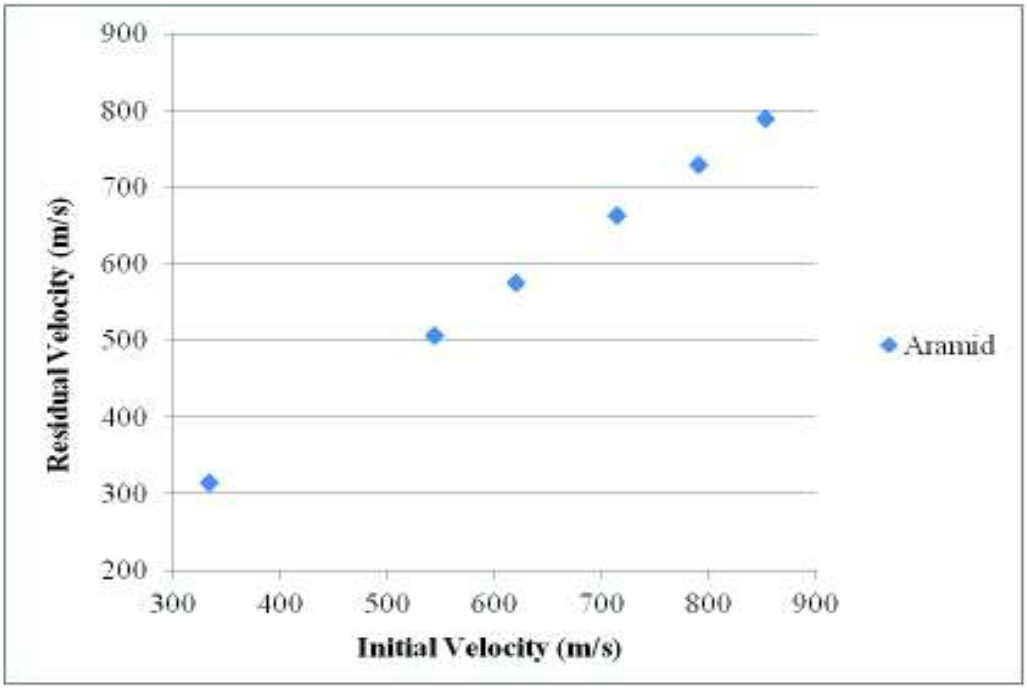


Figure 6.12 Initial vs. residual velocities of layered aramid/epoxy composite with MAT 22 after simulations

After calculating ballistic limit velocities of layered aramid/epoxy composite material with MAT 22; initial, residual and ballistic limit velocities are given in Table 6.5.

Table 6.5 Initial, residual and ballistic limit velocities of layered aramid/epoxy composite with MAT 22 after simulations

Initial velocity V_i (m/s)	Residual velocity V_r (m/s)	Ballistic limit velocity V_b (m/s)
852	789	321.53
790	729	304.40
713	662	264.81
619	575	229.21
543	506	197.01
333	314	110.87
		Average ballistic limit velocity V_b = 248.85 m/s

After finding ballistic limit velocities of layered aramid/epoxy composite with MAT 22, actual function of initial velocity and residual velocity diagram is given in Figure 6.13. As it is seen from Figure 6.13, bilinear behavior is obtained as expected.

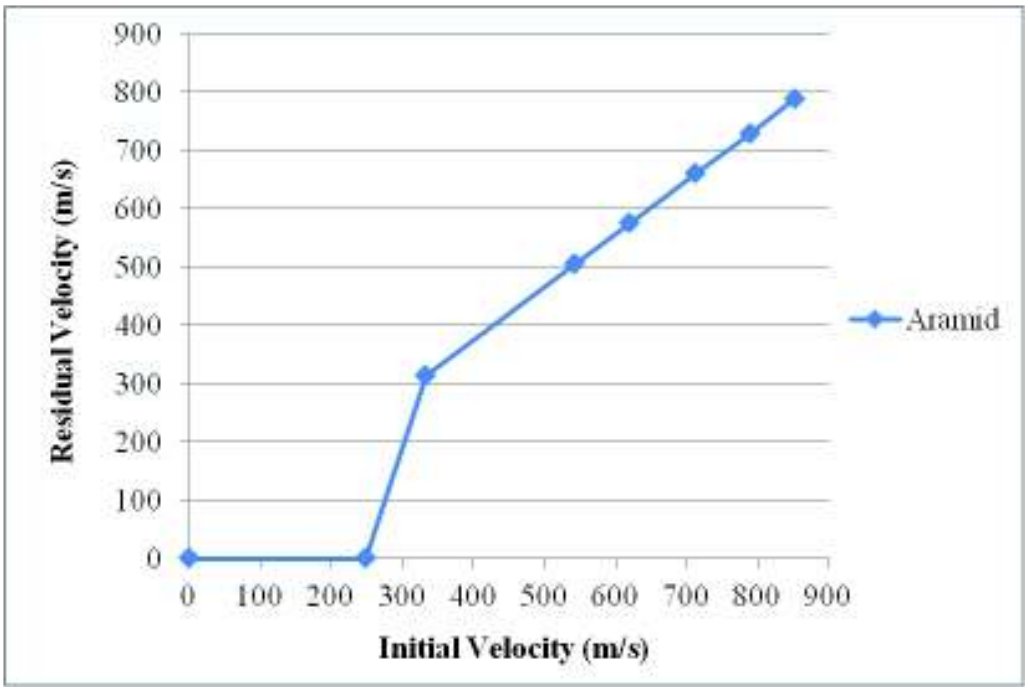


Figure 6.13 Initial velocity vs. residual velocity of layered aramid/epoxy composite with MAT 22 including ballistic limit velocity after simulations

6.2.1.2 Carbon-Aramid/Epoxy Composite

Detailed results are given in Appendix B. Initial velocity versus residual velocity diagram of layered carbon-aramid/epoxy composite with MAT 22 is drawn by using obtained data from simulations and shown in Figure 6.14.

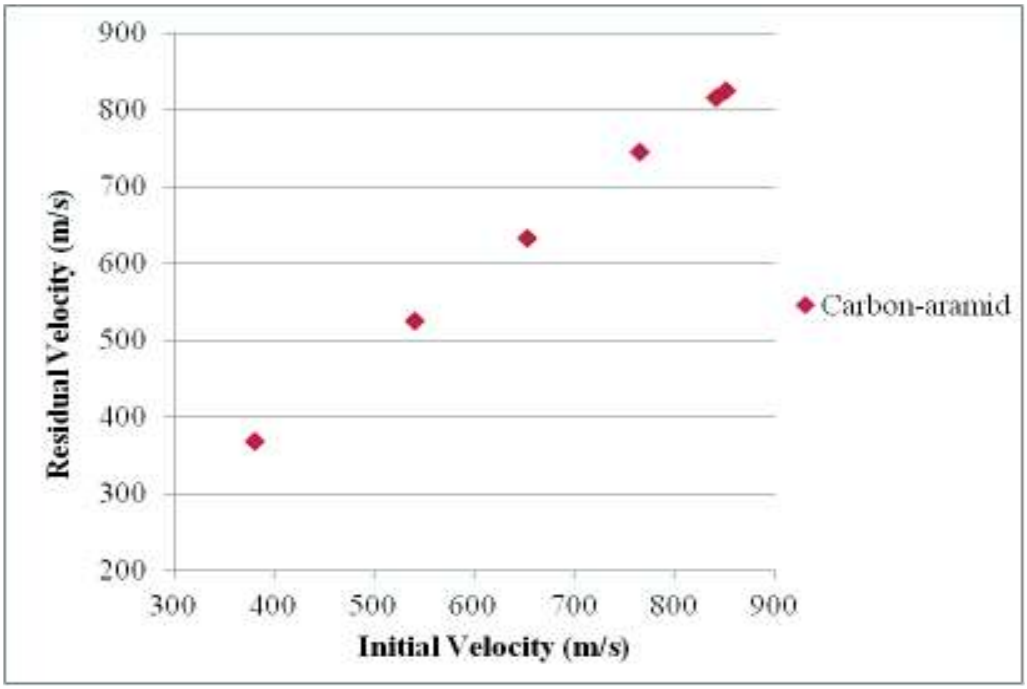


Figure 6.14 Initial velocity vs. residual velocity of layered carbon-aramid/epoxy composite with MAT 22 after simulations

After calculating ballistic limit velocities of layered carbon-aramid/epoxy composite material with MAT 22; initial, residual and ballistic limit velocities are given in Table 6.6.

After finding ballistic limit velocities of layered aramid/epoxy composite with MAT 22, actual function of initial velocity and residual velocity diagram is given in Figure 6.15. As it is seen from Figure 6.15, bilinear behavior is obtained as expected.

Table 6.6 Initial, residual and ballistic limit velocities of layered carbon-aramid/epoxy composite with MAT 22 after simulations

Initial velocity V_i (m/s)	Residual velocity V_r (m/s)	Ballistic limit velocity V_b (m/s)
850	826	200.56
841	816	203.53
764	745	169.32
652	633	156.25
540	525	126.39
381	369	94.87
		Average ballistic limit velocity V_b = 163.13 m/s

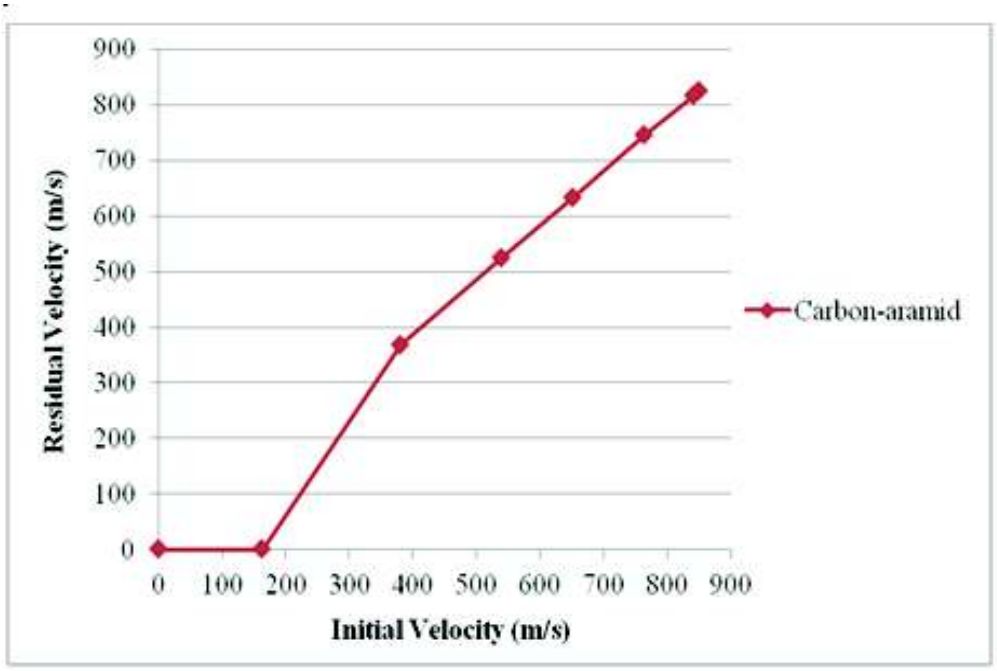


Figure 6.15 Initial velocity vs. residual velocity of layered carbon-aramid/epoxy composite with MAT 22 including ballistic limit velocity after simulations

6.2.2 Numerical Results of Layered Composites with MAT 59

6.2.2.1 Aramid/Epoxy Composite

Detailed results are given in Appendix C. Initial velocity versus residual velocity diagram of layered aramid/epoxy composite with MAT 59 is drawn by using obtained data from simulations and shown in Figure 6.16.

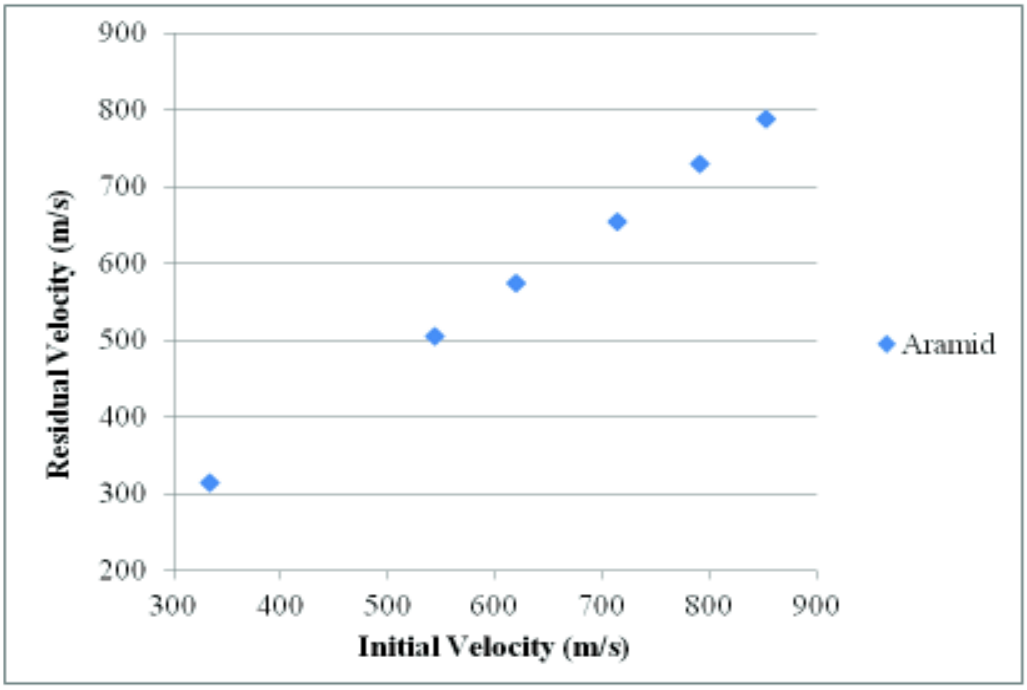


Figure 6.16 Initial velocity vs. residual velocity of layered aramid/epoxy composite with MAT 59 after simulations

After calculating ballistic limit velocities of layered aramid/epoxy composite material with MAT 59; initial, residual and ballistic limit velocities are given in Table 6.7.

After finding ballistic limit velocities of layered aramid/epoxy composite with MAT 59, actual function of initial velocity and residual velocity diagram is given in Figure 6.17. As it is seen from Figure 6.17, bilinear behavior is obtained as expected.

Table 6.7 Initial, residual and ballistic limit velocities of layered aramid/epoxy composite with MAT 59 after simulations

Initial velocity V_i (m/s)	Residual velocity V_r (m/s)	Ballistic limit velocity V_b (m/s)
852	788	321.53
790	730	304.40
713	655	264.81
619	575	229.21
543	506	197.01
333	314	110.87
		Average ballistic limit velocity V_b = 252.47 m/s

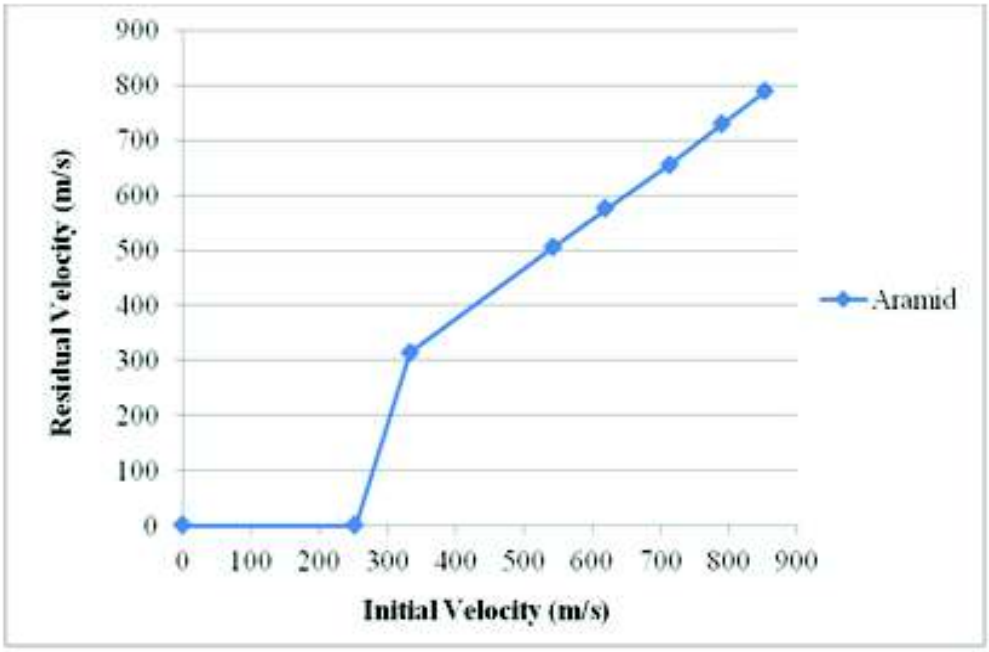


Figure 6.17 Initial velocity vs. residual velocity of layered aramid/epoxy composite with MAT 59 including ballistic limit velocity after simulations

6.2.2.2 Carbon-Aramid/Epoxy Composite

Detailed results are given in Appendix D. Initial velocity versus residual velocity diagram of layered carbon-aramid/epoxy composite with MAT 59 is drawn by using obtained data from simulations and shown in Figure 6.18.

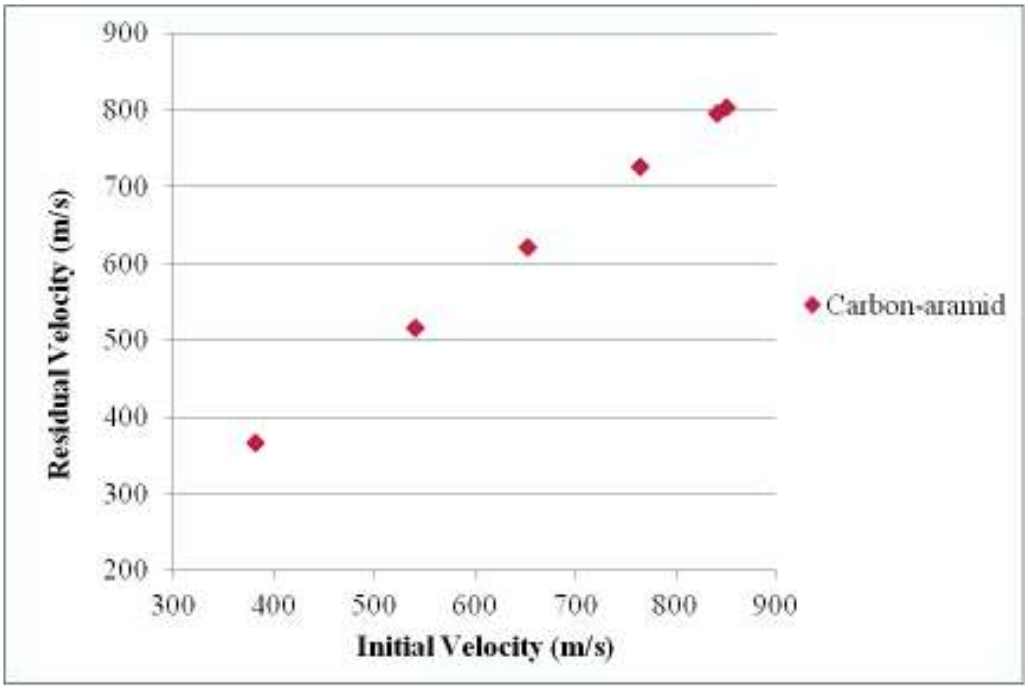


Figure 6.18 Initial velocity vs. residual velocity of layered carbon-aramid/epoxy composite with MAT 59 after simulations

After calculating ballistic limit velocities of layered carbon-aramid/epoxy composite material with MAT 59; initial, residual and ballistic limit velocities are given in Table 6.8.

After finding ballistic limit velocities of layered carbon-aramid/epoxy composite with MAT 59, actual function of initial velocity and residual velocity diagram is given in Figure 6.199. As it is seen from Figure 6.19, bilinear behavior is obtained as expected.

Table 6.8 Initial, residual and ballistic limit velocities of layered carbon-aramid/epoxy composite with MAT 59 after simulations

Initial velocity V_i (m/s)	Residual velocity V_r (m/s)	Ballistic limit velocity V_b (m/s)
850	804	275.83
841	796	271.41
764	726	237.95
652	621	198.65
540	516	159.20
381	366	105.85
		Average ballistic limit velocity V_b = 216.80 m/s

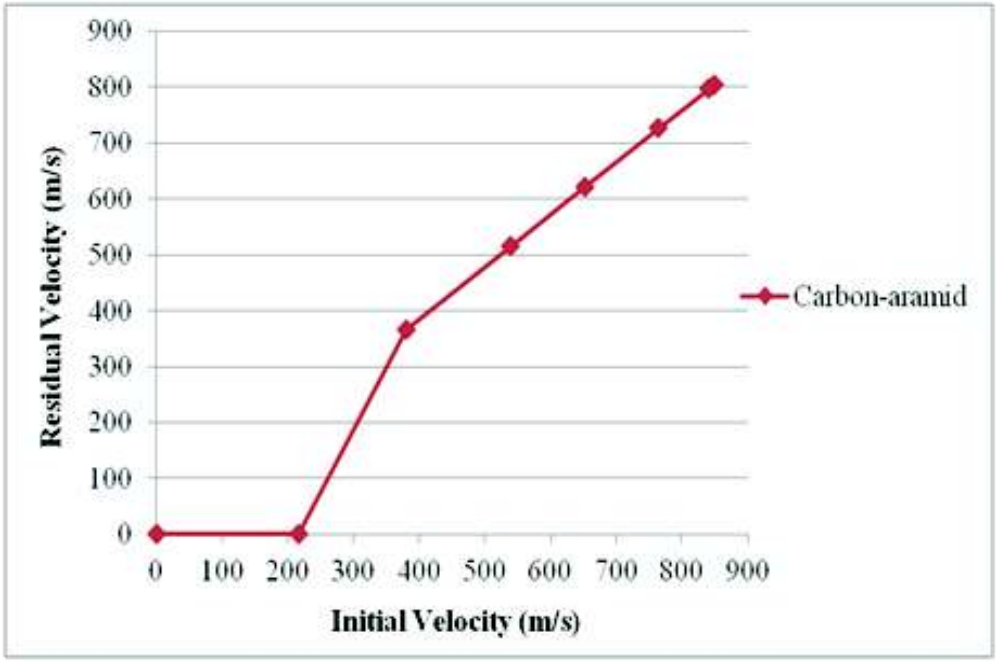


Figure 6.19 Initial velocity vs. residual velocity of layered carbon-aramid/epoxy composite with MAT 59 including ballistic limit velocity after simulations

6.2.3 Numerical Results of Single Layer Composite with MAT 59

6.2.3.1 Aramid/Epoxy Composite

Detailed results are given in Appendix E. Initial velocity versus residual velocity diagram of single layer aramid/epoxy composite with MAT 59 is drawn by using obtained data from simulations and shown in Figure 6.20.

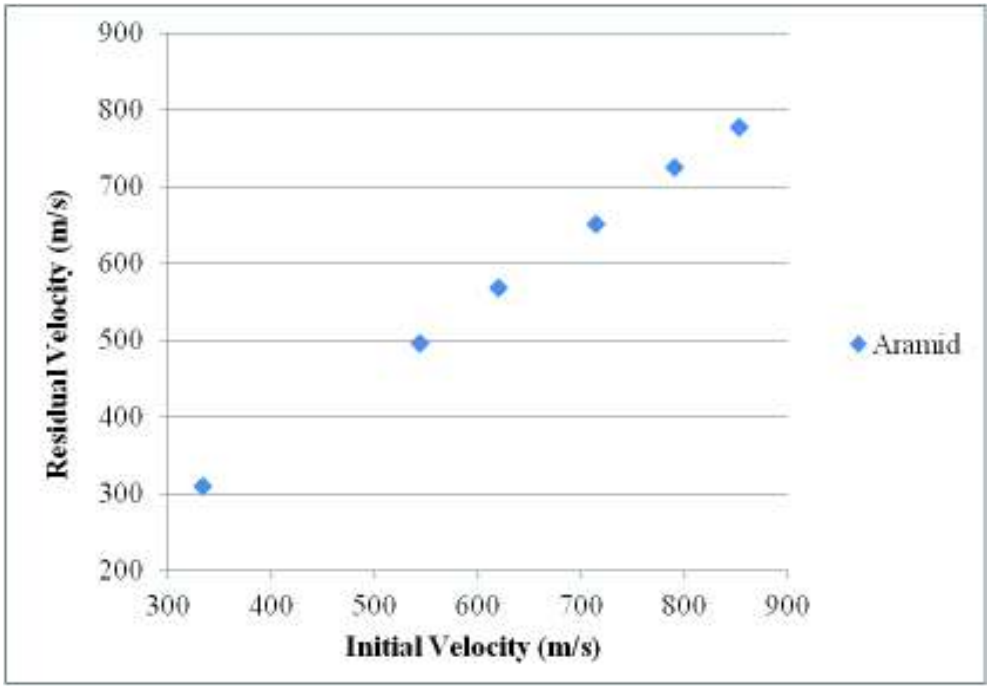


Figure 6.20 Initial velocity vs. residual velocity of single layer aramid/epoxy composite with MAT 59 after simulations

After calculating ballistic limit velocities of single layer aramid/epoxy composite material with MAT 59; initial, residual and ballistic limit velocities are given in Table 6.9.

After finding ballistic limit velocities of single layer aramid/epoxy composite with MAT 59, actual function of initial velocity and residual velocity diagram is given in Figure 6.21. As it is seen from Figure 6.21, bilinear behavior is obtained as expected.

Table 6.9 Initial, residual and ballistic limit velocities of single layer aramid/epoxy composite with MAT 59 after simulations

Initial velocity V_i (m/s)	Residual velocity V_r (m/s)	Ballistic limit velocity V_b (m/s)
852	778	347.30
790	725	313.80
713	651	290.80
619	569	243.72
543	496	220.98
333	310	121.61
		Average ballistic limit velocity V_b = 267.33 m/s

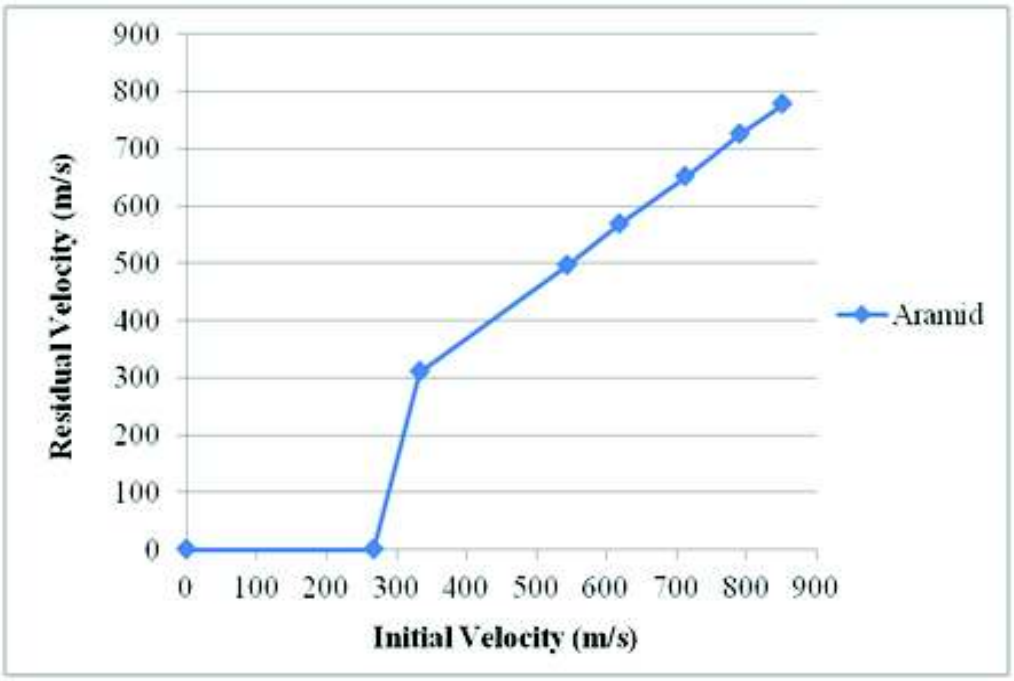


Figure 6.21 Initial velocity vs. residual velocity of single layer aramid/epoxy composite with MAT 59 including ballistic limit velocity after simulations

6.2.3.2 Carbon-Aramid/Epoxy Composite

Detailed results are given in Appendix F. Initial velocity versus residual velocity diagram of single layer carbon-aramid/epoxy composite with MAT 59 is drawn by using obtained data from simulations and shown in Figure 6.22.

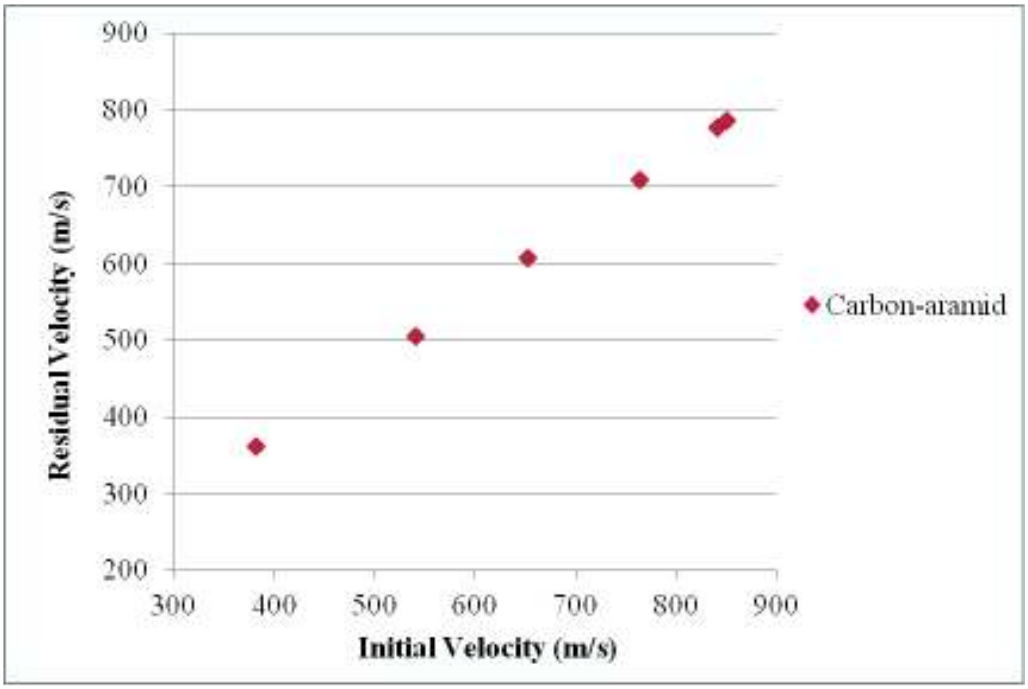


Figure 6.22 Initial velocity vs. residual velocity of single layer carbon-aramid/epoxy composite with MAT 59 after simulations

After calculating ballistic limit velocities of single layer carbon-aramid/epoxy composite material with MAT 59; initial, residual and ballistic limit velocities are given in Table 6.10.

After finding ballistic limit velocities of single layer carbon-aramid/epoxy composite with MAT 59, actual function of initial velocity and residual velocity diagram is given in Figure 6.23. As it is seen from Figure 6.23, bilinear behavior is obtained as expected.

Table 6.10 Initial, residual and ballistic limit velocities of single layer carbon-aramid/epoxy composite with MAT 59 after simulations

Initial velocity V_i (m/s)	Residual velocity V_r (m/s)	Ballistic limit velocity V_b (m/s)
850	787	321.14
841	778	319.37
764	710	282.13
652	608	235.46
540	506	188.58
381	361	121.82
		Average ballistic limit velocity V_b = 256.38 m/s

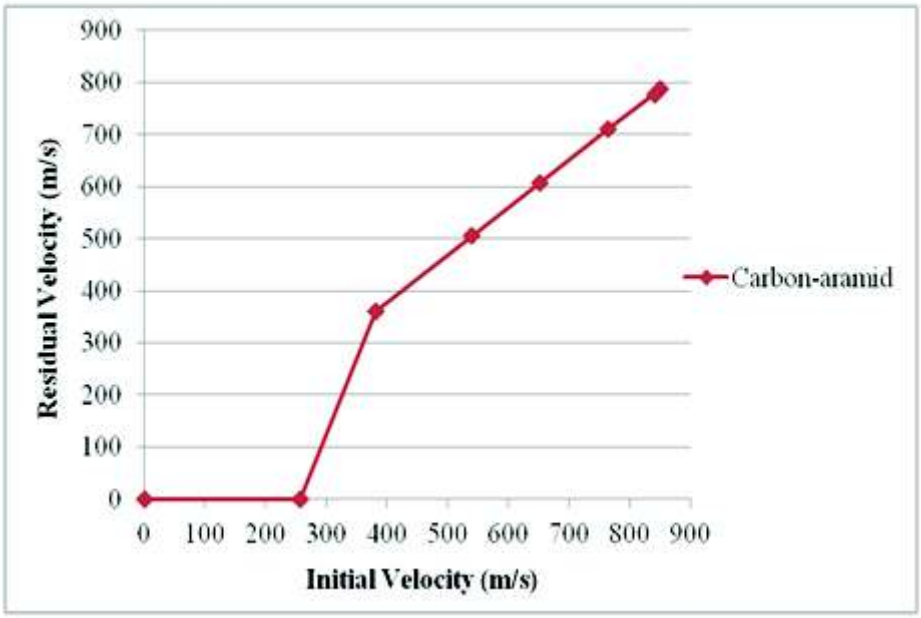


Figure 6.23 Initial velocity vs. residual velocity of single layer carbon-aramid/epoxy composite with MAT 59 including ballistic limit velocity after simulations

6.3 Comparison Between Numerical and Experimental Results

6.3.1 Aramid/Epoxy Composite

Satisfactory results were obtained after comparison between experimental and all numerical methods.

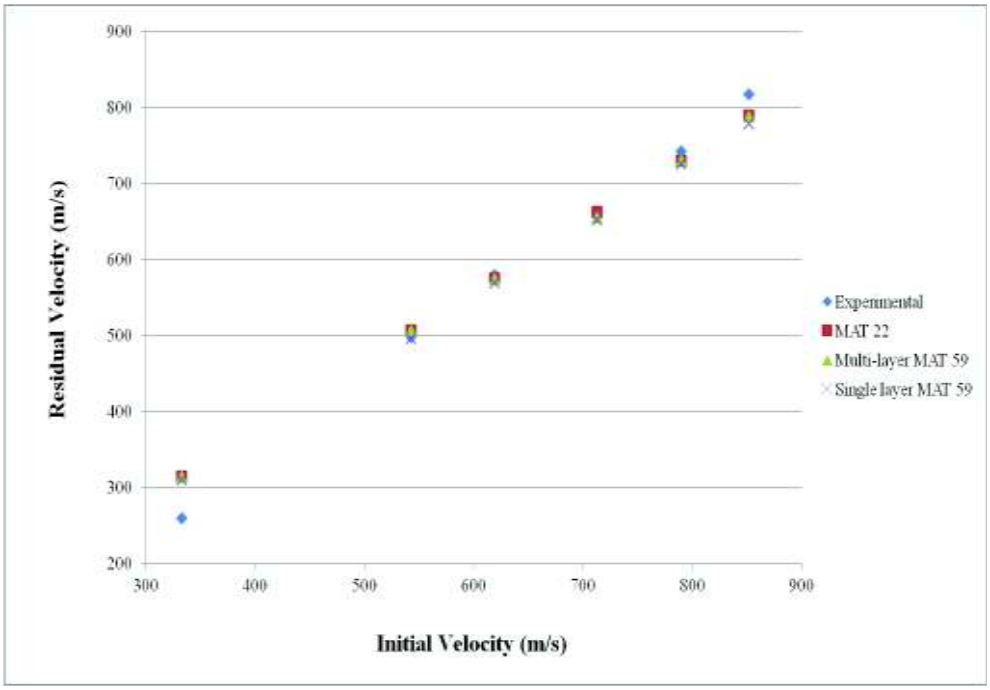


Figure 6.24 Comparison of experimental and numerical results of aramid/epoxy composite

Results occurred with a very low margin of error for the velocities 790 m/s, 713 m/s, 619 m/s, 543 m/s. Different residual velocities were obtained for 852 m/s and 333 m/s between all numerical and experimental results. It is thought that this difference could be because of projectile jacket for 852 m/s. As it was already defined, only core of projectile was modeled as a rigid impactor and jacket and filler effects were ignored before simulations. For 333 m/s, it is thought that this difference in residual velocity could be because of delamination mechanism. As it is known, only delamination initiation is found when stress-based delamination theory is used. Because of this difference, this mechanism may not be fully reflected.

Delamination was seen for all shots in experimental results. For five velocities excluding 333 m/s, this mechanism was less effective than other failures as fiber breakage or matrix cracking and it is seen from close results between experimental and numerical simulations. For 333 m/s, it is thought that delamination was also an effective mechanism.

Layered composites with MAT 22, layered composites with MAT 59 and single layer composite with MAT 59 show similar behaviors. These results show that in-plane strengths show dominant behavior over through-thickness strengths.

Single layer composite with MAT 59 absorbed more energy than layered composite with MAT 59. It can be said that modeling plies has important effect on stiffness of composite materials. Results are close for layered composites with MAT 22 and MAT 59.

Ballistic limit velocities were calculated as 237.05 m/s for experimental method, 248.85 m/s for layered composite with MAT 22, 252.47 m/s for layered composite with MAT 59 and 267.33 m/s for single layer composite with MAT 59 (Table 6.11).

Table 6.11 Error percentages of numerical methods for aramid/epoxy composite considering ballistic limit velocities

	Ballistic limit velocity (m/s)	Error (%)
Experimental	237.05	-
Layered composite with MAT 22	248.85	4.98
Layered composite with MAT 59	252.47	6.5
Single layer composite with MAT 59	267.33	12.78

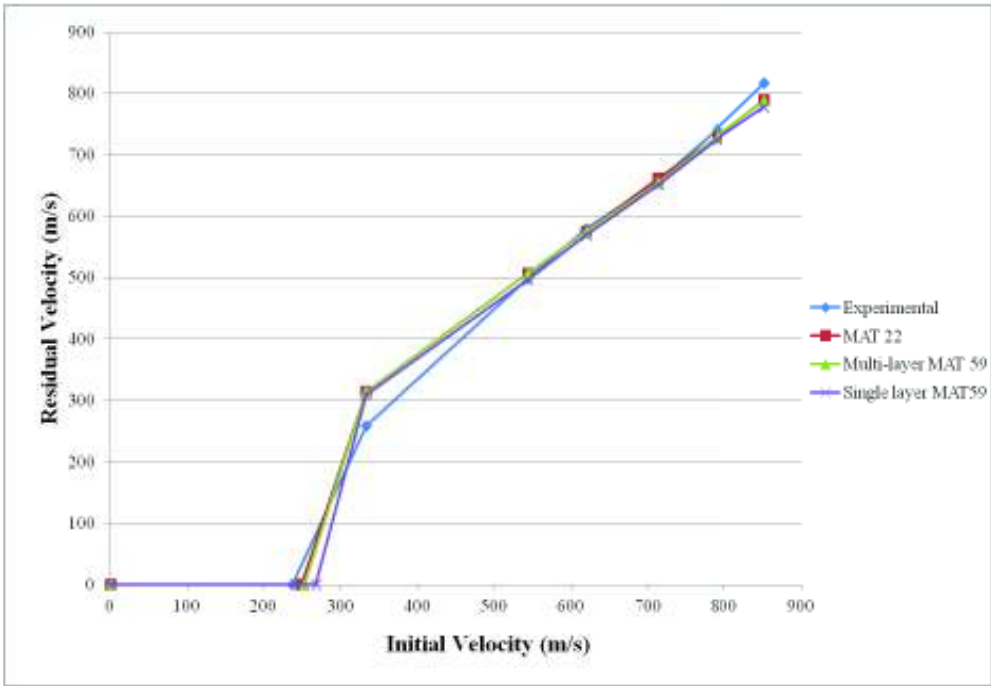


Figure 6.25 Comparison of experimental and numerical results of aramid/epoxy composite including ballistic limit velocity

Although it may seem that results for single layer composite with MAT 59 are close to other two methods in terms of residual velocity. After calculating ballistic limit velocities, ballistic limit velocity is higher than other two methods for single layer composite with MAT 59.

After evaluating the results in terms of residual and ballistic limit velocities, layered composites with MAT 22 and MAT 59 are more appropriate than single layer composite with MAT 59.

6.3.2 Carbon-Aramid/Epoxy Composite

Layered composites with MAT 59 showed better performance than other two methods for carbon-aramid/epoxy composite.

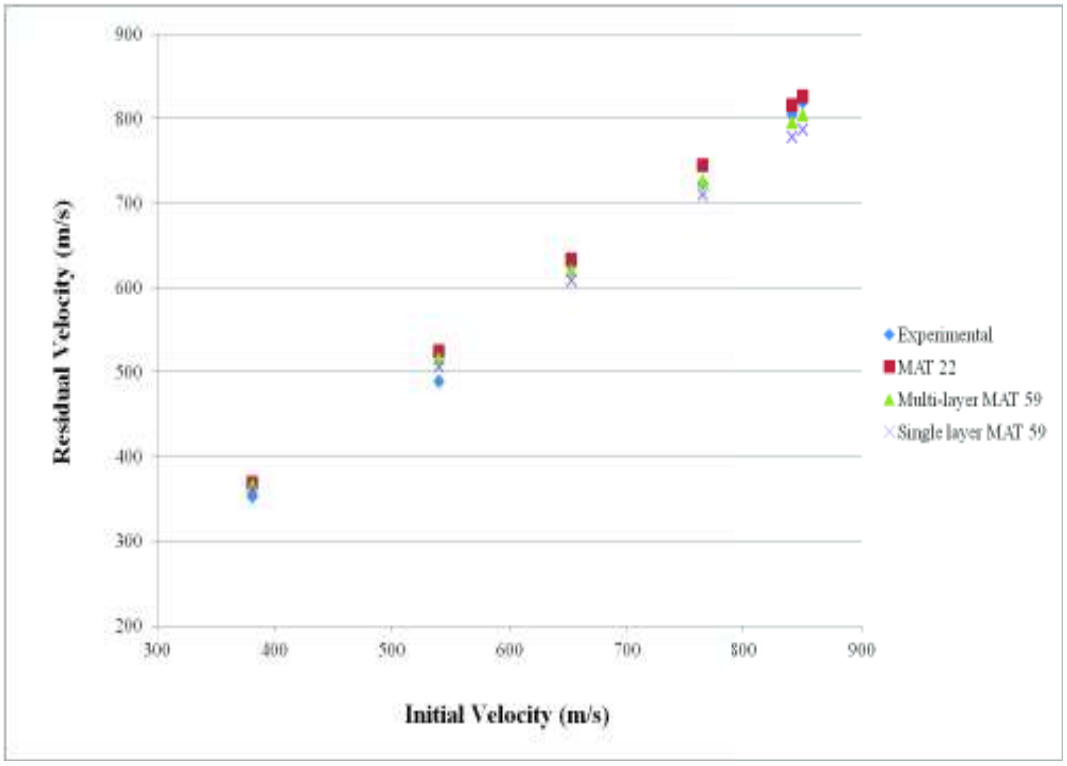


Figure 6.26 Comparison of experimental and numerical results of carbon-aramid/epoxy composite

Layered composite with MAT 22 showed a good performance for velocities 850 m/s and 841 m/s, the composite absorbed less energy than experimental method for lower methods. Single layer composite with MAT 59 showed a good performance

for velocities 540 m/s and 381 m/s, but the composite absorbed more energy than experimental method for high velocities.

Layered composite with MAT 59 showed better performance and results occurred with a very low margin of error than other two methods. Although these differences are small enough to be negligible in terms of residual velocities, state of these differences are also supported by aramid/epoxy composite. For velocities 850 m/s and 841 m/s, difference was caused possibly because of projectile jacket which was modeled as only rigid core and for velocity 381 m/s, difference was caused possibly because of delamination mechanism.

Delamination was not exactly seen in the carbon-aramid/composites after experimental tests, also this comment was supported by the agreement between experimental and numerical results.

Ballistic limit velocities were calculated as 219.79 m/s for experimental method, 163.13 m/s for layered composite with MAT 22, 216.80 m/s for layered composite with MAT 59 and 256.38 m/s for single layer composite with MAT 59 (Table 6.12).

Table 6.12 Error percentages of numerical methods for carbon-aramid/epoxy composite considering ballistic limit velocities

	Ballistic limit velocity (m/s)	Error (%)
Experimental	219.79	-
Layered composite with MAT 22	163.13	25.78
Layered composite with MAT 59	216.80	1.36
Single layer composite with MAT 59	256.38	16.64

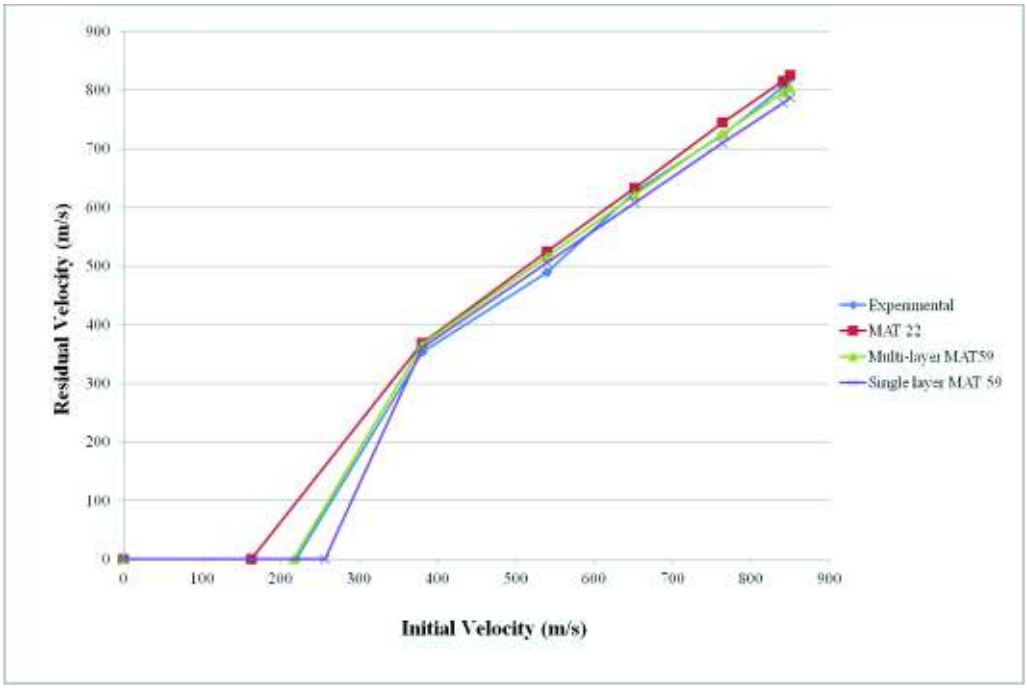


Figure 6.27 Comparison of experimental and numerical results of carbon-aramid/epoxy composite including ballistic limit velocity

After evaluating the results in terms of residual and ballistic limit velocities, layered composites with MAT 59 are more appropriate than other two methods.

CHAPTER SEVEN

CONCLUSION AND DISCUSSION

In this study, effect of reinforcement type and different numerical composite damage material models were investigated in high velocity impact applications. 7.62 mm AP projectile was used experimentally. Layered composites with MAT 22 and MAT 59 and single layer composite with MAT 59 were created as numerical models. Because of three numerical procedures, two composite materials and six different velocities, thirty-six numerical simulations were performed.

For aramid/epoxy composite, all numerical models showed similar behaviors in terms of projectile residual velocity. It is thought that in-plane stiffness has more importance than through-thickness stiffness for aramid/epoxy composite. But layered composites with MAT 22 and MAT 59 showed better performance than single layer MAT 59 in terms of ballistic limit velocity.

For carbon-aramid/epoxy composite, differences were observed between numerical models. Layered composite with MAT 22 showed a good performance for the highest two velocities and single layer composite with MAT 59 showed better performance than other methods for the lowest two velocities. Layered composite with MAT 59 showed better performance and results occurred with a very low margin of error than other two methods in terms of residual and ballistic limit velocities.

Ply modeling had also effect on stiffness of composite materials. Although there was not a major difference in aramid/epoxy composite, high changes were observed in carbon-aramid/epoxy composites.

Some differences were observed in residual velocity between experimental and numerical models for the highest and lowest velocities. For the highest velocities, effect of projectile jacket can be included and should be investigated. For the lowest velocities, differences possibly were caused by delamination mechanism. As we know, delamination is a major topic on composites and some approaches are used numerically for modeling this mechanism. In this study, stress based theory was used

but it was seen that this mechanism was not fully sufficient. Delamination can be modeled by fracture mechanics and can be compared with stress based theory.

For aramid/epoxy layered composite with MAT 22 and MAT 59, for carbon-aramid/epoxy composites layered composite with MAT 59 showed better performance over other methods. In line with these results, it was observed that choosing true material model or technique is also dependent on material mechanical properties.

Aramid/epoxy absorbed more energy than carbon-aramid/epoxy composites both experimentally and numerically as expected. But these energy differences are not too high and even can be said as close, hybrid composite can also be preferred because of lower areal density advantage.

REFERENCES

Abrate, S. (2007). Ballistic impact on composites. *16th International Conference on Composite Materials.* Retrieved June 08, 2014, from http://www.ewp.rpi.edu/hartford/~ernesto/F2011/EP/MaterialsforStudents/Manahan/OldIdea/Abrate2007.PDF

Ahn, J.-H., Nguyen, K.-H., Park, Y.-B., Kweon, J.-H., & Choi, J.-H. (2010). A numerical study of the high-velocity impact response of a composite laminate using LS-DYNA. *International Journal of Aeronautical and Space Sciences*, *11*(3), 221–226.

Azevedo, R., & Alves, M. (2009). Numerical simulation of soft-body impact on GFRP laminate composites: mixed SPH-FE and pure SPH approaches. *Mechanics of Solids in Brazil*. Retrieved May 19, 2013, from http://www.abcm.org.br/pt/wp-content/symposium series/SSSM_Vol2/Contents/SSSM_02.pdf

Balya, B. (2004). *Design and analysis of filament wound composite tubes*. M.Sc Thesis, Middle East Technical University, Turkey

Bundy, C. B. (2005). *Use of pultruded carbon fiber/epoxy inserts as reinforcement in composite structures*. M.Sc Thesis, Montana State University, USA

Davis, D. (2012). *Finite element modeling of ballistic impact on a glass fiber composite armor*. M.Sc Thesis, California Polytechnic State University, USA

Demir, T., Übeyli, M., & Yıldırım, R. O. (2008). Investigation on the ballistic impact behavior of various alloys against 7.62 mm armor piercing projectile. *Materials & Design*, *29*(10), 2009–2016.

Deniz, T. (2010). *Ballistic penetration of hardened steel plates.* M.Sc Thesis*,* Middle East Technical University, Turkey

Deo, R. J. (2010). *Preparation and characterization of polymer matrix composite using natural fiber lantana-camara*. PhD Thesis, National Institute of Technology Rourkela, India

Dhananjayan, K. V. (2013). *Design and analysis of a compression molded carbon composite wheel center*. M.Sc Thesis, The University of Texas, USA

Fawaz, Z., Zheng, W., & Behdinan, K. (2004). Numerical simulation of normal and oblique ballistic impact on ceramic composite armours. *Composite Structures*, *63*(3-4), 387–395.

Goyal, V. K., Huertas, C. A., & Vasko, T. J. (2013). Bird strike modeling based on the Lagrangian formulation using LS-DYNA. *American Transactions on Engineering & Applied Sciences*, *2*(2), 57–81.

Grimsley, B. W. (2005). *Characterization of the vacuum assisted resin transfer molding process for fabrication of aerospace composites,* M.Sc Thesis, Virginia Polytechnic Institute and State University, USA

Guild, F., El-Habti, M., & Hogg, P. (2007). Ballistic impact of composite laminate: Experiments and simulations. *16th International Conference on Composite Materials*. Retrieved September 09, 2012, from http://www.iccm-central.org/Proceedings/ICCM16proceedings/contents/pdf/ThuH/ThHA2-01ge_guildf224287p.pdf

Hallquist, O. J. (2006). *LS-DYNA theory manual*. Retrieved November 07, 2013, from http://www.dynasupport.com/manuals/additional/ls-dyna-theory-manual-2005-beta/view

Heimbs, S., Heller, S., & Middendorf, P. (2008). *Simulation of low velocity impact on composite plates with compressive preload*. Retrieved March 16, 2014, from http://www.heimbs-online.de/Heimbs_Composite%20Plates%20with%20Compressive%20Preload.pdf

Hoof, v. J. (1999). *Modeling of impact induced delamination in composite materials*, PhD Thesis, Carleton University, Canada

Ipek, H. (2005). *Modeling of resin transfer molding for composite manufacturing*, M.Sc Thesis, Middle East Technical University, Turkey

Kamath, M. G. (2004). *Processing and evaluation of cotton-based composites for automotive and other applications*. M.Sc Thesis, University of Tennessee, USA

Keulen, C. (2006). *Design and manufacturing of composite structures using the resin transfer molding technique*. M.Sc Thesis, University of Victoria, Canada

Liu, C. (2010). *Mesophase pitch-based carbon fiber and its composites: Preparation and characterization*, M.Sc Thesis, University of Tennessee, USA

Mallick, P.K. (2007). *Fiber re-inforced composites materials, manufacturing, and design* (3rd ed.). NY: CRC Press.

Manes, A., Lumassi, D., Giudici, L., & Giglio, M. (2013). An experimental–numerical investigation on aluminum tubes subjected to ballistic impact with soft core 7.62 ball projectiles. *Thin-Walled Structures*, *73*, 68–80.

Mansur, A. (2011). *Modeling of mechanical properties of ceramic-metal composites for armor applications*. M.Sc Thesis, University of Ottawa, Canada

Mohan, S., & Velu, S. (2014). Ballistic impact behaviour of unidirectional fibre reinforced composites. *International Journal of Impact Engineering*, *63*, 164–176.

Öğrenci, D. H. (2012). *Mekanik olarak bağlanmış kompozitlerin dayanımı*, M.Sc Thesis, Dokuz Eylül University, Turkey

Ramadhan, A. A., Abu Talib, A. R., Mohd Rafie, A. S., & Zahari, R. (2013). High velocity impact response of Kevlar-29/epoxy and 6061-T6 aluminum laminated panels. *Materials & Design*, *43*, 307–321.

Sevkat, E., Liaw, B., Delale, F., & Raju, B. B. (2009). A combined experimental and numerical approach to study ballistic impact response of S2-glass fiber/toughened epoxy composite beams. *Composites Science and Technology*, *69*(7-8), 965–982.

Shukla, P. S. (2011). *Investigation in to tribo potential of rice husk (RH) char reinforced epoxy composite*. M.Sc Thesis, National Institute of Technology Rourkela, India

Stegmann, H. (2005). *Analysis and optimization of laminated composite shell structures.* PhD Thesis, Aalborg University, Denmark

Vaidya, U. K., Abraham A., & Bhide, S. (2001). Affordable processing of thick section and integral multi-functional composites. *Composites Part A: Applied Science and Manufacturing*, *32*(8), 1133–1142.

Wang, H.Y & Shie, J. J. (2009). Effect of autoclave curing on the compressive strength and elastic modulus of lightweight aggregate concrete. *Journal of ASTM International*, *6*(6).

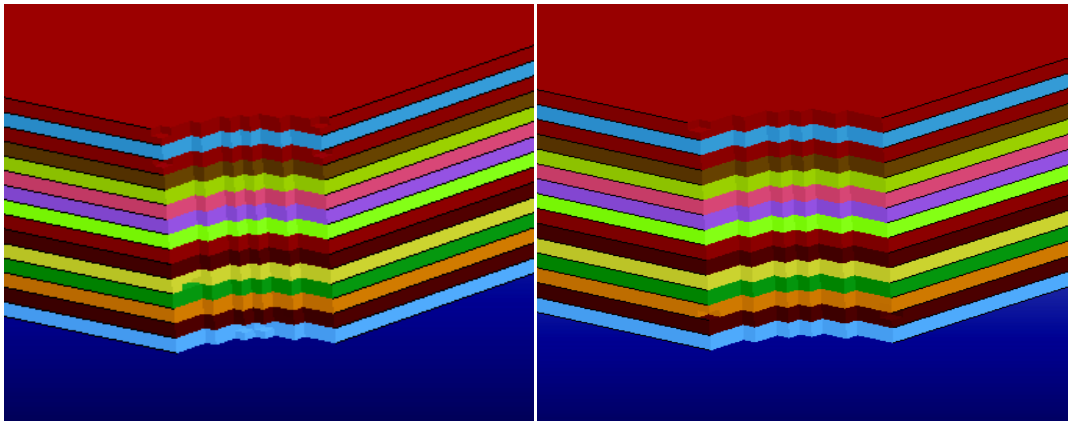
Wielewski, E., Birkbeck, A., & Thomson, R. (2013). Ballistic resistance of spaced multi-layer plate structures: Experiments on fibre reinforced plastic targets and an analytical framework for calculating the ballistic limit. *Materials & Design*, *50*, 737–741.

Yaghoubi, S. A., & Liaw, B. (2013). Effect of lay-up orientation on ballistic impact behaviors of GLARE 5 FML beams. *International Journal of Impact Engineering*, *54*, 138–148.

Yang, J., & Dai, J. (2010). Simulation-based assessment of rear effect to ballistic helmet impact. *Computer-Aided Design and Applications*, *7*(1), 59–73.

APPENDICES

Appendix A



(a) (b)

Figure 1. Perforation view of layered aramid/epoxy composites with MAT 22 after simulations for initial velocities (a) V_i: 713 m/s (b) V_i: 619 m/s

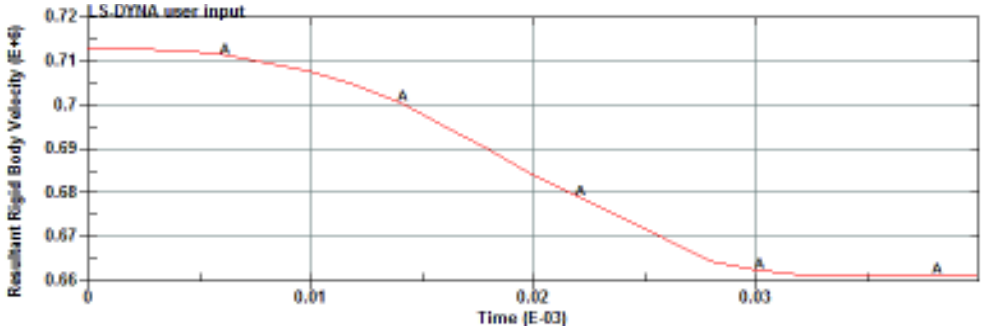


Figure 2. Velocity (mm/s) vs. time (s) curve of layered aramid/epoxy composite with MAT 22 for initial velocity V_i: 713 m/s

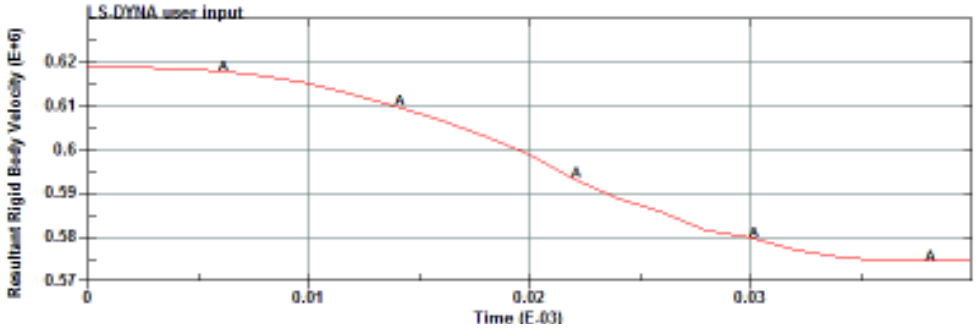
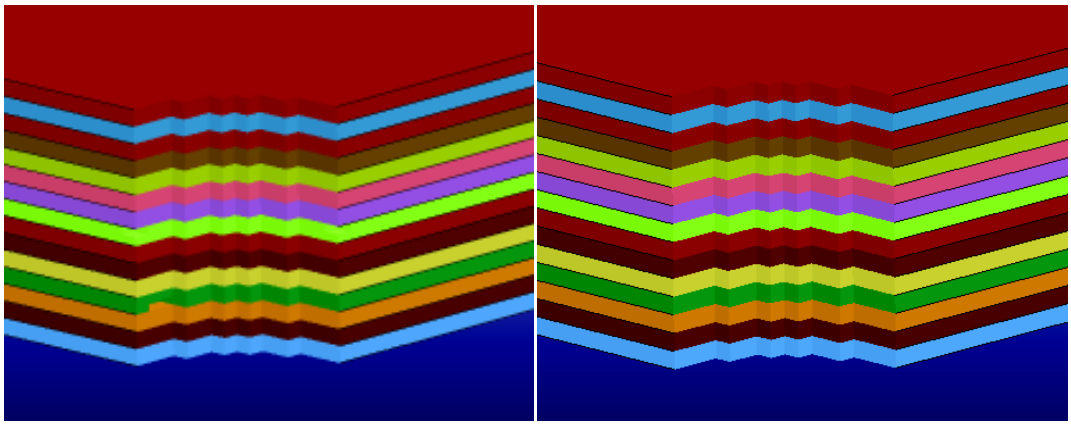


Figure 3. Velocity (mm/s) vs. time (s) curve of layered aramid/epoxy composite with MAT 22 for initial velocity V_i: 619 m/s



(a) (b)

Figure 4. Perforation view of layered aramid/epoxy composites with MAT 22 after simulations for initial velocities (a) V_i: 543 m/s (b) V_i: 333 m/s

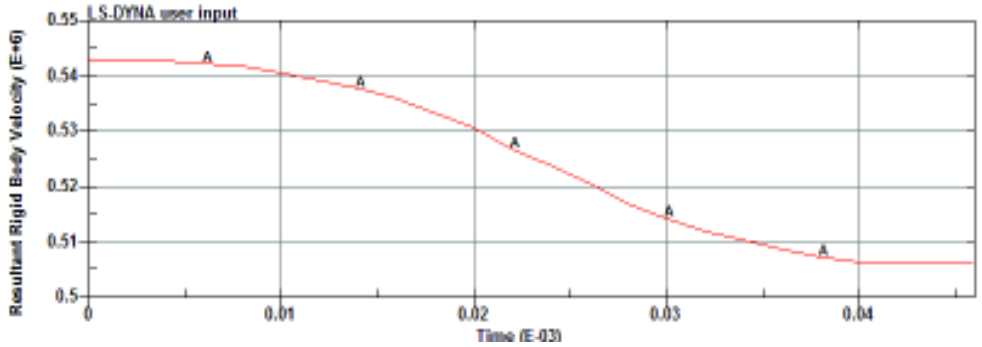


Figure 5. Velocity (mm/s) vs. time (s) curve of layered aramid/epoxy composite with MAT 22 for initial velocity V_i: 852 m/s

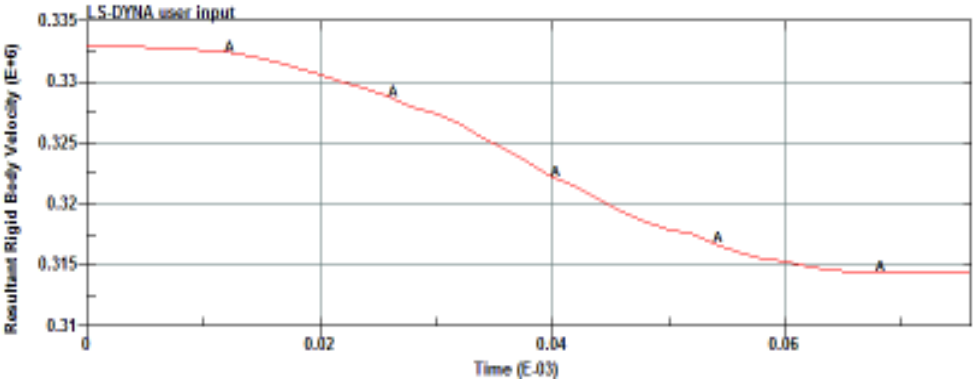
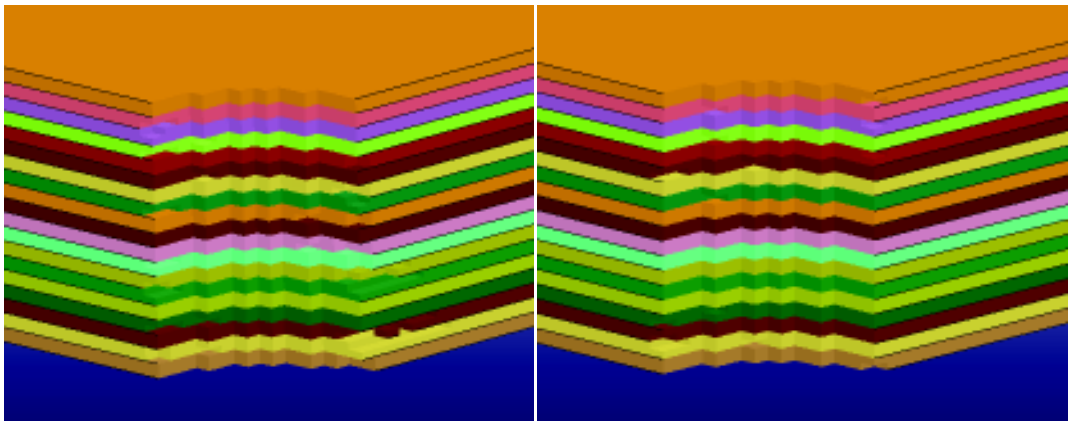


Figure 6. Velocity (mm/s) vs. time (s) curve of layered aramid/epoxy composite with MAT 22 for initial velocity V_i: 333 m/s

Appendix B



(a) (b)

Figure 7. Perforation view of layered carbon-aramid/epoxy composites with MAT 22 after simulations for initial velocities (a) V_i: 850 m/s (b) V_i: 841 m/s

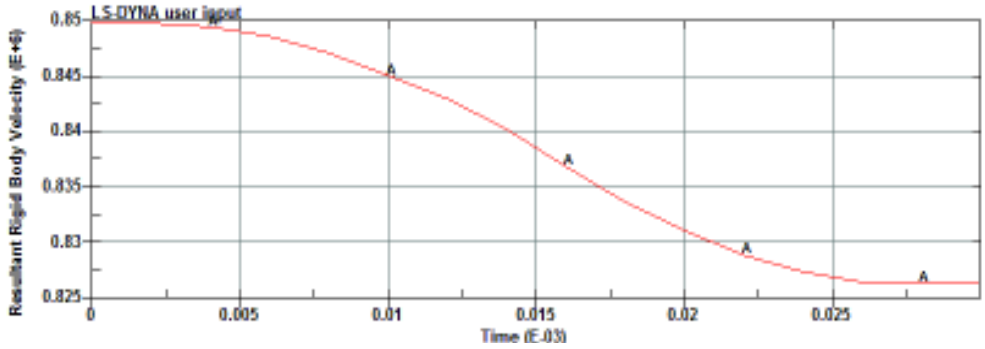


Figure 8. Velocity (mm/s) vs. time (s) curve of layered carbon-aramid/epoxy composite with MAT 22 for initial velocity V_i: 850 m/s

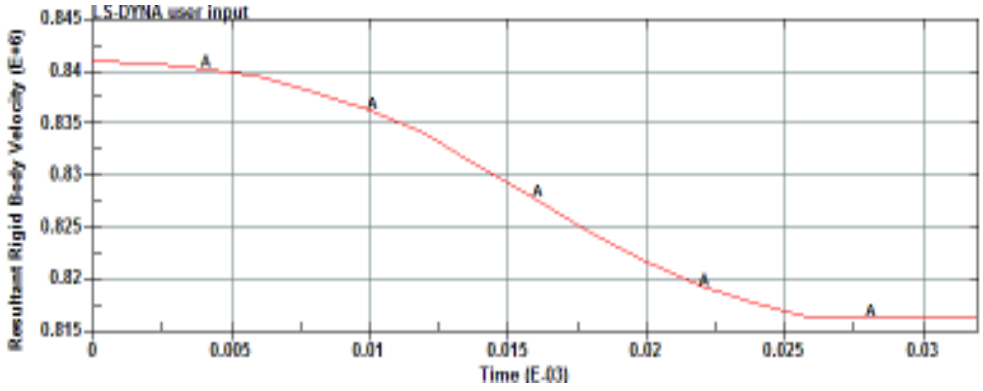
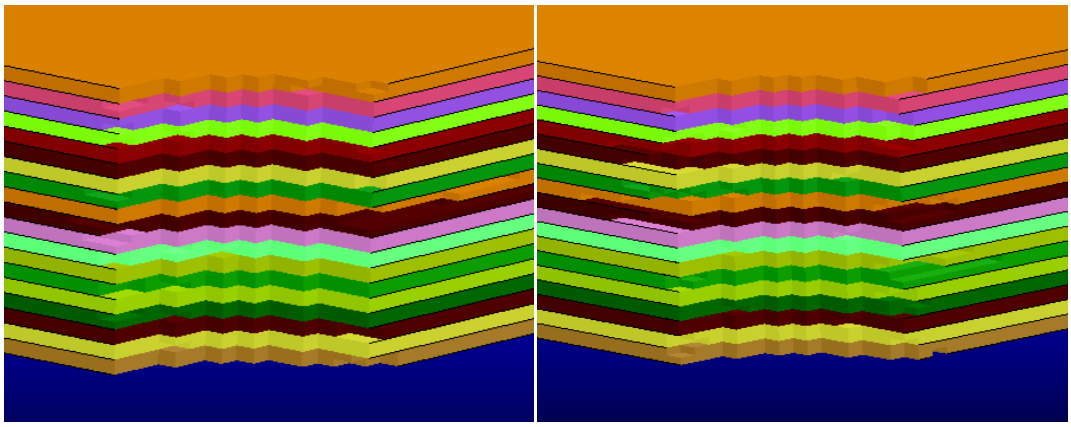


Figure 9. Velocity (mm/s) vs. time (s) curve of layered carbon-aramid/epoxy composite with MAT 22 for initial velocity V_i: 841 m/s



(a) (b)

Figure 10. Perforation view of layered carbon-aramid/epoxy composites with MAT 22 after simulations for initial velocities (a) V_i: 764 m/s (b) V_i: 652 m/s

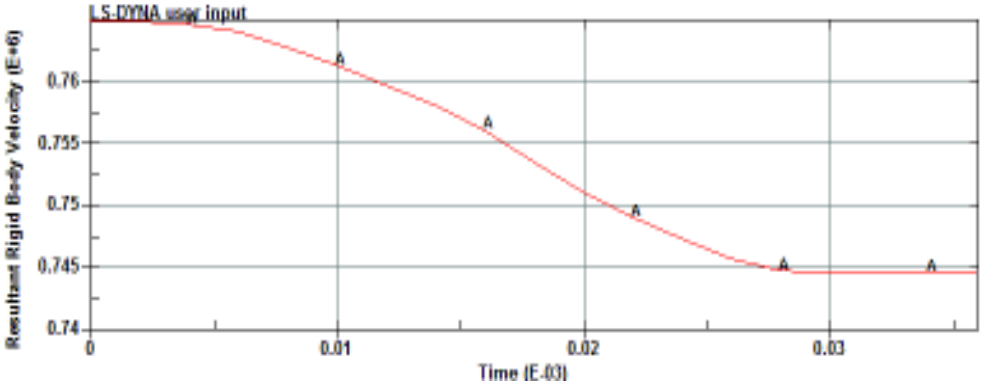


Figure 11. Velocity (mm/s) vs. time (s) curve of layered carbon-aramid/epoxy composite with MAT 22 for initial velocity V_i: 764 m/s

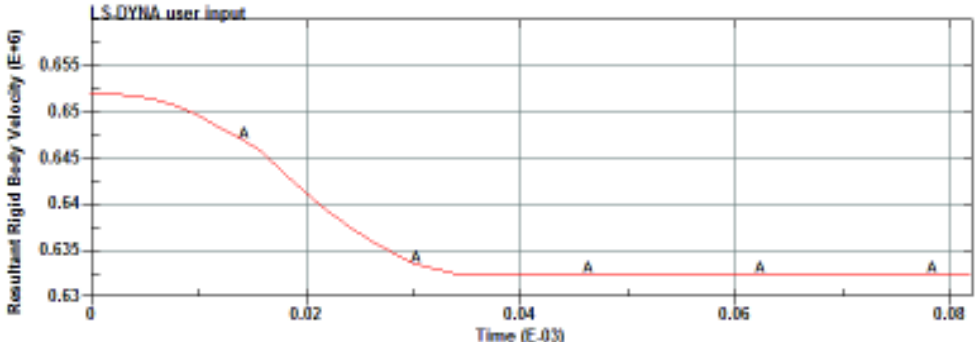
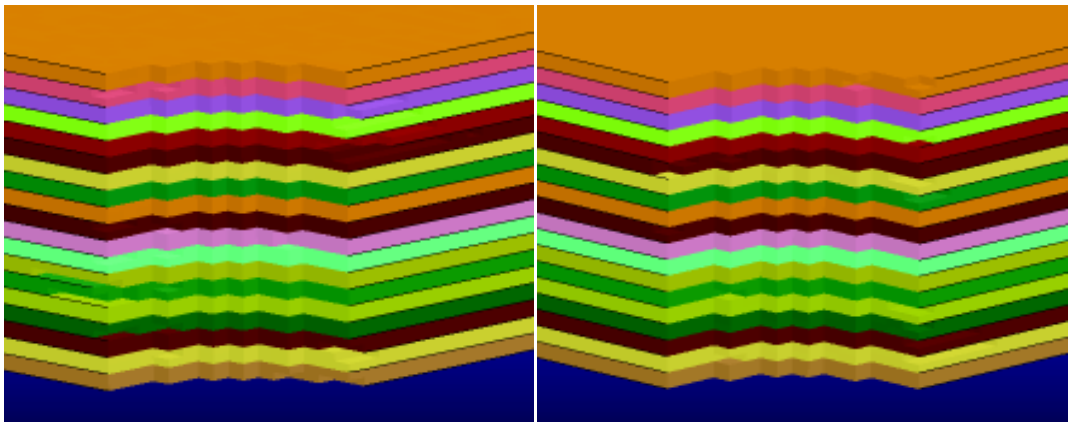


Figure 12. Velocity (mm/s) vs. time (s) curve of layered carbon-aramid/epoxy composite with MAT 22 for initial velocity V_i: 652 m/s



(a) (b)

Figure 13. Perforation view of layered carbon-aramid/epoxy composites with MAT 22 after simulations for initial velocities (a) V_i: 540 m/s (b) V_i: 381 m/s

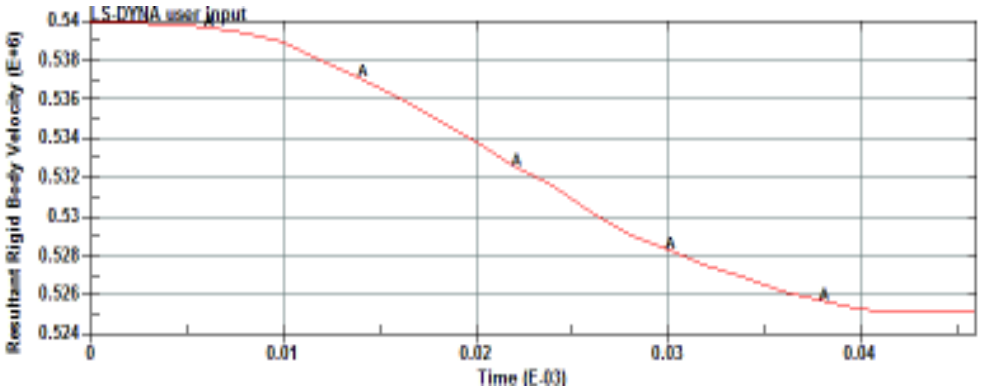


Figure 14. Velocity (mm/s) vs. time (s) curve of layered carbon-aramid/epoxy composite with MAT 22 for initial velocity V_i: 540 m/s

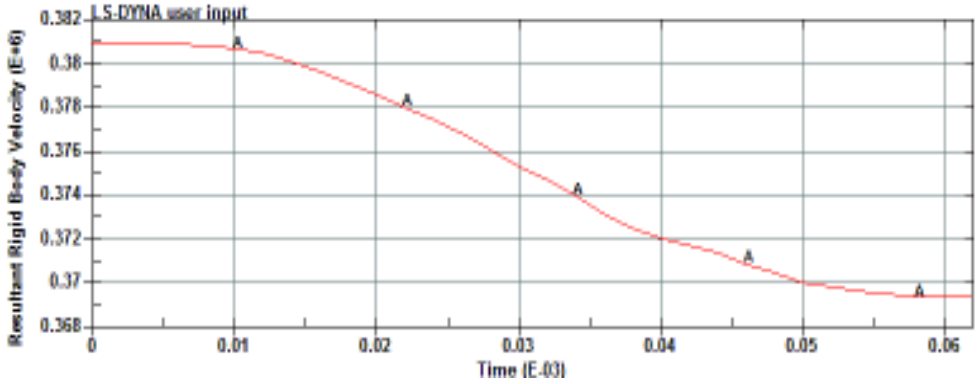
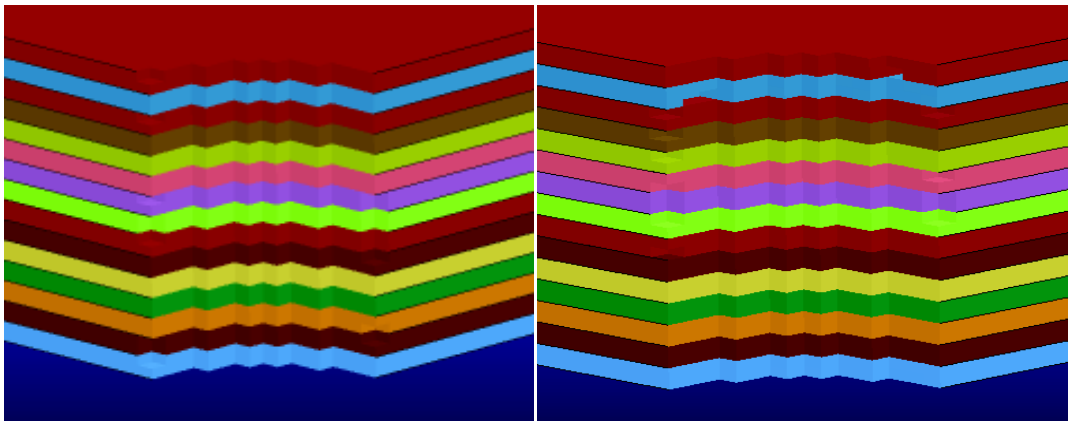


Figure 15. Velocity (mm/s) vs. time (s) curve of layered carbon-aramid/epoxy composite with MAT 22 for initial velocity V_i: 381 m/s

Appendix C



(a) (b)

Figure 16. Perforation view of layered aramid/epoxy composites with MAT 59 after simulations for initial velocities (a) V_i: 852 m/s (b) V_i: 790 m/s

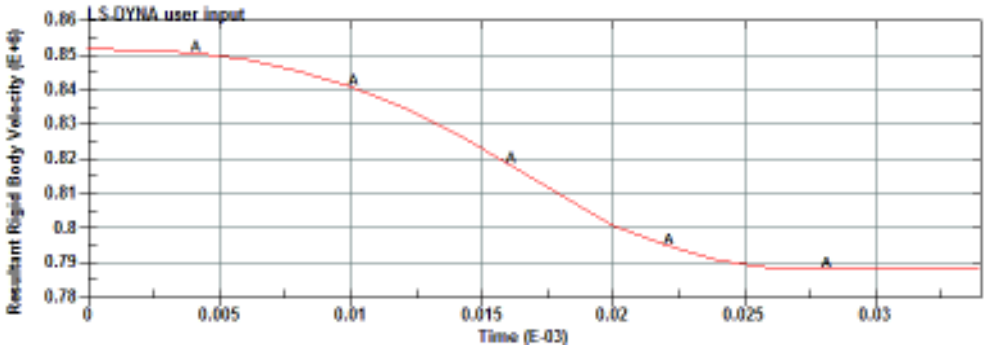


Figure 17. Velocity (mm/s) vs. time (s) curve of layered aramid/epoxy composite with MAT 59 for initial velocity V_i: 852 m/s

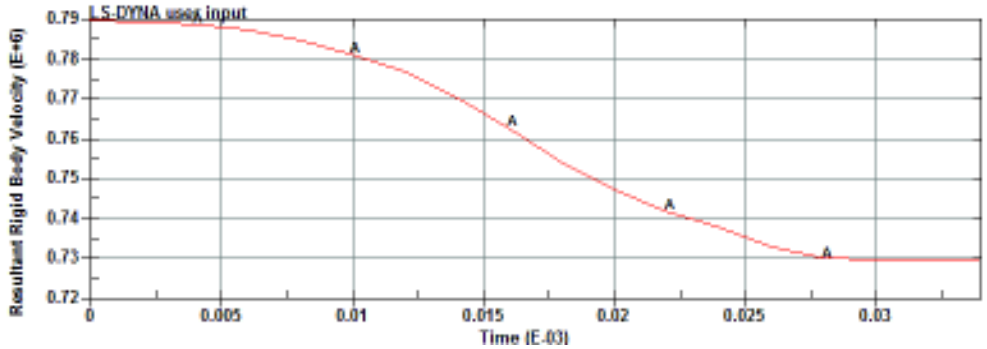
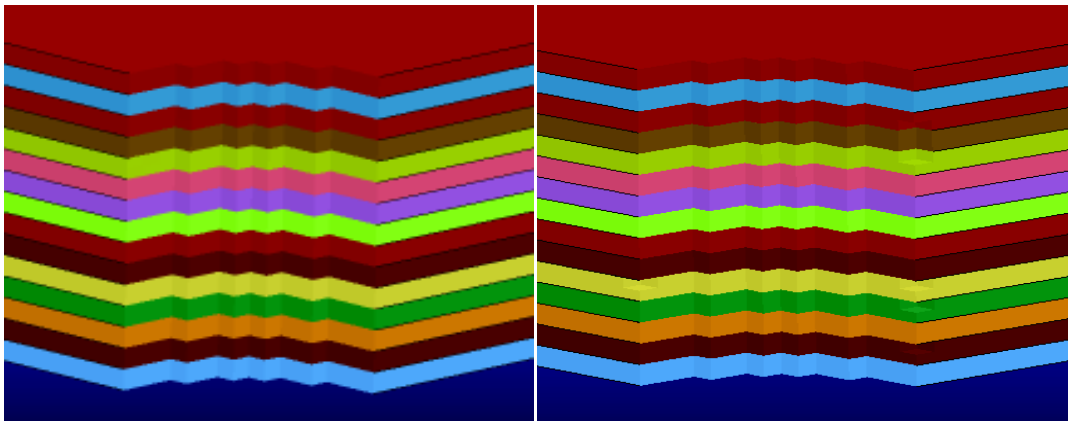


Figure 18. Velocity (mm/s) vs. time (s) curve of layered aramid/epoxy composite with MAT 59 for initial velocity V_i: 790 m/s



(a) (b)

Figure 19. Perforation view of layered aramid/epoxy composites with MAT 59 after simulations for initial velocities (a) V_i: 713 m/s (b) V_i: 619 m/s

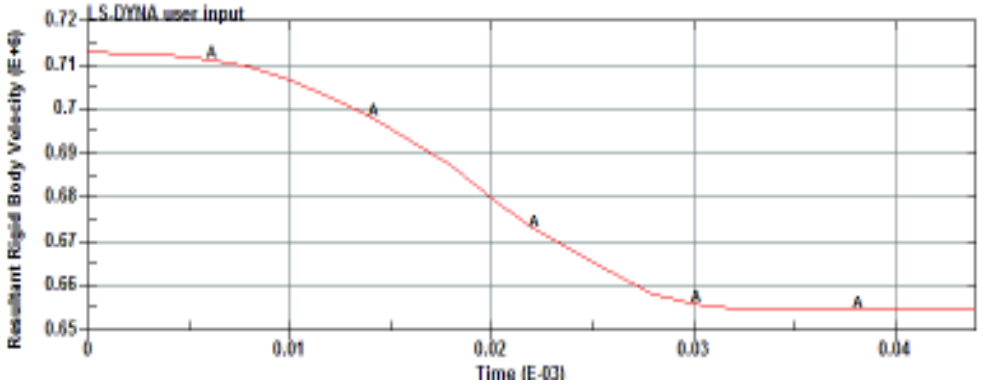


Figure 20. Velocity (mm/s) vs. time (s) curve of layered aramid/epoxy composite with MAT 59 for initial velocity V_i: 713 m/s

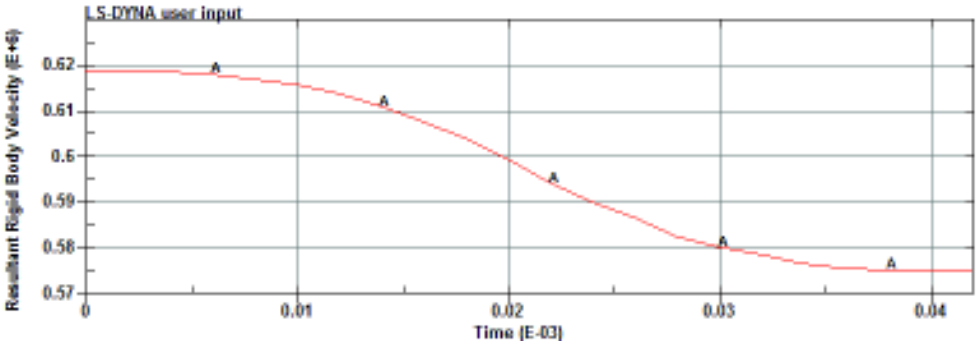
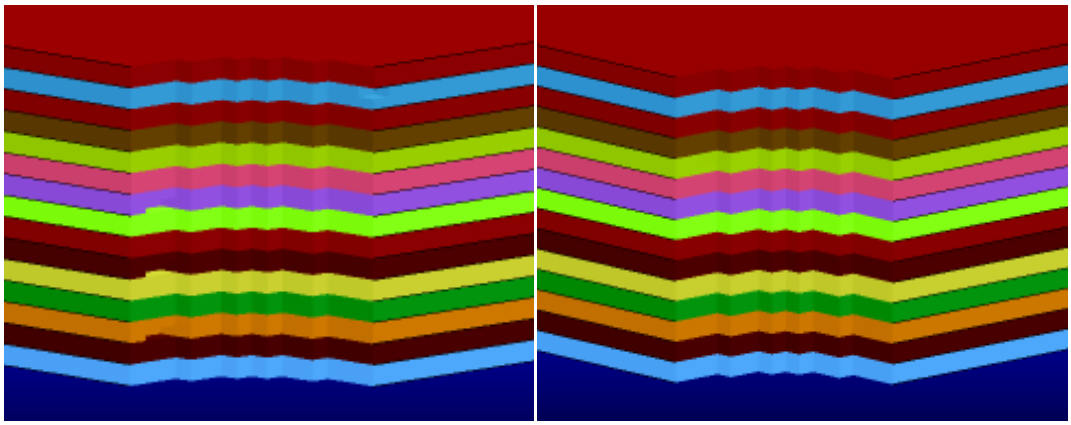


Figure 21. Velocity (mm/s) vs. time (s) curve of layered aramid/epoxy composite with MAT 59 for initial velocity V_i: 619 m/s



(a) (b)

Figure 22. Perforation view of layered aramid/epoxy composites with MAT 59 after simulations for initial velocities (a) V_i: 543 m/s (b) V_i: 333 m/s

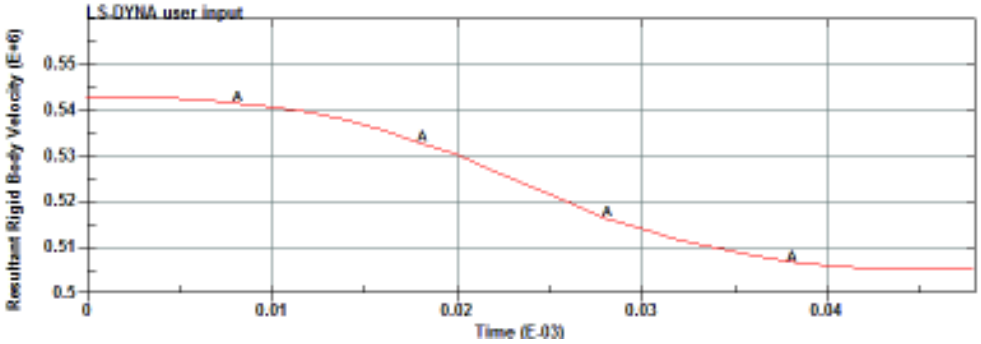


Figure 23. Velocity (mm/s) vs. time (s) curve of layered aramid/epoxy composite with MAT 59 for initial velocity V_i: 543 m/s

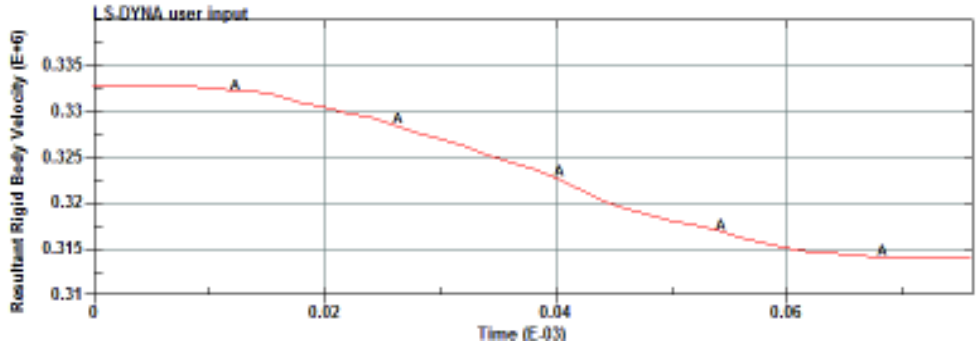
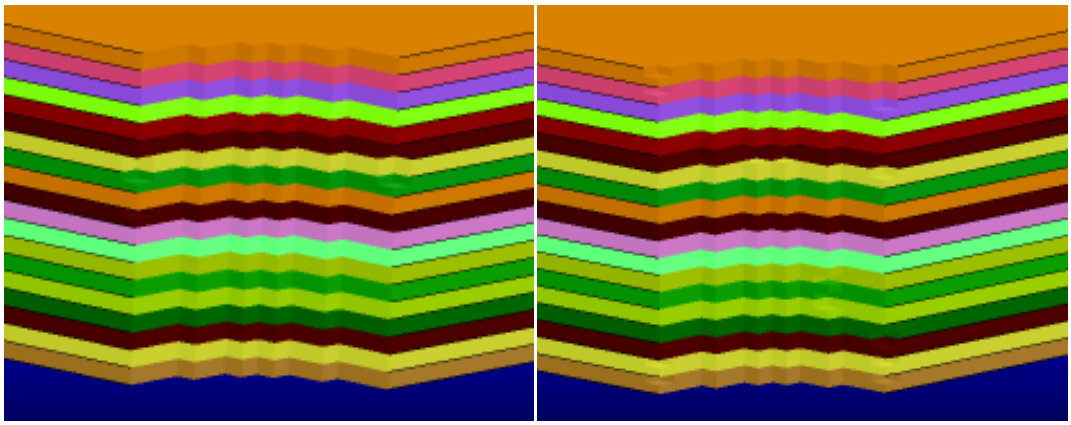


Figure 24. Velocity (mm/s) vs. time (s) curve of layered aramid/epoxy composite with MAT 59 for initial velocity V_i: 333 m/s

Appendix D



(a) (b)

Figure 25. Perforation view of layered carbon-aramid/epoxy composites with MAT 59 after simulations for initial velocities (a) V_i: 850 m/s (b) V_i: 841 m/s

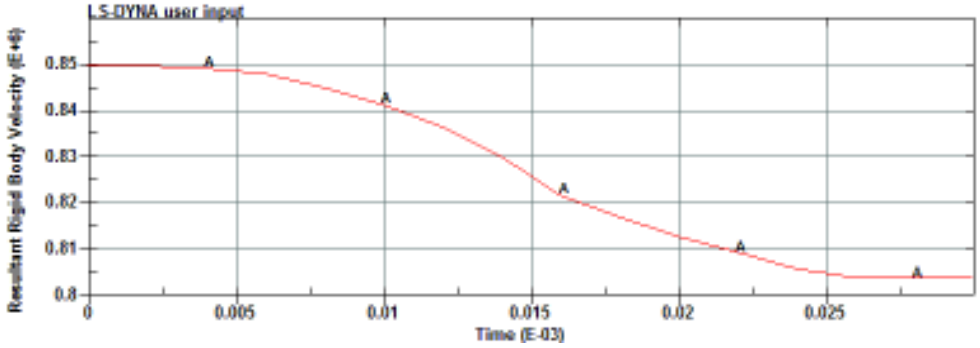


Figure 26. Velocity (mm/s) vs. time (s) curve of layered carbon-aramid/epoxy composite with MAT 59 for initial velocity V_i: 850 m/s

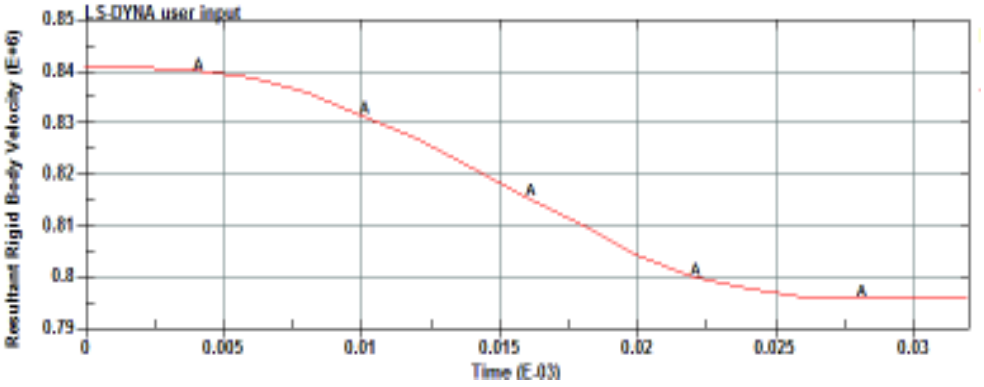
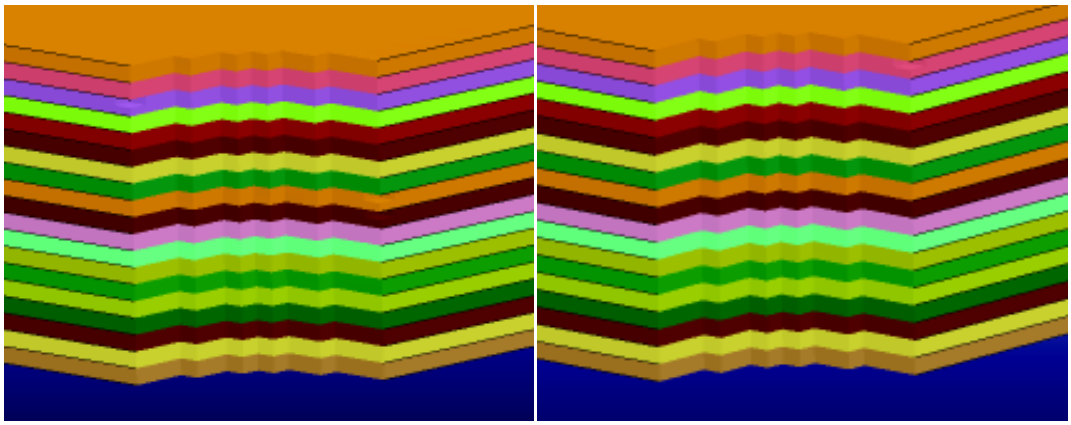


Figure 27. Velocity (mm/s) vs. time (s) curve of layered carbon-aramid/epoxy composite with MAT 59 for initial velocity V_i: 841 m/s



(a) (b)

Figure 28. Perforation view of layered carbon-aramid/epoxy composites with MAT 59 after simulations for initial velocities (a) V_i: 764 m/s (b) V_i: 652 m/s

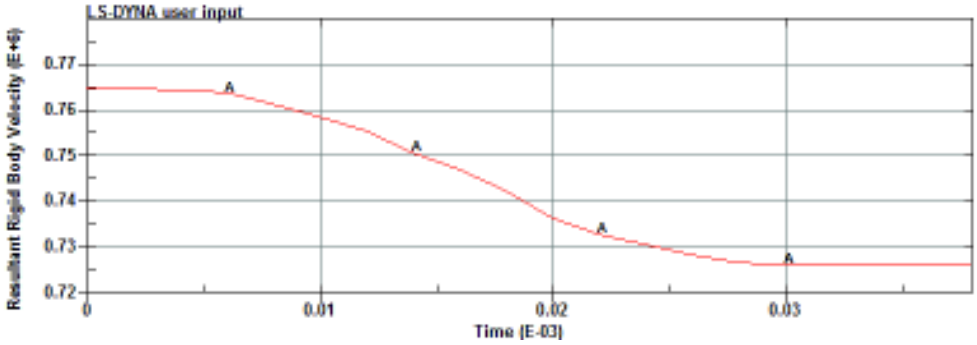


Figure 29. Velocity (mm/s) vs. time (s) curve of layered carbon-aramid/epoxy composite with MAT 59 for initial velocity V_i: 764 m/s

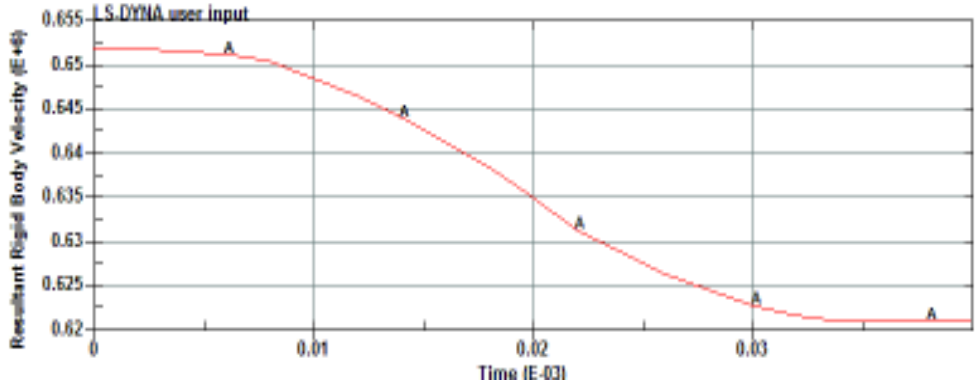
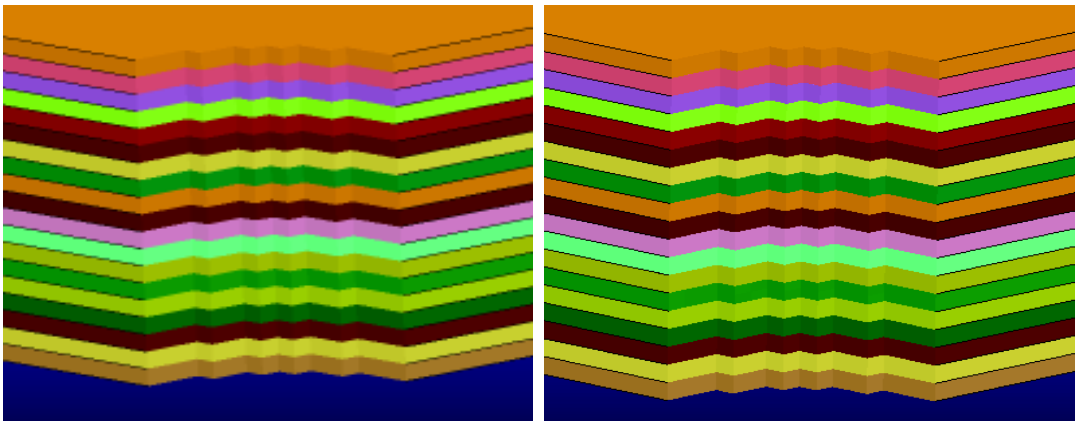


Figure 30. Velocity (mm/s) vs. time (s) curve of layered carbon-aramid/epoxy composite with MAT 59 for initial velocity V_i: 652 m/s



(a) (b)

Figure 31. Perforation view of layered carbon-aramid/epoxy composites with MAT 59 after simulations for initial velocities (a) V_i: 540 m/s (b) V_i: 381 m/s

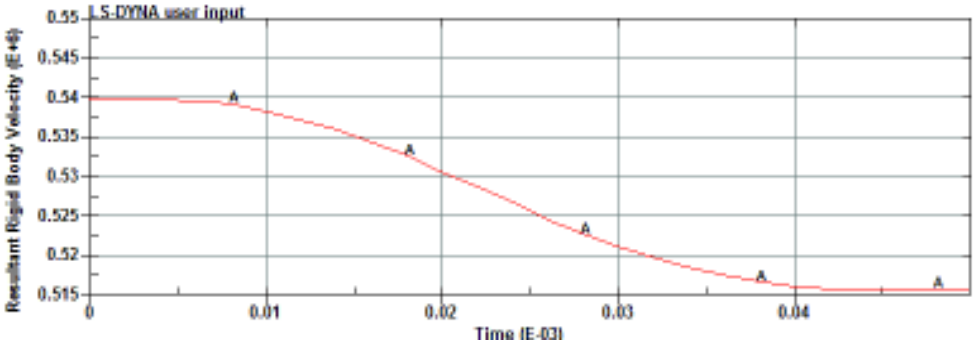


Figure 32. Velocity (mm/s) vs. time (s) curve of layered carbon-aramid/epoxy composite with MAT 59 for initial velocity V_i: 540 m/s

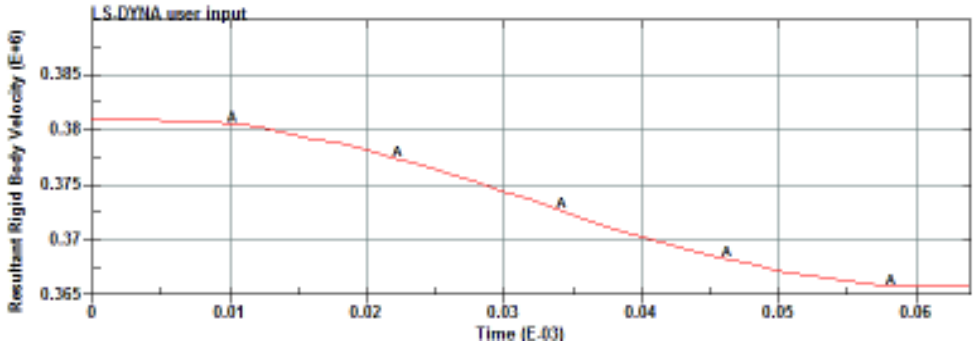
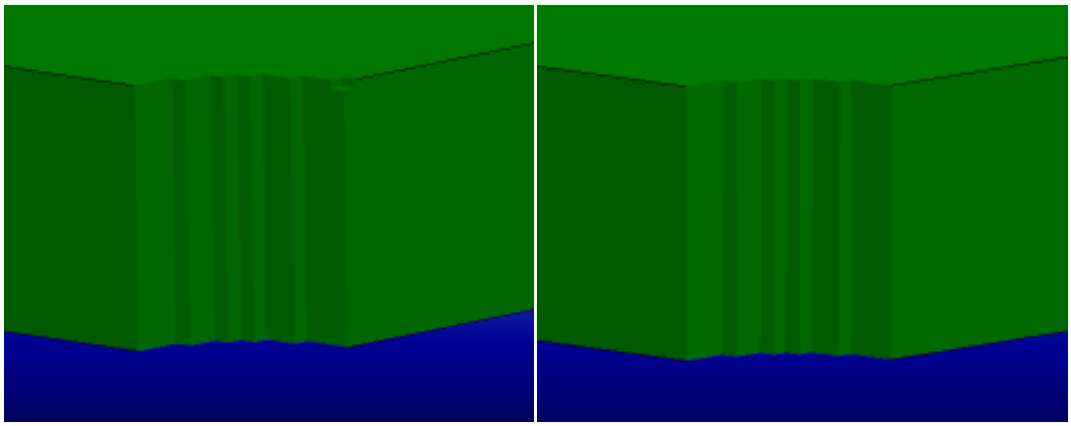


Figure 33. Velocity (mm/s) vs. time (s) curve of layered carbon-aramid/epoxy composite with MAT 59 for initial velocity V_i: 381 m/s

Appendix E



(a) (b)

Figure 34. Perforation view of single layer aramid/epoxy composites with MAT 59 after simulations for initial velocities (a) V_i: 852 m/s (b) V_i: 790 m/s

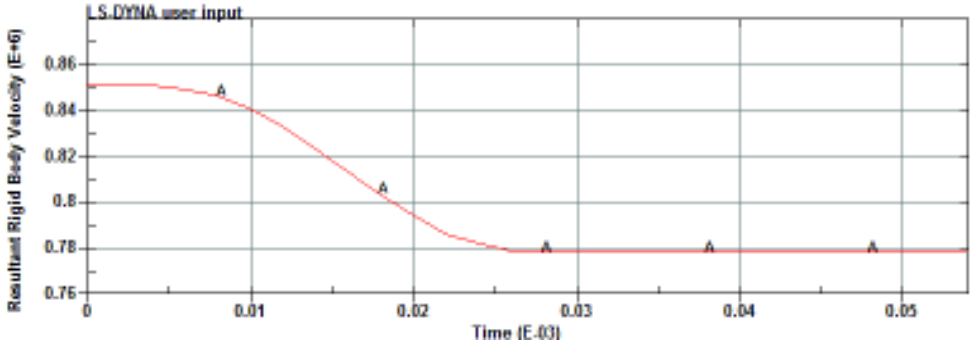


Figure 35. Velocity (mm/s) vs. time (s) curve of single layer aramid/epoxy composite with MAT 59 for initial velocity V_i: 850 m/s

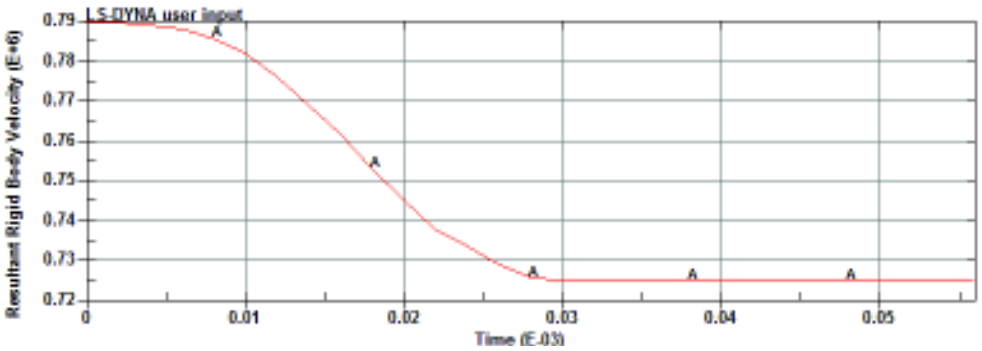
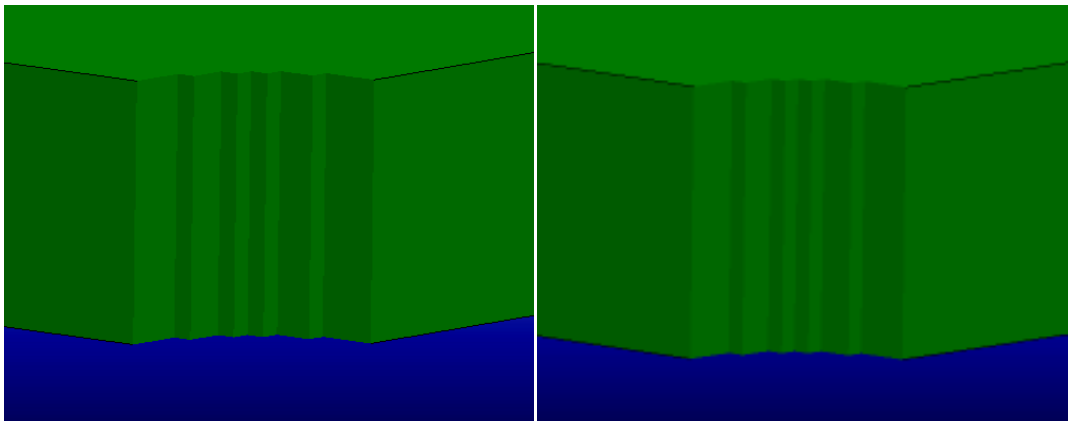


Figure 36. Velocity (mm/s) vs. time (s) curve of single layer aramid/epoxy composite with MAT 59 for initial velocity V_i: 790 m/s



(a) (b)

Figure 37. Perforation view of single layer aramid/epoxy composites with MAT 59 after simulations for initial velocities (a) V_i: 713 m/s (b) V_i: 619 m/s

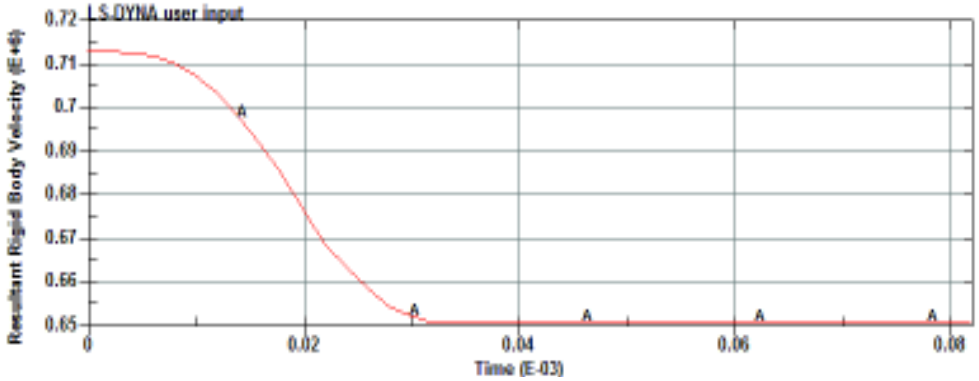


Figure 38. Velocity (mm/s) vs. time (s) curve of single layer aramid/epoxy composite with MAT 59 for initial velocity V_i: 713 m/s

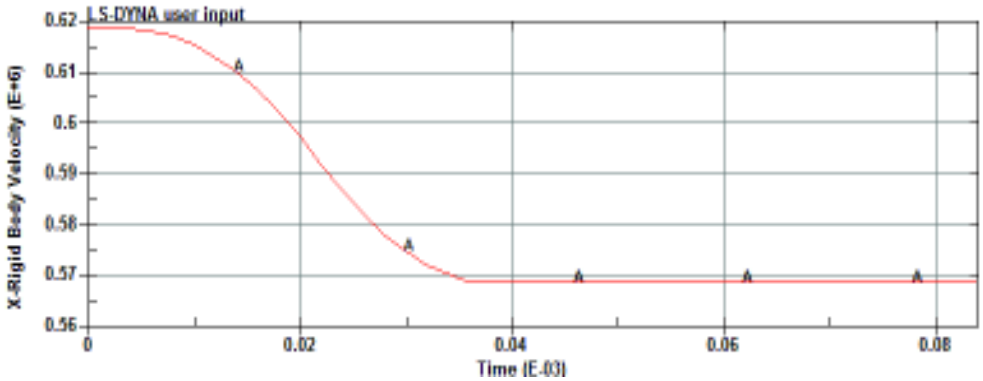
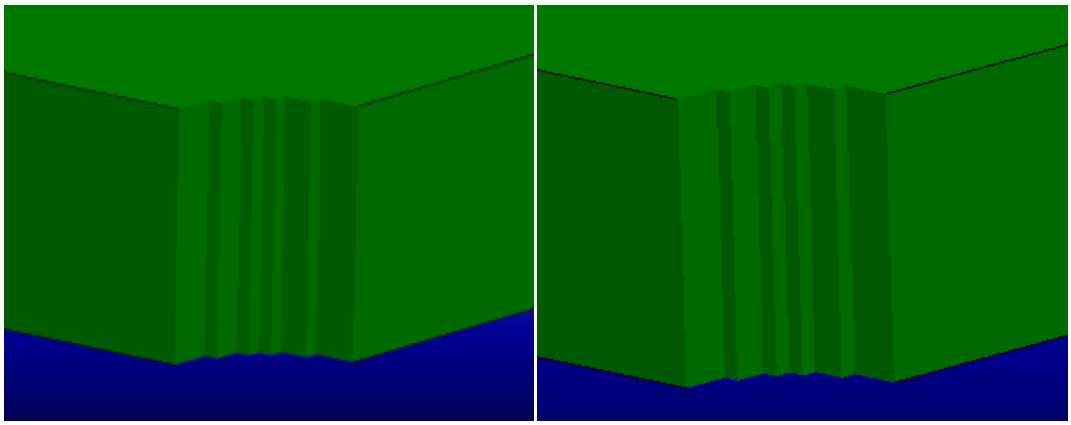


Figure 39. Velocity (mm/s) vs. time (s) curve of single layer aramid/epoxy composite with MAT 59 for initial velocity V_i: 619 m/s



(a) (b)

Figure 40. Perforation view of single layer aramid/epoxy composites with MAT 59 after simulations for initial velocities (a) V_i: 543 m/s (b) V_i: 333 m/s

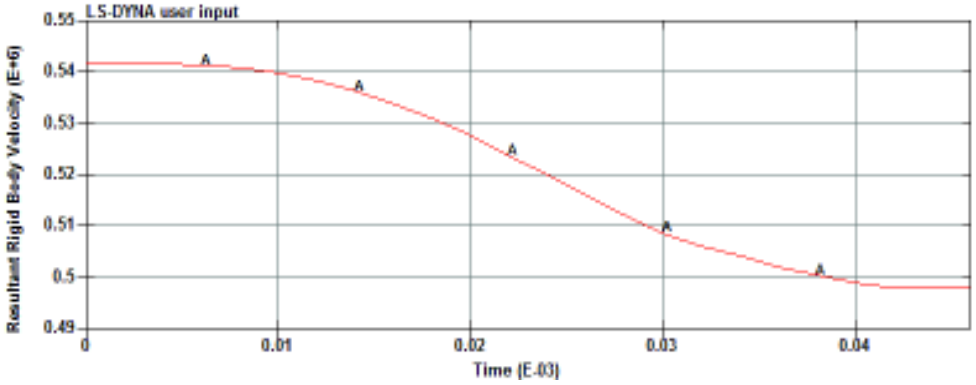


Figure 41. Velocity (mm/s) vs. time (s) curve of single layer aramid/epoxy composite with MAT 59 for initial velocity V_i: 543 m/s

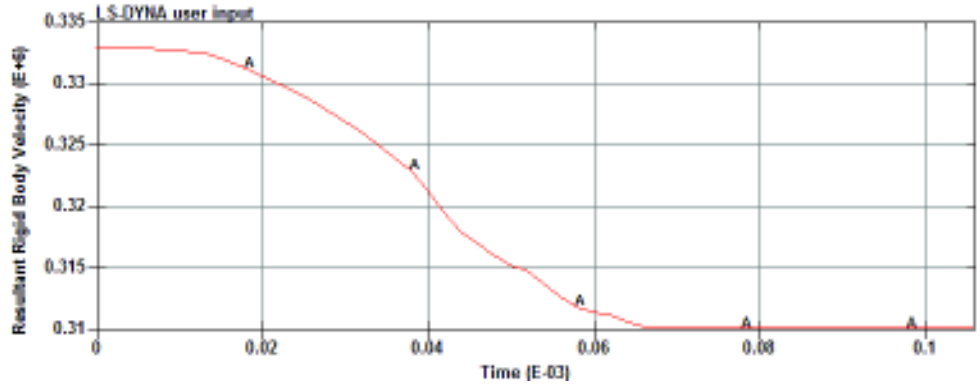
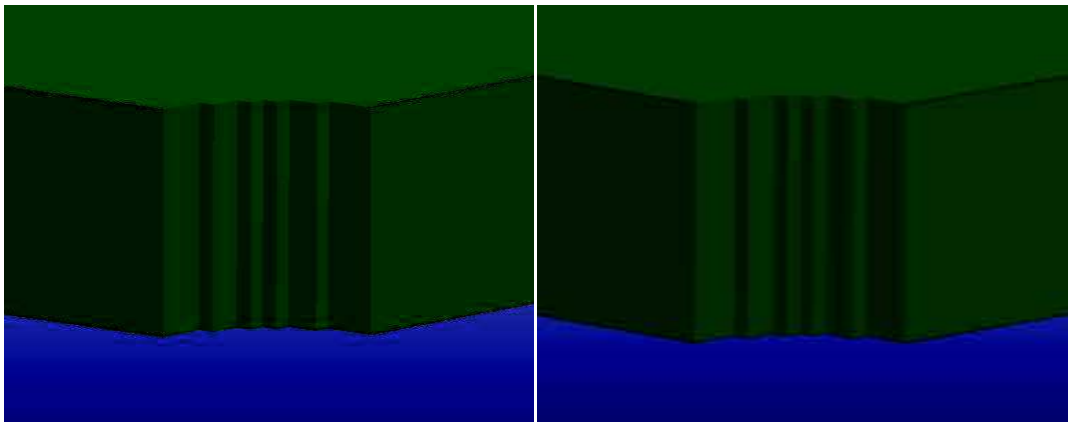


Figure 42. Velocity (mm/s) vs. time (s) curve of single layer aramid/epoxy composite with MAT 59 for initial velocity V_i: 333 m/s

Appendix F



(a) (b)

Figure 43. Perforation view of single layer carbon-aramid/epoxy composites with MAT 59 after simulations for initial velocities (a) V_i: 850 m/s (b) V_i: 841 m/s

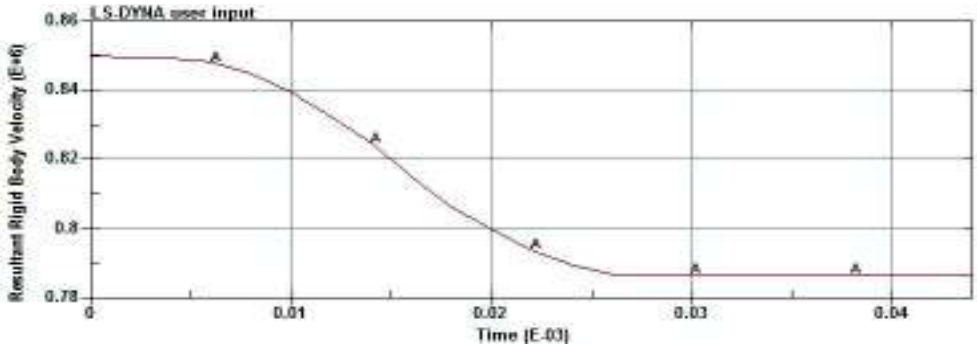


Figure 44. Velocity (mm/s) vs. time (s) curve of single layer carbon-aramid/epoxy composite with MAT 59 for initial velocity V_i: 850 m/s

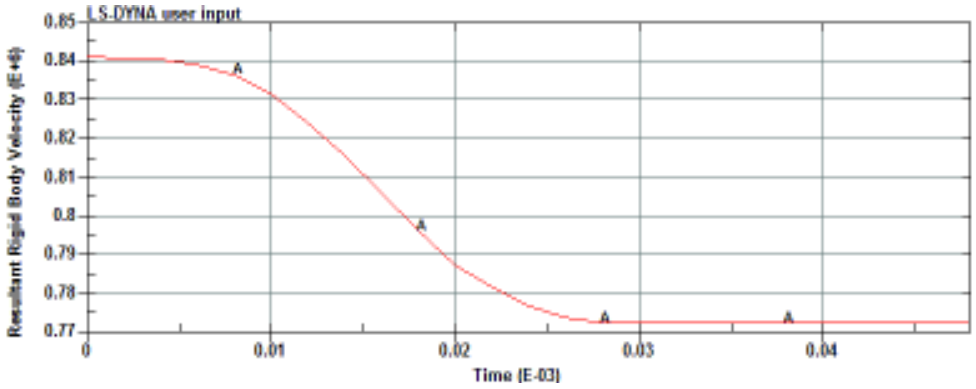
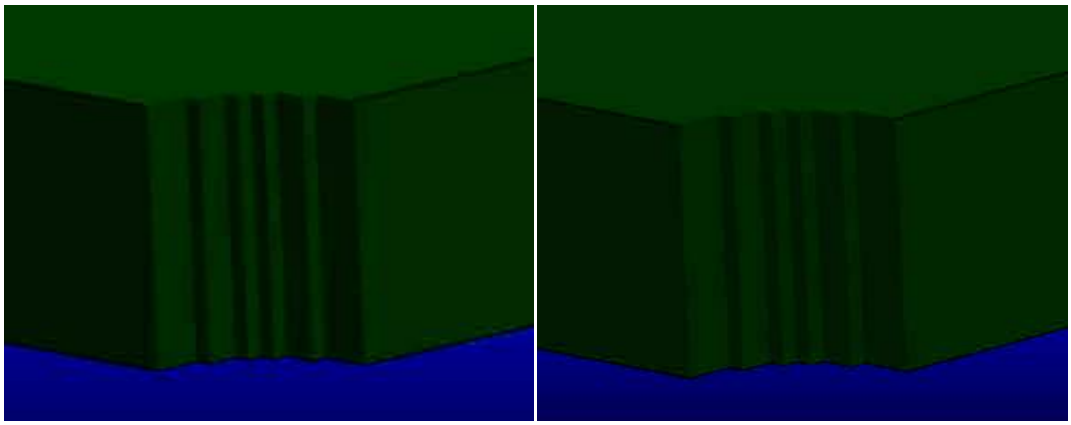


Figure 45. Velocity (mm/s) vs. time (s) curve of single layer carbon-aramid/epoxy composite with MAT 59 for initial velocity V_i: 841 m/s



(a) (b)

Figure 46. Perforation view of single layer carbon-aramid/epoxy composites with MAT 59 after simulations for initial velocities (a) V_i: 764 m/s (b) V_i: 652 m/s

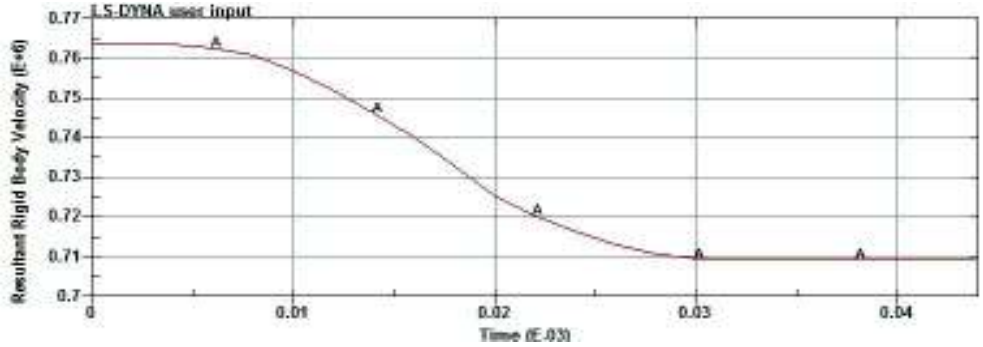


Figure 47. Velocity (mm/s) vs. time (s) curve of single layer carbon-aramid/epoxy composite with MAT 59 for initial velocity V_i: 764 m/s

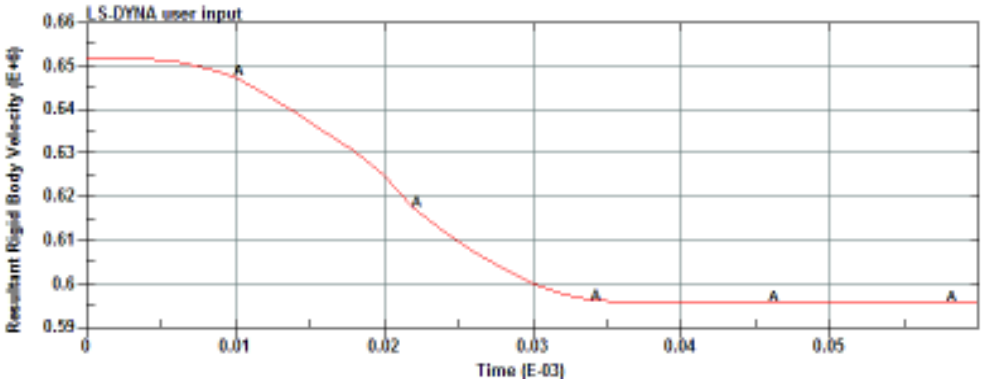
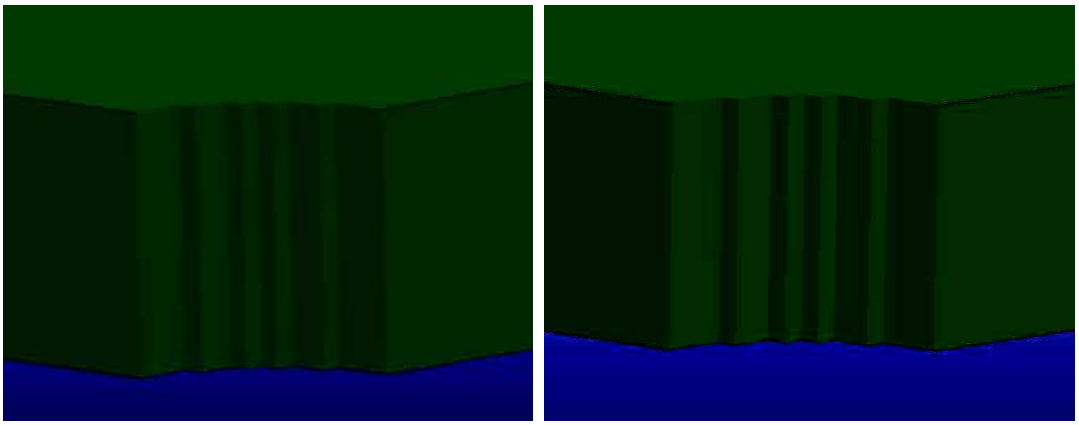


Figure 48. Velocity (mm/s) vs. time (s) curve of single layer carbon-aramid/epoxy composite with MAT 59 for initial velocity V_i: 652 m/s



(a) (b)

Figure 49. Perforation view of single layer carbon-aramid/epoxy composites with MAT 59 after simulations for initial velocities (a) V_i: 540 m/s (b) V_i: 381 m/s

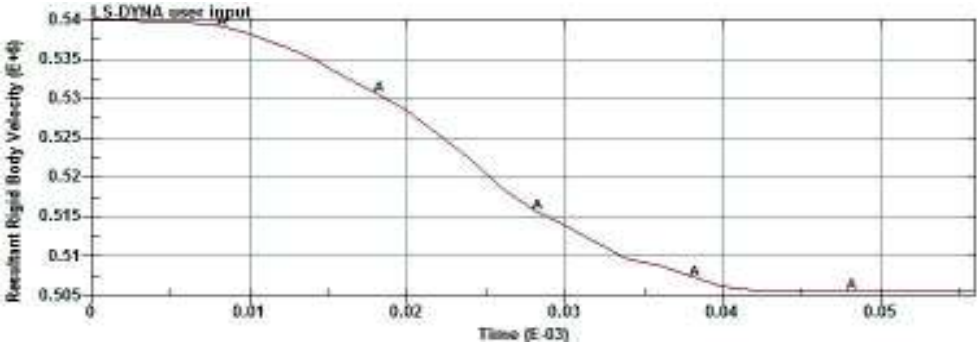


Figure 50. Velocity (mm/s) vs. time (s) curve of single layer carbon-aramid/epoxy composite with MAT 59 for initial velocity V_i: 540 m/s

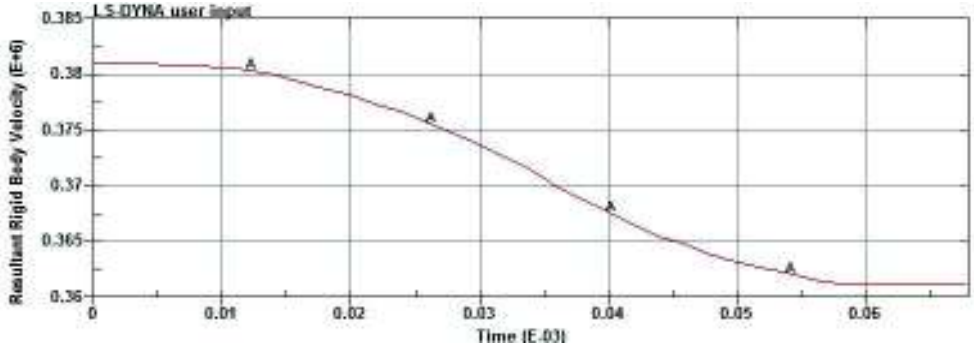


Figure 51. Velocity (mm/s) vs. time (s) curve of single layer carbon-aramid/epoxy composite with MAT 59 for initial velocity V_i: 381 m/s